CHAPTER-IV

RESULTS AND DISCUSSIONS

Chapter-IV
RESULTS AND DISCUSSIONS

This chapter deals with a detailed description of the outcomes obtained from the experimental investigations. It also deals with the statistical representation of the data obtained from the various tools, software, and experimental work. Interpret the data from the studies and their scientific background and compare them with the relevant recent scientific work. Overall, it includes the interrelation between the experimental combinations and outcomes of the investigations and their interpretation.

4.0 Results and discussion

4.1 Stability of CP-treated PPO and POD enzymes

The effects of varying voltage and treatment times on enzyme activity are presented in Figs. 4.1, 4.2, and 4.3. Pineapple pulp treated under different sample depths of 2, 3, and 4 mm with voltages applied from 15 kV to 25 kV for treatment times of (3-15) min showed a positive impact on pineapple pulp. The relative activity of these enzymes was reduced with the combined effect of voltage and treatment times, indicating that the higher the voltage, more the inactivation of enzymes. The maximum PPO and POD inactivation was about 85% and 66% at 25 kV and 2 mm sample depth. Relative activity of the enzymes was significantly ($p<0.05$) reduced with the increased experimental conditions, as presented in Figs. 4.1, 4.2, and 4.3. The reactive species generated during DBD plasma treatment significantly reduced the enzymes in pineapple pulp at $p<0.05$. Tappi et al. (2014) successfully inactivated the PPO enzymes in fresh-cut apples by applying DBD plasma. The activity of these enzymes also showed a similar pattern of inactivation upon exposure to high-voltage cold plasma treatments (Fig. 4.1, 4.2, and 4.3). However, the inactivation rate was higher in PPO than in POD for all the treatment conditions. For both PPO and POD, the inactivation was due to the combined effect of voltage and plasma exposure time, not because of the temperature. This was confirmed by utilizing a digital thermometer to record the temperature rise, which showed a maximum temperature rise of 3 ^{o}C from room temperature (25 ^{o}C) for all the samples. Both the parameters had a significant impact on the reduction activity ($p<0.05$). Voltages significantly affected the inactivation rate for all the treatment conditions, as seen in Fig. 4.1 ($p<0.05$).

(a)

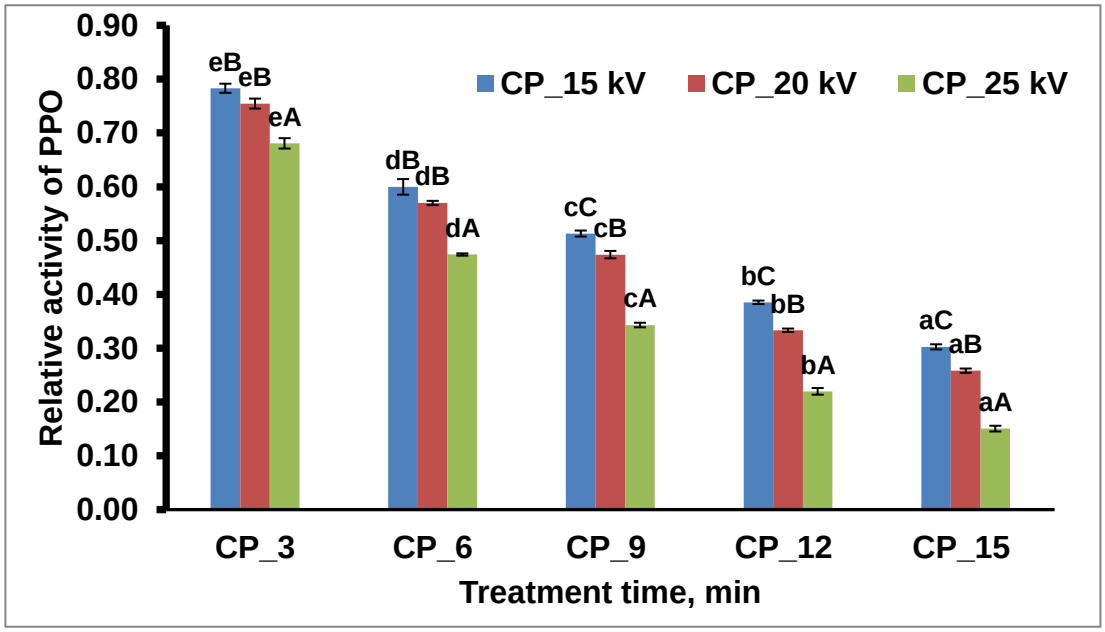

(b)

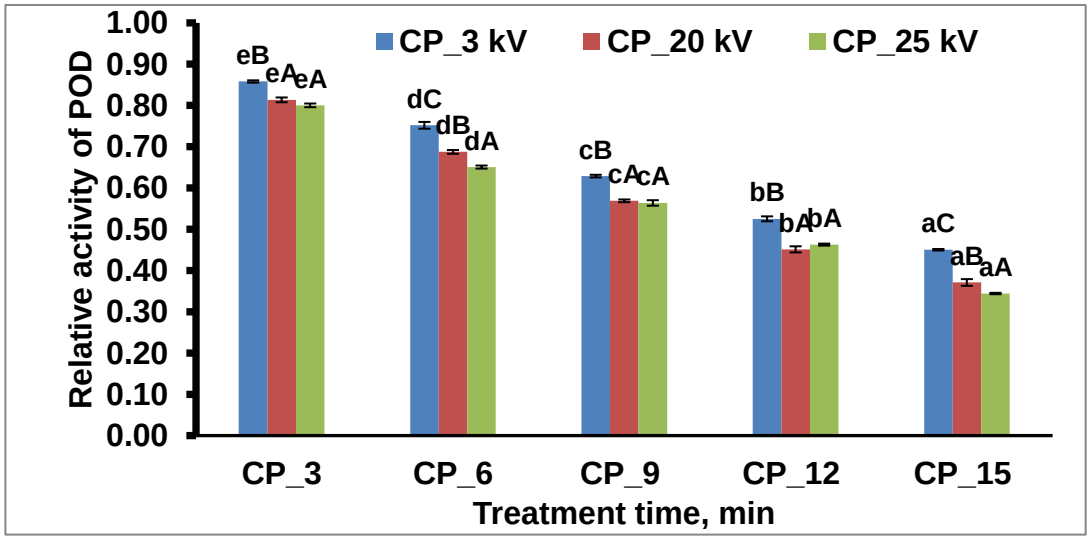

Figure 4.1: Relative activity of (a) PPO, (b) POD of cold plasma-treated pineapple pulp at 2 mm sample depth under different voltages of 15-25 kV and treatment time for 3-15 min.

**mean± SD that do not share a small letter are significantly different with the treatment time, and capital letters are significantly different with the voltages

(a)

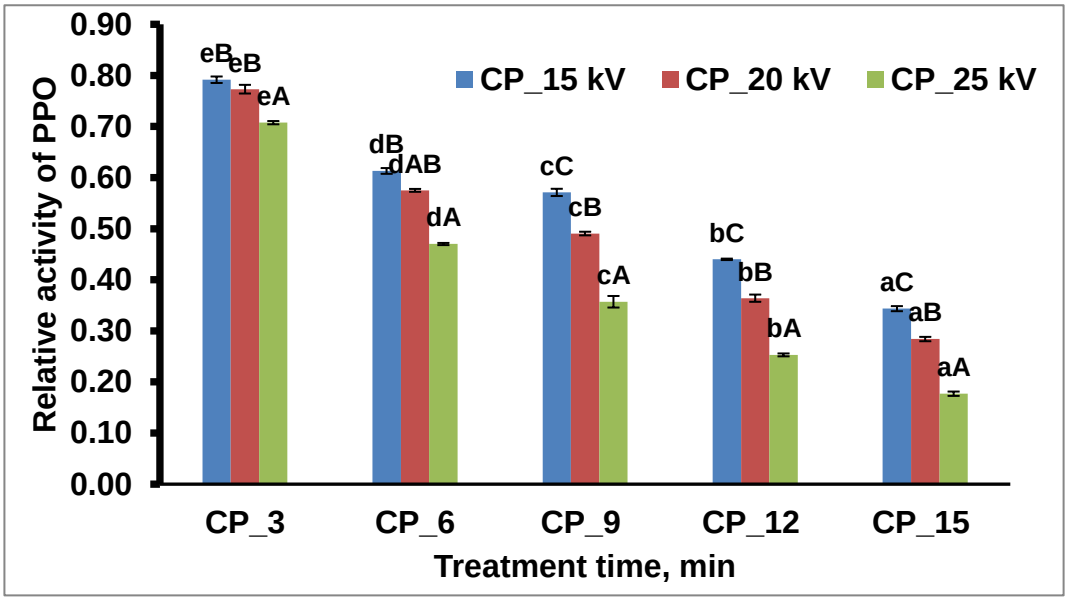

(b)

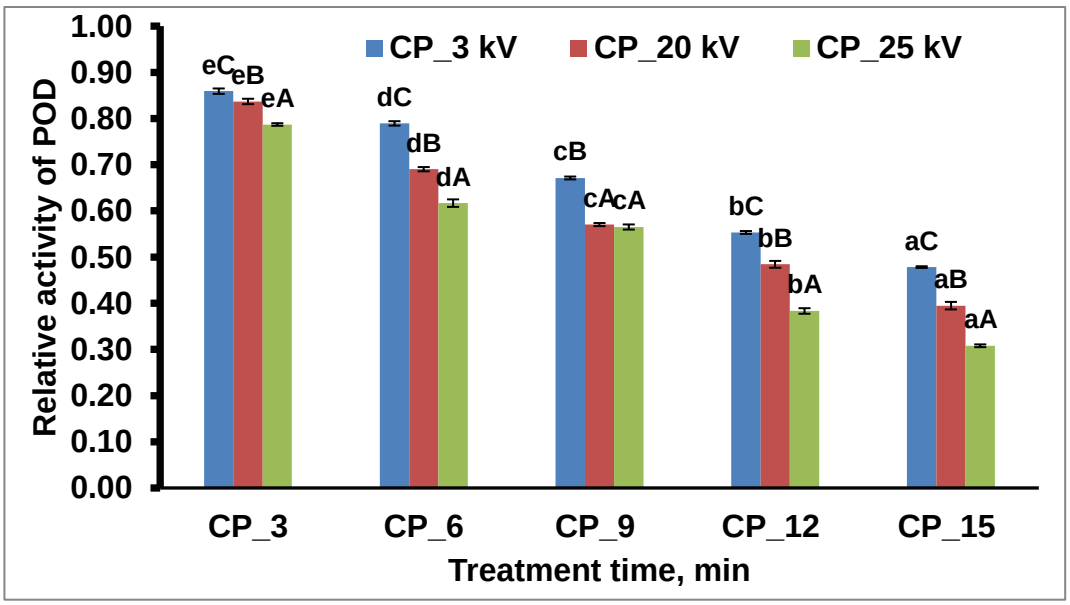

Figure 4.2: Relative activity of (a) PPO, (b) POD of cold plasma-treated pineapple pulp at 3 mm sample depth under different voltages of 15-25 kV and treatment time for 3-15 min

**mean± SD that do not share small letters are significantly different with the treatment time, and capital letters are significantly different with the voltages

(a)

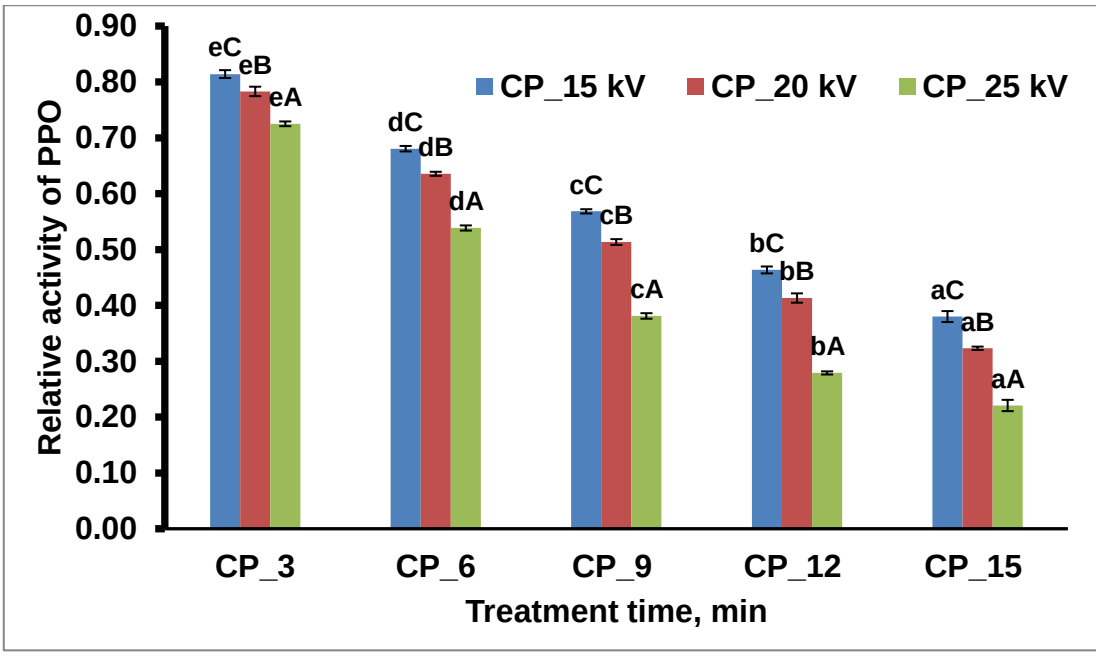

(b)

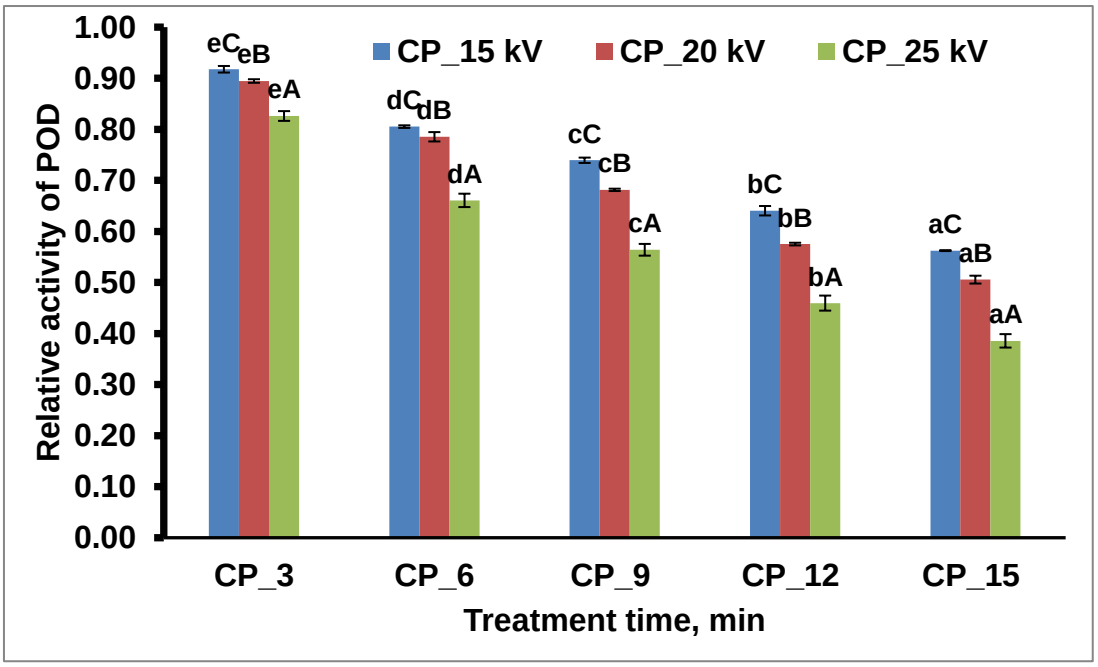

Figure 4.3: Relative activity of (a) PPO, (b) POD of cold plasma-treated pineapple pulp at 4 mm sample depth under different voltages of 15-25 kV and treatment time for 3-15 min

**mean± SD that do not share small letters are significantly different with the treatment time, and capital letters are significantly different with the voltage

Similar changes can also be observed from other experimental conditions, as presented in Figs 4.2 and 4.3. Atmospheric DBD plasma treatment could significantly reduce the PPO enzyme in apple juice, as reported by Illera et al. (2019). Similar patterns were also obtained for the degradation kinetic study of enzymes in pineapple pulp. Upon exposure to DBD treatments, the secondary structure of the protein gets denatured, and enzyme inactivation is caused. Reactive species, free radicals such as hydroxyl, superoxide anion, hydroperoxy radicals, and nitrogen oxide generated during the plasma, modify the chemical changes in the amino acids, breaking of peptide bonds, and oxidative degradation of proteins, which might result in enzyme inactivation (Takai et al., 2012). Pankaj et al. (2013) investigate the peroxidase inactivation of tomato extract upon exposure to cold plasma treatment. They reported that both parameters substantially impacted the levels of inactivation. According to their studies, the inactivation was caused by the reaction between the generated species (O_2, N_2) with the side chains of the protein. The relative content analysis of secondary structure motifs of the oxidative enzymes is studied by Surowsky et al. (2013). Their investigations also revealed that the Circular dichroism spectroscopy reduced the number of α-helices and β-structure. Plasma exposure in fresh-cut apples and potatoes significantly reduced the enzymes (Bubler et al., 2016). According to their investigations, the rate of inactivation is attributed to the modification in the α-helices structure of the protein in enzymes. Zhong et al. (2007) also studied the electric field effect on the inactivation of the PPO and POD enzymes. Their studies reveal that the enzymes' inactivation is due to the protein's secondary (α-helices) structural modification. According to Davies and Delsignore (1987), plasma-inherent ROS and UV photons are most likely the initiators of many reactions that could result in conformational changes in the complex plasma chemistry. The inactivation of enzymes in DBD-treated pulp was due to the reduction of α-helices. The destruction of β-structure was due to the denaturation of protein bonds (C-H, C-N, and N-H) caused by the oxidation of active species of oxygen-containing plasma into CO_2, NO_2, and H_2O (Hayashi et al., 2009). Plasma exposure is effectively applied to fruits such as apple juice, tomato, kiwifruit, and melon (Illera et al., 2019; Mishra et al., 2014; Ramazzina et al., 2015).

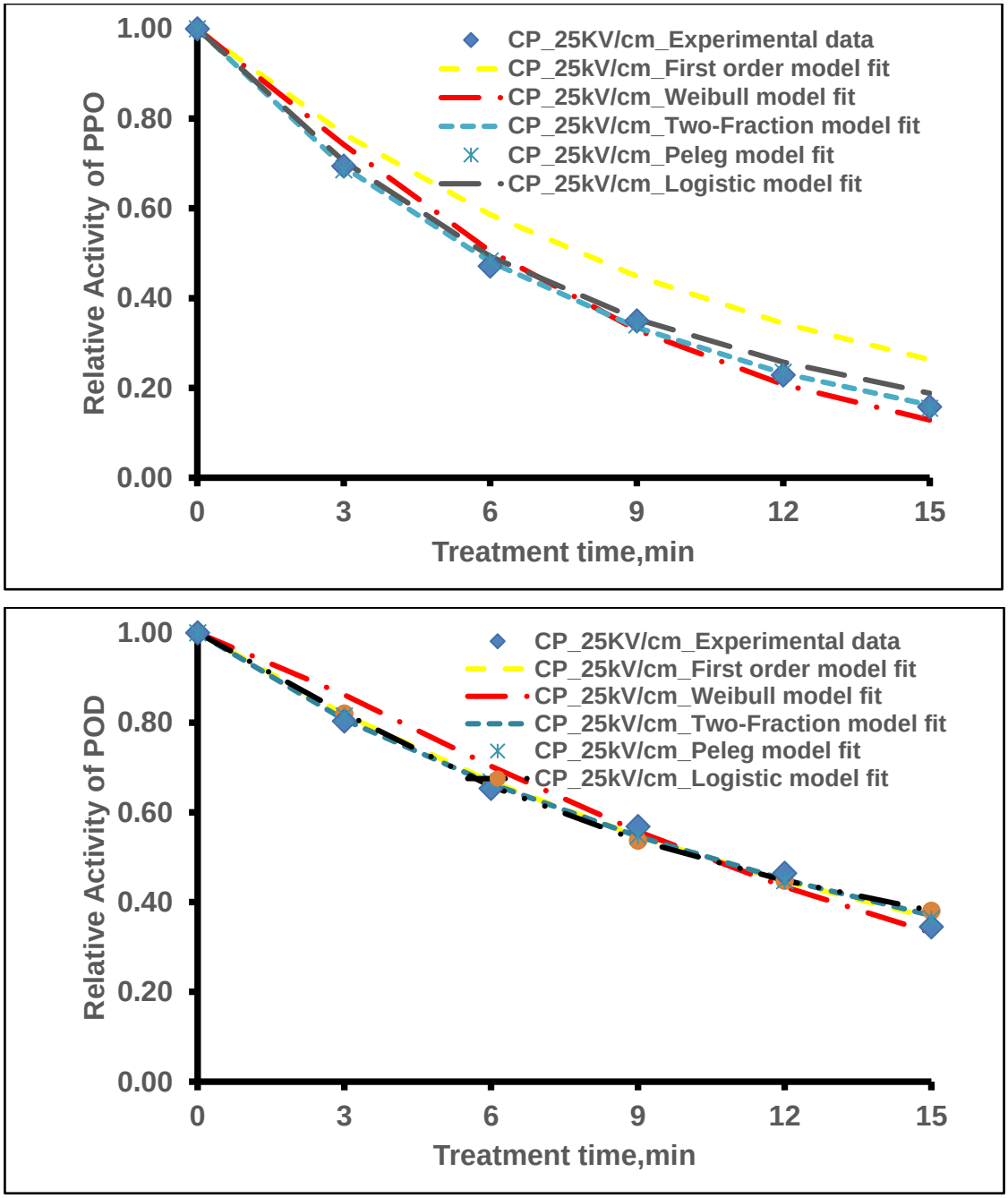

Figure 4.4: Relative activity of PPO and POD of cold plasma-treated pineapple pulp at 2 mm sample depth fitted to first-order kinetic model, Weibull model, Two-Fractional model, Peleg and Logistic model

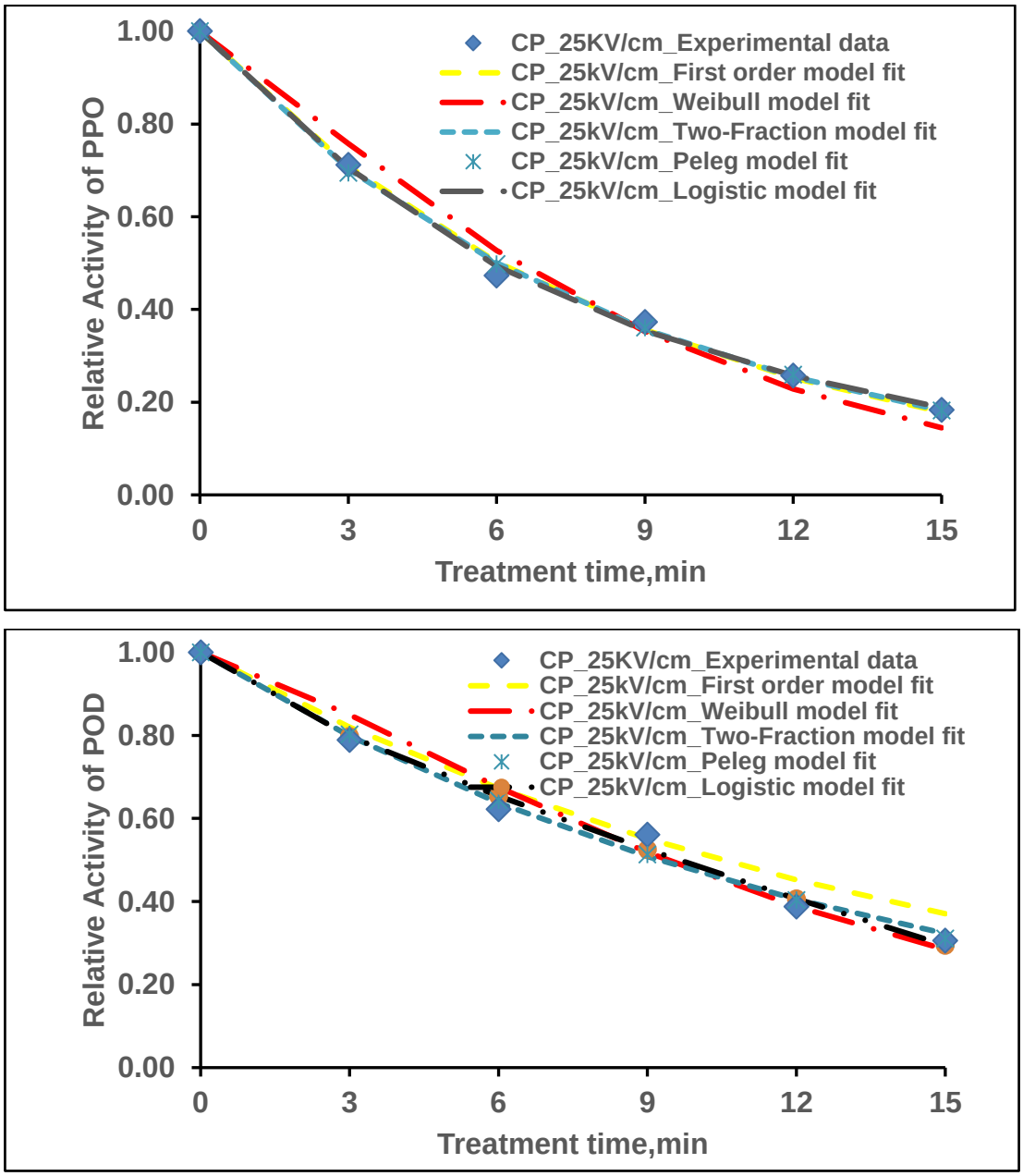

Figure 4.5: Relative activity of PPO and POD of cold plasma-treated pineapple pulp at 3 mm sample depth fitted to first-order kinetic model, Weibull model, Two-Fractional model, Peleg and Logistic model

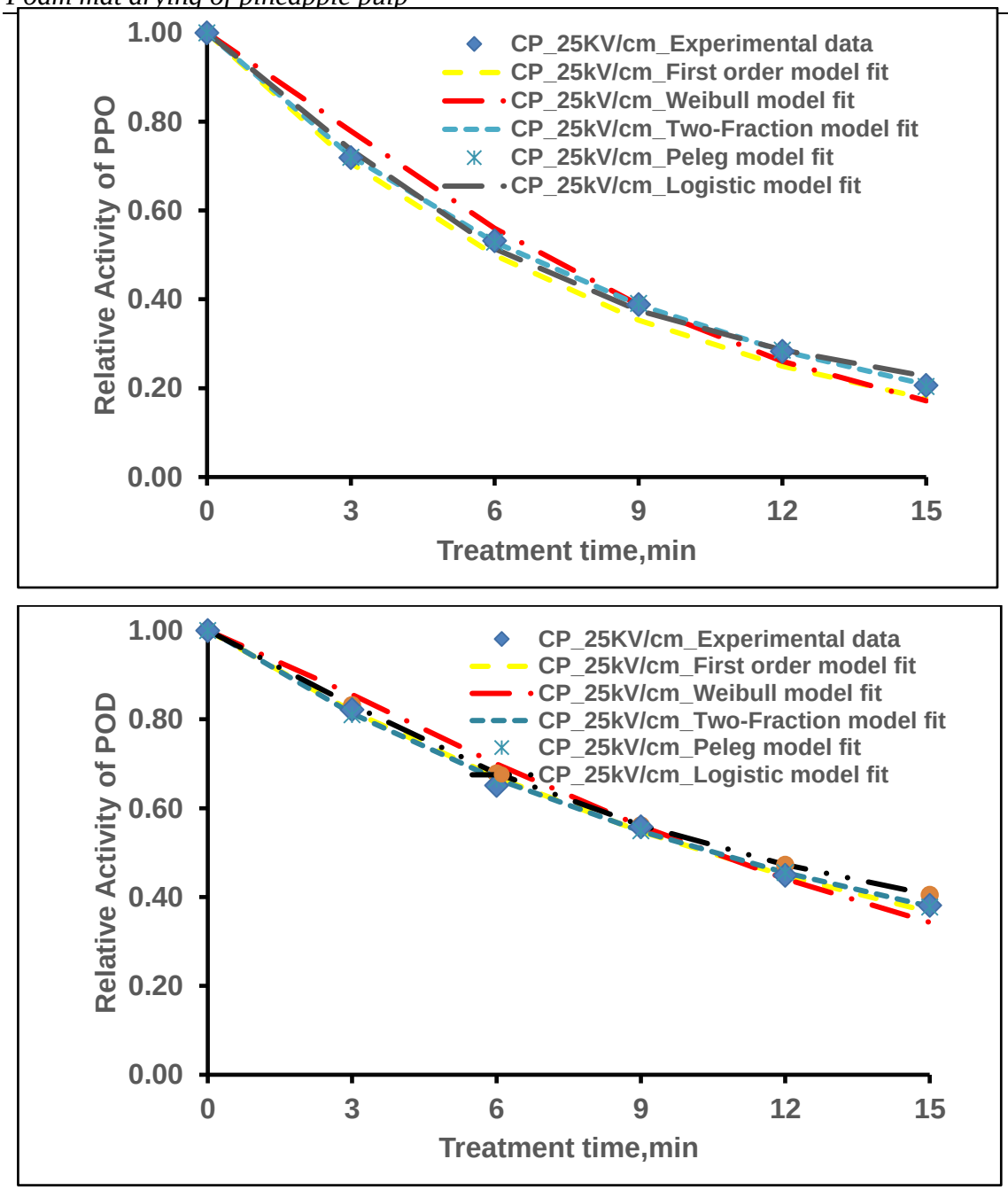

Figure 4.6: Relative activity of PPO and POD of cold plasma-treated pineapple pulp at 4 mm sample depth fitted to first-order kinetic model, Weibull model, Two-Fractional model, Peleg and Logistic model

In the present investigation, PPO inactivation exceeded 85% under several treatment conditions (e.g., 25 kV, 2 mm depth, 12–15 min), meeting the PPO inactivation target for high-quality dried pineapple products. POD inactivation reached up to 66% under the same conditions, which, while slightly above the optimal target, is still sufficient to significantly retard oxidative deterioration. Importantly, these inactivation levels were achieved without substantial temperature rise (≤3 °C), preserving thermolabile nutrients.

Based on the combined inactivation efficiency, model fitting, and minimal thermal effects, the optimal plasma treatment conditions for producing high-quality pineapple pulp product were 25 kV, 2 mm sample depth, and 12–15 min treatment time**.** These parameters enable industry professionals to meet enzymatic inactivation thresholds while maintaining product integrity, making the process effective and scalable for commercial adoption.

The sample plot shown in Figures 4.4, 4.5, and 4.6 implied the effect of the treatment time on the relative activity of the enzymes in pineapple pulp. The plots shown in the figure represent the activity of both enzymes gradually decreasing with the increased treatment times, voltages, and sample depth. Enzyme inactivation was greatly influenced by the plasma exposure time, as reported by Surowsky et al. (2013). The present investigation also signifies a similar significant effect of time on the inactivation of the enzyme in pineapple pulp ($p<0.05$). All the predicted models close to the experimental conditions indicate a better prediction of the model for enzyme inactivation.

4.2 Mathematical modeling of enzymes (PPO and POD)

4.2.1 First-order kinetics

First-order model parameters (reaction rate constant, k_F) for PPO and POD were observed to be increased from (0.080-0.115 s^{-1}) and (0.037-0.067 s^{-1}), respectively, with the voltage gradients (Table 4.1-4.6). The higher value of the reaction rate constant of PPO than POD signifies that the POD was more stable during the cold plasma treatment. The coefficients of regression (R^2) for PPO and POD at 2 mm depth were (0.995-0.996) and (0.994-0.998), respectively. Similar patterns can also be observed from the samples treated under sample depths of 3 and 4 mm (Tables 4.3, 4.4, 4.5, and 4.6). It is seen from the observations of R^2 >0.99, while the RMSE/error was not satisfactory. This model's unsatisfactory error/RMSE values describe its poor fitness for explaining the enzyme activity.

Table 4.1 PPO Enzymatic modeling kinetic parameters of Cold plasma-treated pineapple pulp at 2 mm sample depth

Enzyme	Model (s)	Treatment (kV/cm)	k (s^{-1})	b	n	A_L	A_S	T_{50}	a	k_1	k_2	R^2	RMSE
PPO	First order	15	0.080									0.996	0.0166
		20	0.089									0.997	0.0156
		25	0.089									0.997	0.0156
	Weibull	15		0.034	1.447							0.953	0.0560
		20		0.049	1.279							0.979	0.0406
		25		0.080	1.207							0.989	0.0319
	Two-fraction	15				0.9403	0.0053			0.2893	0.0740	0.996	0.0244
		20				0.9922	0.0611			0.4422	0.0881	0.997	0.0245
		25				0.8848	0.0077			0.8307	0.1211	0.993	0.0132
	Peleg	15								11.46	0.6826	0.997	0.0170
		20								10.78	0.6285	0.997	0.0159
		25								7.51	0.6819	0.999	0.0091
	Logistic	15				$1.32x10^{-9}$		15.01	1.189			0.985	3.195
		20				-41.94		9.758	1.021			0.997	1.910
		25				-17.63		7.599	1.178			0.998	1.697

Table 4.2 POD Enzymatic modeling kinetic parameters of Cold plasma-treated pineapple pulp at 2 mm sample depth

Enzyme	Model (s)	Treatment (kV/cm)	k (s^{-1})	b	n	A_L	A_S	T_{50}	a	k_1	k_2	R^2	RMSE
POD	First order	15	0.052									0.997	0.0123
		20	0.065									0.998	0.0097
		25	0.067									0.994	0.0180
	Weibull	15		0.027	1.279							0.989	0.0217
		20		0.035	1.267							0.985	0.0286
		25		0.038	1.243							0.975	0.0376
	Two-fraction	15				1.207	0.209			0.0631	0.1551	0.998	0.0124
		20				1.416	0.4185			0.0777	0.1198	0.998	0.0123
		25				0.9795	0.7948			0.06486	7.713	0.995	0.027
	Peleg	15								20.910	0.412	0.998	0.009
		20								15.930	0.523	0.999	0.008
		25								14.410	0.610	0.995	0.019
	Logistic	15				-86.680		34.010	0.855			0.998	1.070
		20				-350.200		24.100	0.984			0.996	0.649
		25				0.000		10.150	1.059			0.990	2.641

Table 4.3 PPO Enzymatic modeling kinetic parameters of Cold plasma-treated pineapple pulp at 3 mm sample depth

Enzyme	Model (s)	Treatment (kV/cm)	k (s^{-1})	b	n	A_L	A_S	T_{50}	a	k_1	k_2	R^2	RMSE
PPO	First order	15	0.070									0.987	0.027
		20	0.084									0.996	0.016
		25	0.115									0.998	0.015
	Weibull	15		0.024	1.447							0.918	0.068
		20		0.044	1.279							0.971	0.046
		25		0.074	1.207							0.984	0.040
	Two-fraction	15				0.960	0.040			2.14	0.065	0.989	0.032
		20				0.983	0.017			2.11	0.081	0.997	0.020
		25				0.983	0.017			1.89	0.113	0.998	0.019
	Peleg	15								12.84	0.710	0.989	0.028
		20								10.96	0.678	0.997	0.017
		25								7.703	0.708	0.998	0.016
	Logistic	15				-59.87		17.89	1.019			0.986	3.195
		20				-41.94		15.01	1.021			0.997	1.910
		25				-17.63		7.599	1.178			0.998	1.697

Table 4.4 POD Enzymatic modeling kinetic parameters of Cold plasma-treated pineapple pulp at 3 mm sample depth

Enzyme	Model (s)	Treatment (kV/cm)	k (s^{-1})	b	n	A_L	A_S	T_{50}	a	k_1	k_2	R^2	RMSE
POD	First order	15	0.047									0.988	0.021
		20	0.062									0.998	0.011
		25	0.066									0.998	0.011
	Weibull	15		0.022	1.307							0.987	0.023
		20		0.032	1.279							0.973	0.037
		25		0.040	1.269							0.974	0.042
	Two-fraction	15		0.022		0.379	0.023			0.049	0.032	0.991	0.030
		20		0.032		0.227	0.035			0.073	0.079	0.998	0.017
		25		0.040		0.102	0.127			0.079	3.668	0.989	0.043
	Peleg	15								25.200	0.223	0.995	0.016
		20								15.260	0.649	0.998	0.013
		25								13.560	0.547	0.990	0.028
	Logistic	15				$-1.090x10^5$		23.56	0.5824			0.994	2.022
		20				-9.238		12.88	0.7766			0.998	1.274
		25				$-2.0x10^4$		11.96	0.9796			0.992	3.056

Table 4.5 PPO Enzymatic modeling kinetic parameters of Cold plasma-treated pineapple pulp at 4 mm sample depth

Enzyme	Model (s)	Treatment (kV/cm)	k (s^{-1})	b	n	A_L	A_S	T_{50}	a	k_1	k_2	R^2	RMSE
PPO	First order	15	0.063									0.969	0.0390
		20	0.075									0.927	0.0540
		25	0.105									0.972	0.0490
	Weibull	15		0.017	1.545							0.931	0.0604
		20		0.039	1.287							0.979	0.0369
		25		0.066	1.213							0.989	0.0314
	Two-fraction	15				0.992	0.008			1.937	0.063	0.998	0.0030
		20				0.990	0.010			1.699	0.074	0.9999	0.0037
		25				0.985	0.015			1.533	0.104	0.9999	0.0033
	Peleg	15								14.990	0.633	0.9999	0.0021
		20								12.510	0.648	0.9999	0.0023
		25								8.673	0.677	0.9999	0.0021
	Logistic	15				$4.18x10^{-14}$		10.780	1.252			0.9982	1.0710
		20				$2.41x10^{-12}$		8.959	1.292			0.9978	1.3150
		25				$3.34x10^{-11}$		6.248	1.402			0.9972	1.7440

Table 4.6 POD Enzymatic modeling kinetic parameters of Cold plasma-treated pineapple pulp at 4 mm sample depth

Enzyme	Model (s)	Treatment (kV/cm)	k (s^{-1})	b	n	A	B	T50	P	k_1(s^{-1})	k_2(s^{-1})	R^2	RMSE
POD	First order	15	**0.037**									**0.901**	**0.049**
		20	**0.045**									**0.927**	**0.054**
		25	**0.066**									**0.995**	**0.019**
	Weibull	15		**0.013**	**1.415**							**0.982**	**0.022**
		20		**0.022**	**1.298**							**0.986**	**0.023**
		25		**0.042**	**1.197**							**0.982**	**0.032**
	Two-fraction	15				**0.992**	**0.023**			**0.046**	**0.046**	**0.997**	**0.017**
		20				**0.974**	**0.035**			**0.168**	**0.058**	**0.999**	**0.014**
		25				**0.875**	**0.127**			**0.144**	**0.055**	**0.999**	**0.014**
	Peleg	15								**31.810**	**0.141**	**0.996**	**0.012**
		20								**23.710**	**0.407**	**0.998**	**0.011**
		25								**13.780**	**0.646**	**0.998**	**0.010**
	Logistic	15				**0.6853**		**21.61**	**1.192**			**1.000**	**0.231**
		20				**$7.32x10^{-12}$**		**19.94**	**1.201**			**0.999**	**0.633**
		25				**$3.61x10^{-10}$**		**14.99**	**1.234**			**0.999**	**0.818**

This can be seen in Fig.4.4, where the fitted model is slightly away from the experimental data for both the enzymes in pineapple pulp. This might be due to the complex nature of the enzymes and variations that occur in the different mechanisms involved in the breakdown of their structure. However, the parameters obtained from the first-order models showed that the PPO was more inactivated than the POD. Pankaj et al. (2013) also reported similar results for enzyme degradation in tomatoes. The data fitted with this model showed adj. R^2 (0.949-0.972) and RMSE (0.48-0.71) for the inactivation of ozonation-treated sugarcane juice (Panigrahi et al., 2021). Another mathematical model has been proposed to check their fitness with error.

4.2.2 Weibull model

Weibull-model parameters (b and n) for the PPO and POD were estimated to study the significance of treatment on pineapple pulp. The Weibull non-linear parameter ('b') value for PPO and POD varied from (0.017-0.066) and (0.013-0.042) with the increased voltages, while the opposite trends can be seen for 'n' values (Table 4.5 and Table 4.6). Shape factors for PPO and POD decreased from (1.545-1.213) and (1.415-1.197), respectively. The shape factor for both enzymes was n>1, indicating their downward concavity. The downward concavity of the enzymes implied their decreasing rate of enzymes with the applied voltage and treatment time combinations, as seen from Figs 4.4, 4.5, and 4.6. The Weibull model parameter was well-fitted with the $R^2 \geq \left| 0.931 \right|$ and RMSE$\leq$0.060 (Table 4.5). The coefficient of adjustment R^{2}-values for the Weibull model were higher with lower RMSE/error than the first order, indicating the good prediction of this model in the reduction of PPO and POD. Similar patterns of PPO and POD inactivation were observed for the samples treated under 2 mm and 3 mm sample depths, as shown in Tables 4.1-4.4. The relative activity of experimental data and predicted models versus treatment time is shown in Figs. 4.4, 4.5, and 4.6 signify that the model was well fitted with the observations, but due to their higher variations/RMSE in model parameters, which describes the inadequacy for model fitting (Tables 4.1 and 4.2). Hence, the Two-fraction kinetic model was considered to further explain enzyme behavior with their regression coefficient.

4.2.3 Two-fraction kinetic model

Model parameter A_L significantly decreased with voltage gradients, possibly due to the increased inactivation of enzymes. A_L value was reduced with the increasing voltage (Table 4.5). While the A_S value was higher in both the PPO and POD, it might be due to the various

reactive species generated upon exposure to plasma treatment, which causes the denaturation of the enzymes. The K_L value was higher in PPO than in POD, revealing more inactivation than in POD, which can also be obtained from the first-order reaction rate constant (k_F value). Two-fraction kinetic models were better fitted with the experimental values, with the highest $R^2 \leq 0.99$ and RMSE$\leq$0.037 for the PPO and POD. Similar results of PPO and POD can also be obtained from the other conditions, as shown in Tables 4.1-4.6. All the kinetic models fitted well with $R^2 \geq \left| 0.927 \right|$ and RMSE$\leq$2.40. However, the two-fraction kinetic model was best fitted among the three models with the highest R^2 ($0.989>|r|\leq 0.999$) and lowest RMSE value. Due to the highest correlation coefficient and lowest RMSE obtained in the two-fraction kinetic model, it can fit the enzymes with more inactivation. Illera et al. (2019) also revealed that the two-fraction model was best for the inactivation in cloudy apple juice by CP treatment. The plots shown in Figs. 4.1-4.3 represent the decreasing trend of these enzymes with the voltage gradients. Predicted models were well fitted with their experimental values, which showed their accuracy with the minimum variation.

4.2.4 Peleg model

The model parameters of the non-linear regression were presented in Tables 4.1-4.6 for the inactivation kinetics of enzymes. The significance of this model is that it can predict the maximum inactivation of enzymes with short experimental observations. The regression coefficient (R^2) under different treatment conditions varied from 0.990 to 0.999 for PPO and POD, while the error had low values, RMSE<0.028. The statistical parameter fulfilling the desirable criteria indicates that Peleg's model was suitable for describing the inactivation kinetics behavior of enzymes in pineapple pulp. Peleg's constant ($K_1$and K_2) was changed with the treatment time for both the PPO and POD. However, the value of ($K_1>K_2$) was higher for both enzymes, which was expected. The Peleg constant K_1 is related to the mass transfer rate and the inactivation rate of the enzymes. The K_1 value was found to be decreased with the cold plasma voltage, which implied the higher rate ($1/K_1$) of inactivation due to plasma exposure, and the highest observed at 25 kV. Peleg's constant K_2 is related to the maximum inactivation capacity or the extent to which the enzyme inactivation may occur. The K_2 value for both the PPO and POD enzymes was slightly increased with the applied voltages (Tables 4.5 and 4.6). PPO and POD of samples treated under depths of 2 and 3 mm also showed similar findings in Tables 4.1-4.6. Drying carrot cubes using Peleg's model also showed findings identical to those of Planinic et al. (2005).

Peleg's model successfully modeled the inactivation kinetics of enzymes with the highest regression coefficient and lowest RMSE. All the models fit the experimental data well. However, it is clear from the table data and plots (Fig. 4.4) that the Peleg model was best fitted for both the activity of enzymes in pineapple pulp. However, a logistic model was proposed to explain their accuracy in the present context to reduce the error to a minimum value.

4.2.5 Logistic model

Logistic model parameters (A_{min}, t_{50}, and p) were determined by fitting the experimental RA versus time plot with the eq. 3.6. The t_{50} value for the enzymes found to be decreased from (10.780-6.248) and (21.610-14.990), respectively (Table 4.5 and 4.6.) t_{50} was the time taken to diminish the activity to its half before the treatment and its value were found to be decreased with the plasma voltage for both the PPO and POD (Panigrahi et al., 2021). A decreased t_{50} value with voltage gradients significantly affected enzyme inactivation. However, for all the voltages applied, t_{50} values for POD at 15, 20, and 25 were 21.610, 19.940, and 14.990, respectively, which were higher than PPO as presented in Table 4.6, indicating the peroxidase was less inactivated during the plasma treatment. A similar trend was observed in treated sugarcane Juice (Panigrahi et al., 2021). The Logistic model was well fitted for all the treatment conditions with the PPO enzymes with (R^2) ≤ |0.998| and RMSE/error less <1.744. The data presented for the samples treated under 2 mm and 3 mm depth also obtained similar observations.

4.3 Process standardization

All the treatment conditions positively impacted the inactivation of PPO activity, as seen in Table 4.7 of ANOVA. The p-value <0.05 signifies the model was found to be significant. The p-value for the treatment parameters (Voltage, Treatment time, and sample depth) was p<0.05, implying their significant effect on the inactivation of the PPO enzymes. The interaction of the voltage and treatment time also significantly impacted the enzyme inactivation, as seen from the ANOVA Table. The ANOVA Table 4.8 for the response POD also showed a similar behavior. All the treatment parameters found to be p<0.05 implied their positive impact on the POD inactivation. The science behind their inactivation of PPO and POD was explained in detail in section 4.1. Criteria for all the process parameters for standardizing the process have been selected in the range, and the responses were minimal, while giving importance to 3.

Table 4.7 ANOVA Table for the response PPO

Source	Sum of Squares	df	Mean Square	F-value	p-value	
Model	1.11	16	0.0694	168.59	< 0.0001	**significant**
A-Voltage	0.0045	2	0.0022	5.46	< 0.0001	
B-Treatment time	0.6705	4	0.1676	407.12	0.0015	
C-Sample depth	0.0087	2	0.0043	10.52	< 0.0001	
AB	0.4269	8	0.0534	129.62		
Residual	0.0115	28	0.0004			
Cor Total	1.120	44				

Table 4.8 ANOVA Table for the response POD

Source	Sum of Squares	df	Mean Square	F-value	p-value	
Model	0.8048	16	0.0503	105.91	< 0.0001	**significant**
A-Voltage	0.0079	2	0.0040	8.34	0.0014	
B-Treatment time	0.4969	4	0.1242	261.55	< 0.0001	
C-Sample depth	0.0129	2	0.0064	13.58	< 0.0001	
AB	0.2871	8	0.0359	75.56	< 0.0001	
Residual	0.0133	28	0.0005			
Cor Total	0.8181	44				

Based on the selection criteria, the solution for the process parameters, viz., voltage, treatment time, and sample depth, was 25 kV, 15 min, and 2 mm, respectively. Treatment conditions were selected based on the selection criteria and desirability (Table 4.9). The highest desirability value suggests a better prediction for selecting the process parameters for standardization and optimization. The process parameters were validated, and their outcomes were compared with the model values in Table 4.10. The closeness of the actual values to their predicted values implied the validation of the process parameters with minimum error (Table 4.11).

4.4 Effect of DBD plasma treatment on the colour value of Pineapple Pulp

DBD plasma-treated pineapple pulp showed increased L^* values with the treatment time and voltages (Table 4.12). After the plasma exposure, the increased L^* value tends towards the brightness level, while the a^* values signify the red colour of the pineapple pulp. Treatment time significantly affected the L^* value of pulp ($p<0.05$). However, no significant change was observed at 15 kV even after the pineapple pulp was exposed longer

to plasma treatment. No significant changes had also been observed on a* values, though the values were slightly changed. The slight changes in the *a** values may lead to the stabilization of the anthocyanin in pineapple pulp. The stabilized red hues might be due to the inactivation of the pineapple pulp enzymes, which may prevent oxidation in juices and reduce colour loss. Similar observations can also be seen in the work reported by Ozen and Singh (2020). Meanwhile, the *b** values significantly change with the treatment combinations. The increasing *b** values after the CP treatment led to a yellowish color of the pulp. Increased *L** values might be due to increasing phenolic compounds upon exposure to cold plasma. A decrease in *b** values observed in some treatment conditions could be linked to the breakdown of some bioactive compounds that promote the production of yellow-brown colour. Increasing processing time also showed changes in the **Δ**E ($p<0.05$) (Table 4.13). The significant changes in the **Δ**E value might be due to the changes in the *L** values of the pulp, as seen in Table 4.12. The experimental conditions showed negligible changes in the colour value, signifying that the plasma exposure may preserve the color of the treated pulp after the plasma exposure. Cold plasma-treated grape juice showed a similar color change to that reported by Pankaj et al. (2017). More prolonged exposure of DBD plasma to apple juice resulted in high color variations (Dasan & Boyaci, 2018). Both treatment parameters had a significant role in the Chroma *(C*)* of the cold plasma-treated pineapple pulp at 15-25 kV ($p<0.05$). Plasma exposure denatures the structural changes in the phenolic compounds, resulting in the increased Chroma *(C*)* of the cold plasma-treated pineapple pulp. Pineapple pulp showed insignificant changes in the Hue *(H*)* values even after longer exposure to plasma treatments. Maintaining the original hue indicated minimal nutrient degradation during processing. Significant changes might be observed for some conditions due to the loss of bioactive compounds.

Table 4.9 Selection criteria for the process standardization

Name	Goal	Lower Limit	Upper Limit	Lower Weight	Upper Weight	Importance
A: Voltage	is in range	15	25	1	1	3
B: Treatment time	is in range	3	15	1	1	3
C: Sample depth	is in range	2	4	1	1	3
PPO	minimize	0.134	0.819	1	1	3
POD	minimize	0.217	0.922	1	1	3

Table 4.10 Solutions of the process standardization of PPO and POD

Number	Voltage	Treatment time	Sample depth	PPO	POD	Desirability	
1	**25**	**15**	**2**	**0.153**	**0.237**	**0.957**	**Selected**

Table 4.11 Validation of the standardized combination

Parameters	Unit	Predicted	Actual	% Error
PPO		**0.153**	**0.157**	2.61
POD		**0.237**	**0.231**	2.59

4.5 Model validation

In the present study, the performance of the various fitted models was validated by determining the values of the Accuracy factor (A_f) and Bias factor (B_f) (Tables 4.14 and 4.15). The A_f values for the Weibull model and the Two-fraction model, Peleg's model, and the Logistic models were varied from (1.001-1.016), (1.000-1.022), (1.000-1.013), and (1.000-1.029), respectively. The Weibull model and Peleg showed almost similar patterns of enzyme inactivation in pineapple pulp with the highest accuracy. In contrast, the Two-fraction and Logistic models also showed a similar pattern. However, these models slightly deviate from the observation value, as shown in the values (Table 4.14). The A_f values for the first-order kinetic model varied from 1.001 to 1.045, which indicates that the value is comparatively higher than the other fitted models. The higher A_f value of the first-order model implies a variation in predicted models from the observation values, which pertains to unsatisfactory models for describing their inactivation behavior. The B_f value of the two-fraction and Peleg models was very close to 1, which suggests the reliability of these models for the present investigations. The B_f value for other models (First order, Weibull, and Logistic) was also good. However, due to the slight variation in predictions, it indicated the limiting nature of the predicted models over experimental observations. Similar results had also been obtained from the studies of enzymes in sugarcane juice (Panigrahi et al., 2021).

Table 4.12 Color value of cold plasma-treated Pineapple pulp

	L*			***a****			***b****		
Treatment time, min	**15 kV**	**20 kV**	**25 kV**	**15 kV**	**20 kV**	**25 kV**	**15 kV**	**20 kV**	**25 kV**
0	37.99±0.50^{a}	37.99±0.05^{d}	37.99±0.05^{a}	-1.70±0.01^{a}	-1.70±0.03^{a}	-1.70±0.04^{a}	7.59±0.02^{a}	7.59±0.07^{b}	7.59±0.01^{abc}
3	31.79±0.20^{c}	44.54±2.55^{bc}	32.46±0.43^{bc}	-1.94±0.22^{a}	-2.31±0.20^{a}	-2.11±0.12^{a}	6.96±0.17^{a}	15.98±1.50^{b}	6.97±0.43^{bc}
6	32.97±1.01^{c}	45.52±0.58^{b}	33.67±0.91^{b}	-2.01±0.12^{a}	-2.26±0.22^{a}	-2.07±0.08^{a}	7.66±0.44^{a}	15.54±2.37^{b}	7.28±0.14^{abc}
9	31.60±0.24^{c}	40.78±1.79^{cd}	30.10±0.91^{d}	-1.90±0.11^{a}	-2.88±0.11^{a}	-2.05±0.11^{a}	7.29±0.27^{a}	24.06±2.92^{ab}	6.89±0.18^{c}
12	35.57±0.90^{b}	46.04±1.07^{b}	30.76±0.47^{cd}	-1.90±0.06^{a}	-2.43±0.20^{a}	-1.87±0.06^{a}	5.88±0.40^{b}	30.15±5.04^{a}	7.55±0.15^{ab}
15	39.05±0.18^{a}	52.76±1.97^{a}	30.65±0.61^{d}	-1.77±0.17^{a}	-2.80±1.03^{a}	-2.00±0.13^{a}	6.94±0.16^{a}	31.42±8.19^{a}	7.89±0.11^{a}

**mean± SD that do not share a letter are significantly different with the treatment time

Table 4.13 Total Color change, chroma, and hue of cold plasma-treated Pineapple pulp

		ΔE			**C***			**H***	
Treatment time, min	**15 kV**	**20 kV**	**25 kV**	**15 kV**	**20 kV**	**25 kV**	**15 kV**	**20 kV**	**25 kV**
0	-	-	-	10.40±0.05^{bc}	2.48±0.02^{a}	10.46±0.15^{c}	-0.17±0.01^{b}	-0.63±0.01^{a}	-0.18±0.03^{b}
3	7.22±0.22^{d}	3.67±0.28^{a}	6.22±0.17^{b}	9.47±0.29^{b}	4.64±0.60^{b}	9.46±0.43^{a}	-0.19±0.02^{b}	-0.44±0.03^{b}	-0.23±0.01^{a}
6	5.91±1.22^{c}	3.86±0.93^{a}	5.23±0.44^{a}	10.77±0.9^{c}	4.48±0.08^{b}	9.87±0.40^{ab}	-0.19±0.01^{b}	-0.45±0.03^{b}	-0.20±0.01^{ab}
9	7.42±0.38^{d}	5.07±0.96^{a}	8.57±0.49^{c}	9.93±.0.04^{bc}	6.74±0.37^{c}	9.72±0.01^{a}	-0.19±0.01^{b}	-0.37±0.01^{c}	-0.21±0.02^{ab}
12	3.74±0.23^{b}	7.34±0.16^{b}	8.04±0.13^{c}	7.74±0.87^{a}	8.09±0.18^{d}	10.25±0.16^{bc}	-0.22±0.03^{a}	-0.26±0.01^{d}	-0.18±0.01^{b}
15	1.70±0.06^{a}	9.47±1.96^{c}	8.17±0.07^{c}	9.38±0.11^{b}	8.33±1.00^{d}	11.01±0.07^{d}	-0.19±0.01^{b}	-0.25±0.02^{d}	-0.19±0.01^{b}

*mean± SD that do not share a letter are significantly different with the treatment time

4.6 AIC and BIC for model selection

AIC and BIC values were studied and reported in Tables 4.16 and 4.17 to compare the fitted models and select the best model suited for the enzyme inactivation in pineapple pulp. The lowest AIC values were obtained by the Peleg model, followed by the two-fraction, Logistic, and first-order kinetic models. Illera et al. (2019) also revealed that the two-fraction model was best for the inactivation in cloudy apple juice by CP treatment. BIC of Logistic and Peleg were found to be -0.009 to -6.039 and -0.059 to -7.706, respectively. All three models showed good prediction of the enzyme inactivation with the lowest AIC values. However, with the lowest value observed for the Peleg model, BIC showed a better prediction for describing the enzymes in cold plasma-treated pineapple pulp.

A similar pattern was also observed for all the models fitted for the POD enzyme inactivation. Panigrahi et al. (2021 reported that the Weibull model was selected for the enzyme study in ozone-treated sugarcane juice. The Weibull model was best fitted for the PPO kinetics in high-pressure treated sugarcane juice (Sreedevi et al., 2019). However, in the case of PEF-treated carrot juice, POD activity was reduced and showed better prediction with the first-order model than with the Fractional conversion and the Weibull model (Quintao et al., 2013).

4.7 Interrelation between the model kinetic parameters

The PCA biplot shown in Figure 4.7 represents the interrelation between the kinetic parameters of DBD-treated pineapple pulp. The first component 1 of the PCA biplot is shown on the x-axis, while the second component 2 is shown on the y-axis. The total variation of these two components is more than 99%, indicating the PCA method's suitability for correlating their interrelation. PCA biplot shown in Fig. 4.7 represents that the Weibull model parameter (b value), logistic parameters (a and Alogi), Peleg's parameter (k2Peleg), two fraction constants (Al and K1two and k2two) formed a single loop, which represents their strong correlation among themselves. However, the model coefficient predicted by Weibull (n), Peleg (k1Peleg), and the logistic model (T50) lied in a separate quadrant. They were positioned in opposite quadrants, implying their inverse relationship with the first loop. The coefficients in the first quadrant implied similar significance on the enzyme inactivation rate. The coefficients showed a significant impact on the rate of their inactivation. The same trend can also be seen in Tables 4.1-4.6. A slight deviation between the K_2 Peleg, K_{1two}, K_{2two}, and k predicted by model equations implied their strong relation among themselves. The detailed science behind their inactivation is described in section 4.1.

Table 4.14 Model Validation by A_f and B_f-value of PPO enzymes

Enzymes	Treatment (kV/cm)	First-order model		Weibull model		Two-fraction model		Peleg's model		Logistic model	
		A_f	B_f	A_f	B_f	A_f	B_f	A_f	B_f	A_f	B_f
PPO_2 mm depth	15	1.001	1.000	1.005	0.996	1.000	1.000	1.000	1.000	1.001	1.000
	20	1.000	1.000	1.002	0.998	1.000	1.000	1.000	1.000	1.000	1.000
	25	1.000	1.000	1.001	1.000	1.000	1.000	1.000	1.000	1.000	1.000
PPO_3 mm depth	15	1.001	0.999	1.004	0.996	1.000	1.000	1.000	1.000	1.000	1.000
	20	1.000	1.000	1.002	0.998	1.000	1.000	1.000	1.000	1.000	1.000
	25	1.000	1.000	1.001	0.999	1.000	1.000	1.000	1.000	1.000	1.000
PPO_4 mm depth	15	1.003	0.997	1.005	0.996	1.000	0.999	1.000	0.999	1.000	0.999
	20	1.003	0.997	1.004	0.996	1.000	0.999	1.000	0.999	1.016	0.984
	25	1.045	0.971	1.002	0.998	1.000	0.999	1.003	0.999	1.029	0.971

Table 4.15 Model Validation by A_f and B_f-value of POD enzymes

Enzymes	Treatment (kV/cm)	First-order model		Weibull model		Two-fraction model		Peleg's model		Logistic model	
		A_f	B_f	A_f	B_f	A_f	B_f	A_f	B_f	A_f	B_f
PPO_2 mm depth	15	1.001	1.000	1.002	0.999	1.000	1.000	1.000	1.000	1.001	1.000
	20	1.000	1.000	1.016	0.985	1.013	0.987	1.013	0.987	1.000	1.000
	25	1.009	0.991	1.007	0.994	1.009	0.992	1.008	0.992	1.001	1.000
PPO_3 mm depth	15	1.001	1.000	1.001	0.999	1.000	1.000	1.000	1.000	1.001	0.999
	20	1.000	1.000	1.015	0.985	1.013	0.987	1.013	0.987	1.000	1.000
	25	1.009	0.991	1.007	0.994	1.009	0.992	1.008	0.992	1.001	1.000
PPO_4 mm depth	15	1.005	0.995	1.001	0.999	1.010	0.990	1.000	0.999	1.001	0.999
	20	1.009	0.991	1.001	0.999	1.022	0.978	1.001	0.998	1.002	0.997
	25	1.007	0.993	1.002	0.998	1.000	0.999	1.003	0.996	1.008	0.991

Table 4.16 Model Validation by AIC and BIC-value of PPO enzymes

Enzymes	Treatment (kV/cm)	First-order model		Weibull model		Two-fraction model		Peleg's model		Logistic model	
		AIC	BIC	AIC	BIC	AIC	BIC	AIC	BIC	AIC	BIC
PPO_2 mm depth	15	-62.770	-5.744	-38.019	-6.020	-84.537	-4.206	-73.499	-7.331	-69.876	-5.495
	20	-78.923	-5.213	-47.467	-6.461	-92.946	-4.299	-98.722	-7.706	-86.066	-5.899
	25	-75.796	-5.811	-62.907	-7.021	-81.710	-4.054	-77.967	-7.448	-92.432	-6.039
PPO_3 mm depth	15	-59.072	-5.046	-34.321	-2.322	-84.839	-0.508	-69.801	-3.633	-66.178	-1.797
	20	-75.225	-5.515	-43.769	-2.763	-89.248	-0.601	-85.024	-4.008	-82.368	-2.201
	25	-62.098	-6.113	-59.209	-3.323	-78.012	-0.356	-74.269	-3.750	-88.734	-2.341
PPO_4 mm depth	15	-62.770	-5.744	-38.019	-6.020	-88.537	-4.206	-73.499	-7.331	-69.876	-5.495
	20	-78.923	-5.213	-47.467	-6.461	-72.946	-4.299	-88.722	-7.706	-86.066	-5.899
	25	-85.796	-5.811	-62.907	-7.021	-81.710	-4.054	-77.967	-7.448	-92.432	-6.039

Table 4.17 Model Validation by AIC and BIC-value of POD enzymes

Enzymes	Treatment (kV/cm)	First-order model		Weibull model		Two-fraction model		Peleg's model		Logistic model	
		AIC	BIC	AIC	BIC	AIC	BIC	AIC	BIC	AIC	BIC
PPO_2 mm depth	15	-57.837	-1.446	-43.027	0.797	-83.577	2.572	-55.837	0.346	-49.990	-2.983
	20	-85.717	-2.381	-39.392	0.945	-76.438	3.275	-70.102	-0.059	-92.802	-4.065
	25	-24.395	0.050	-39.403	0.945	-13.685	5.766	-60.379	0.208	-55.005	-3.144
PPO_3 mm depth	15	-61.516	-5.125	-46.706	-2.882	-77.256	-1.107	-59.516	-3.333	-53.669	-1.416
	20	-69.396	-6.060	-43.071	-2.734	-80.117	-0.404	-73.781	-3.738	-96.481	-2.498
	25	-28.074	-3.629	-43.082	-2.734	-17.364	2.087	-64.058	-3.471	-58.684	-1.577
PPO_4 mm depth	15	-32.232	-3.888	-45.988	-2.854	-19.230	1.945	-68.498	-3.597	-61.022	-1.648
	20	-28.219	-3.639	-47.086	-2.897	-10.123	2.759	-72.896	-3.715	-38.956	-0.850
	25	-27.494	-3.590	-46.398	-2.870	-96.194	-0.739	-94.574	-3.758	-23.530	-0.009

4.8 Effect of CP on physicochemical properties

4.8.1 TPC

TPC in pineapple pulp after the cold plasma treatment is shown in Table 4.18. It can be observed that there were significant changes in TPC with the treatment times. Compared to a control sample, 15 kV for 9 min exposure time showed the TPC increased by 7.06% at 2 mm sample depth. Lower voltage gradients and longer plasma exposure time enhanced the TPC content. However, the more exposure to voltage gradients, the slightly reduced the TPC value. Besides, initially, the TPC slightly decreases and then significantly increases after 6 min at 25 kV. The degradation of TPC at the beginning of the treatment might be due to the phenolic content's ability to scavenge free radicals.

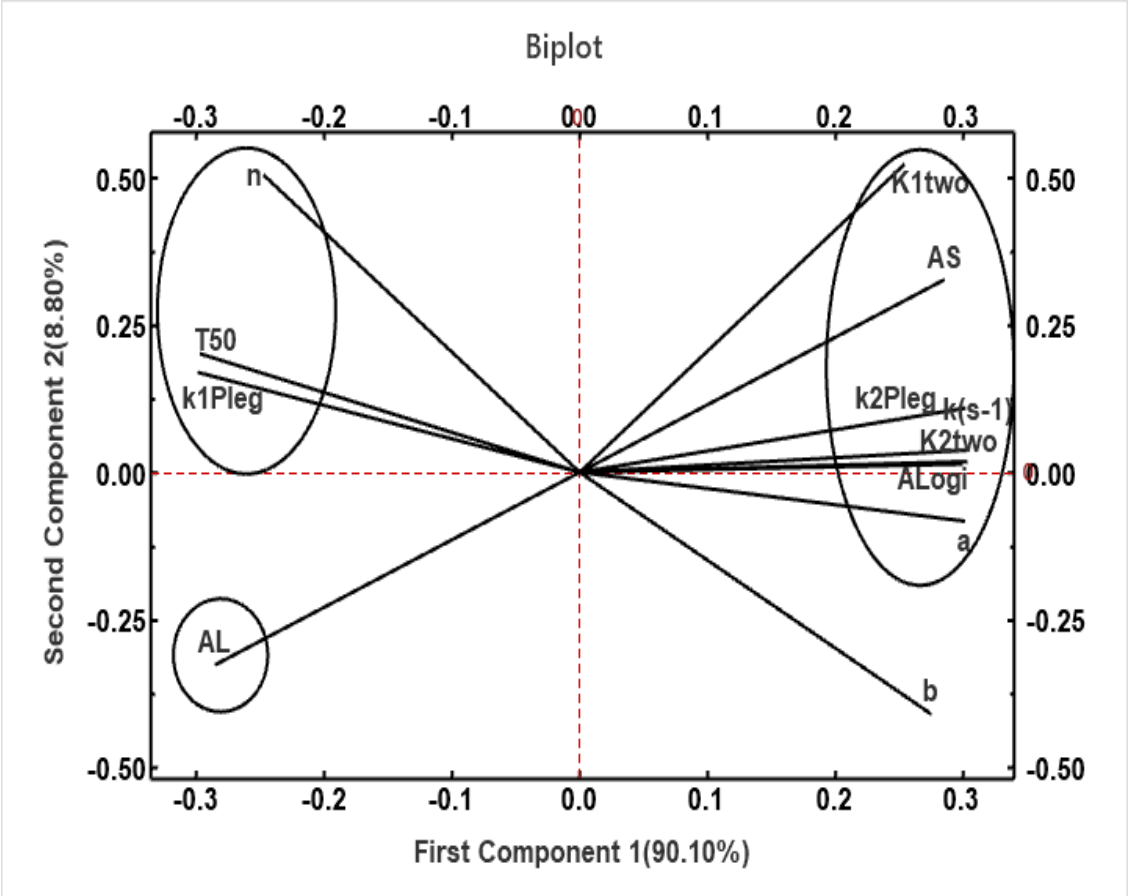

Figure 4. 7 PCA Biplot of kinetic parameters for cold plasma-treated pineapple pulp

The increased TPC observed after a specific treatment period may be due to the plasma-generated reactive species, which have enough energy to disrupt covalent bonds and cause several chemical processes that could break the cell membrane. According to Pankaj et al. (2017), treatment time negatively impacted the phenolic content in grape juice. Similar

observations were also observed in the orange and lettuce juice (Grzegorzewski et al., 2011; Almeida et al., 2015). The phenolic components in plant materials are usually connected with the polysaccharides in plant cell walls. Several chemical reactions are produced during plasma exposure, but plasma active species may destroy the phenolic cell wall matrix. This breakdown may be attributed to higher TPC release at longer exposure times. Initially, the TPC decreases and then increases after a treatment time of 6 min. According to Rodriguez et al. (2017), cold plasma treatment significantly improves the TPC content in apple juice. A similar observation was also obtained by Illera et al. (2019). Both investigations reveal an increase in phenolic content after cold plasma exposure, possibly due to the cell membrane disintegration of compounds. The generated plasma reactive species may cause the cell wall disintegration, thus enhancing the TPC value. Phenolics may rise due to phenolics being extracted from the cell due to cell membrane breakdown. The depolymerization of tannins can also increase the extraction of phenolics. When plants are subjected to plasma-reactive species, phenolic levels can rise due to the activation of cell defense mechanisms. The decrease in phenolics might be due to the oxidation of the compounds upon exposure to plasma (Fernandes et al., 2021).

4.8.2 Effect of CP on DPPH

The DPPH inhibition of plasma-treated pineapple pulp is shown in Table 4.19. The DPPH inhibition of plasma-treated pineapple pulp increased. DPPH inhibition was maximum at 3 min of treatment, while a drastic decreasing trend can be observed afterward. Decreased DPPH values were observed after the treatment time of 9 min. However, the treatment time showed insignificant changes in the DPPH values at 15 and 25 kV ($p>0.05$). The decreasing trend of DPPH in pineapple pulp might be due to the sample's ability to scavenge the free radicals generated by the plasma treatment. The decreasing DPPH radical signifies the decreasing total phenolic content observed in section 4.8. In the present investigations, the treatment time and voltage had insignificant effects on the DPPH values ($p>0.05$). However, slight significant changes can be observed in the treatment values at 4 mm sample depth. According to Pankaj et al. (2017), grape juice's antioxidant and DPPH free radical scavenging properties decreased as treatment duration increased. However, additional information is necessary to examine the chemical reactions between the plasma reactive species and the antioxidant in pineapple pulp.

4.8.3 pH and conductivity of Pineapple Pulp

pH of the cold plasma-treated pineapple pulp with varying voltages of (15-30 kV) and treatment time from 3-15 min has been presented in Table 4.20. From the table, it can be observed that the pH values change with the treatment combinations. Treatment time showed significant changes in the pH values when the samples were treated under 2 and 3 mm sample depths.

Table 4.18 Effect of Cold plasma treatment on the TPC of pineapple pulp

Treatment time(min)	TPC (g GAE / L juice)		
	15 kV	20 kV	25 kV
Fresh	5.93 ±0.20^{abAB}	6.58±0.10^{cB}	5.55±0.30^{bA}
CP_3_2mm	5.808±0.12^{aC}	4.284±0.07^{bA}	5.171±0.132^{abB}
CP_6_2mm	5.774±0.15^{aB}	4.388±0.03^{bA}	4.608±0.09^{aA}
CP_9_2mm	6.349±0.16^{bC}	4.400± 0.05^{bA}	5.121±0.14^{abB}
CP_12_2mm	6.099±0.07^{abC}	4.221±0.06^{bA}	5.454±0.25^{bB}
CP_15_2mm	5.953±0.133^{abC}	3.050±0.07^{aA}	4.854±0.379^{abB}
Fresh	5.93 ±0.20^{abAB}	6.58±0.10^{cB}	5.55±0.30^{cA}
CP_3_3mm	5.765±0.07^{aB}	4.260±0.04^{bA}	5.094±0.06^{abcB}
CP_6_3mm	5.731±0.10^{aB}	4.365±0.01^{bA}	4.531±0.01^{aA}
CP_9_3mm	6.306±0.12^{bC}	4.377± 0.03^{bA}	5.044±0.07^{abcB}
CP_12_3mm	6.056±0.022^{abC}	4.198±0.04^{bA}	5.377±0.17^{bcB}
CP_15_3mm	5.910±0.09^{abC}	3.027±0.04^{aA}	4.777±0.302^{abB}
Fresh	5.93 ±0.20^{abAB}	6.58±0.10^{cB}	5.55±0.30^{cA}
CP_3_4mm	5.71±0.05^{aC}	4.21±0.02^{bA}	5.04±0.04^{abcB}
CP_6_4mm	5.68±0.12^{aB}	4.31±0.03^{bA}	4.48±0.03^{aA}
CP_9_4mm	6.26±0.10^{bC}	4.33± 0.01^{bA}	4.99±0.05^{abcB}
CP_12_4mm	6.01±0.04^{abC}	4.15±0.02^{bA}	5.33±0.19^{bcB}
CP_15_4mm	5.86±0.07^{abC}	2.98±0.02^{aA}	4.74±0.28^{abB}

**mean± SD that do not share small letters are significantly different with the treatment time, and capital letters are significantly different with the voltage

Table 4.19 DPPH free radical scavenging activity of cold plasma-treated pineapple pulp

Treatment time(min)	DPPH free radical scavenging activity (%)		
	15 kV	**20 kV**	**25 kV**
Fresh	66.67±6.86^{aA}	66.25±4.22^{bA}	74.96±0.96^{aA}
CP_3_2mm	75.325±3.32^{aA}	66.115±1.15^{bA}	64.357±3.15^{aA}
CP_6_2mm	68.677±0.48^{aA}	66.578±2.13^{bA}	50.915±0.36^{aA}
CP_9_2mm	67.723±0.36^{aA}	41.733± 0.23^{abA}	60.678±2.14^{aA}
CP_12_2mm	55.967±1.65^{aA}	44.024±0.25^{abA}	57.709±1.25^{aA}
CP_15_2mm	51.459±0.23^{aA}	26.323±0.35^{aA}	48.428±1.23^{aA}
Fresh	66.67±6.86^{aA}	66.25±4.22^{aA}	74.96±0.96^{aA}
CP_3_3mm	72.85±3.15^{aA}	72.85±2.14^{aA}	61.83±0.06^{aA}
CP_6_3mm	65.98±0.11^{aA}	65.98±3.15^{aA}	48.44±0.01^{aA}
CP_9_3mm	65.03±2.31^{aA}	65.03± 1.32^{aA}	58.15±0.07^{aA}
CP_12_3mm	53.04±1.65^{aA}	53.14±3.14^{aA}	55.18±0.17^{aA}
CP_15_3mm	48.63±0.85^{aA}	48.63±3.04^{aA}	45.90±0.302^{aA}
Fresh	66.67±6.86^{bcA}	66.25±4.22^{cA}	74.96±0.96^{dA}
CP_3_4mm	72.59±0.15^{cA}	63.49±4.59^{cA}	61.51±3.70^{cA}
CP_6_4mm	65.69±2.04^{abcB}	63.96±3.15^{cB}	48.07±2.58^{abA}
CP_9_4mm	64.73±4.89^{abcB}	39.00±0.06^{bA}	57.83±3.44^{bcB}
CP_12_4mm	53.02±5.66^{abA}	41.30±1.61^{bA}	54.87±3.73^{abcA}
CP_15_4mm	48.51±2.95^{aB}	24.08±2.29^{aA}	45.58±1.09^{aB}

**mean± SD that do not share small letters are significantly different with the treatment time, and capital letters are significantly different with the voltages

Cold plasma voltages also showed negligible effects from the pH value treated at a 4 mm depth. Pankaj et al. (2017) also observed insignificant pH changes in the cold plasma-treated white grape juice. Samples treated under lower treatment time showed significant changes in the conductivity values, as presented in Table 4.21. However, the values after the treatment time of 6 min showed insignificant changes ($p>0.05$). Samples treated at a depth of 4 mm showed insignificant changes in the conductivity values with the treatment times ($p>0.05$). Similar results were also obtained for the pH values.

Table 4.20 Effect of Cold plasma treatment on the pH of pineapple

Treatment time(min)	pH		
	15kV	**20kV**	**25kV**
Fresh	3.630 ± 0.01^{aA}	3.63 ± 0.04^{abA}	3.61 ± 0.04^{aA}
CP_3_2mm	3.745 ± 0.041^{bB}	3.755 ± 0.029^{cB}	3.41 ± 0.01^{bA}
CP_6_2mm	3.715 ± 0.015^{abA}	3.715 ± 0.017^{bcA}	3.445 ± 0.03^{cA}
CP_9_2mm	3.625 ± 0.027^{aB}	3.700 ± 0.013^{bcB}	3.235 ± 001^{cA}
CP_12_2mm	3.725 ± 0.013^{bC}	3.665 ± 0.011^{abcB}	3.145 ± 0.07^{cA}
CP_15_2mm	3.777 ± 0.015^{bC}	3.555 ± 0.031^{aB}	3.215 ± 0.01^{cA}
Fresh	3.63 ± 0.01^{aA}	3.63 ± 0.04^{abA}	3.61 ± 0.04^{aA}
CP_3_3mm	3.775 ± 0.035^{cA}	3.785 ± 0.049^{cA}	3.790 ± 0.057^{bA}
CP_6_3mm	3.745 ± 0.007^{bcA}	3.745 ± 0.025^{bcA}	3.805 ± 0.003^{bA}
CP_9_3mm	3.655 ± 0.040^{abA}	3.730 ± 0.014^{bcAB}	3.810 ± 0.014^{bB}
CP_12_3mm	3.755 ± 0.008^{cB}	3.685 ± 0.007^{abcA}	3.835 ± 0.005^{bC}
CP_15_3mm	3.800 ± 0.028^{cB}	3.585 ± 0.021^{aA}	3.765 ± 0.007^{bB}
Fresh	3.63 ± 0.01^{aA}	3.63 ± 0.04^{abA}	3.86 ± 0.01^{abA}
CP_3_4mm	3.79 ± 0.04^{cA}	3.80 ± 0.05^{cA}	3.79 ± 0.06^{cA}
CP_6_4mm	3.76 ± 0.01^{bcA}	3.76 ± 0.04^{cA}	3.74 ± 0.01^{cA}
CP_9_4mm	3.67 ± 0.04^{abA}	3.74 ± 0.01^{bcA}	3.73 ± 0.00^{bcA}
CP_12_4mm	3.76 ± 0.01^{cB}	3.71 ± 0.01^{abcA}	3.70 ± 0.01^{abcA}
CP_15_4mm	3.81 ± 0.02^{cB}	3.60 ± 0.02^{aA}	3.59 ± 0.01^{aA}

**mean± SD that do not share small letters are significantly different with the treatment time, and capital letters are significantly different with the voltages

Cold plasma voltages showed changes in the conductivity values. The reactions of the sample's constituents with the reactive species produced during plasma exposure cause these modifications. Pankaj et al. (2017) also obtained an increased conductivity value for plasma-treated grape juice. Additionally, their research revealed that the increased conductivity value may contribute to the solubilization of the reactive gas species. The generation of the species and their reactions, which might affect the original values of the constituents, is explained in detail in section 4.1.

Table 4.21 Effect of Cold plasma treatment on the conductivity of pineapple pulp

Treatment time(min)	Conductivity		
	15kV	**20kV**	**25kV**
Fresh	2.700 ± 0.197^{bA}	2.660 ± 0.127^{aA}	4.195 ± 0.021^{aB}
CP_3_2mm	2.108 ± 0.007^{aA}	3.358 ± 0.035^{bB}	4.484 ± 0.056^{aC}
CP_6_2mm	5.803 ± 0.028^{cB}	4.403 ± 0.084^{cA}	6.019 ± 0.219^{bB}
CP_9_2mm	6.258 ± 0.021^{dB}	4.543 ± 0.014^{cA}	6.309 ± 0.063^{bB}
CP_12_2mm	6.298 ± 0.035^{dB}	5.298 ± 0.049^{dA}	6.219 ± 0.021^{bB}
CP_15_2mm	6.383 ± 0.042^{dB}	5.793 ± 0.169^{eA}	6.289 ± 0.021^{bB}
Fresh	2.700 ± 0.197^{bA}	2.660 ± 0.127^{aA}	4.195 ± 0.021^{aB}
CP_3_3mm	2.065 ± 0.007^{aA}	3.315 ± 0.035^{bB}	4.483 ± 0.056^{aC}
CP_6_3mm	5.760 ± 0.028^{cB}	4.360 ± 0.084^{cA}	6.018 ± 0.219^{bB}
CP_9_3mm	6.215 ± 0.021^{dB}	4.500 ± 0.014^{cA}	6.308 ± 0.063^{bB}
CP_12_3mm	6.255 ± 0.035^{dB}	5.255 ± 0.049^{dA}	6.218 ± 0.021^{bB}
CP_15_3mm	6.340 ± 0.072^{dB}	5.750 ± 0.196^{eA}	6.288 ± 0.020^{bB}
Fresh	2.700 ± 0.197^{bA}	2.660 ± 0.127^{aA}	4.195 ± 0.021^{aB}
CP_3_4mm	2.04 ± 0.01^{aA}	3.285 ± 0.035^{bB}	4.440 ± 0.056^{aC}
CP_6_4mm	5.73 ± 0.03^{cB}	4.330 ± 0.084^{cA}	5.975 ± 0.219^{bB}
CP_9_4mm	6.19 ± 0.02^{dB}	4.470 ± 0.014^{cA}	6.265 ± 0.063^{bB}
CP_12_4mm	6.23 ± 0.04^{dB}	5.225 ± 0.049^{dA}	6.175 ± 0.021^{bB}
CP_15_4mm	6.31 ± 0.03^{dB}	5.720 ± 0.169^{eA}	6.245 ± 0.023^{bB}

**mean± SD that do not share small letters are significantly different with the treatment time, and capital letters are significantly different with the voltages

4.9 Foaming properties

The pineapple pulp was subjected to Cold plasma treatment at 25 kV for 15 min. After the cold plasma treatment, the treated pineapple pulp was foamed with the varying SMP concentrations from 2-4 % (w/w) and WT from 60-120 s (3 levels). A full factorial design has been carried out, and a total of 9 experiments were obtained. After the foam's immediate preparation, the foaming properties, viz., foam expansion, foam density, and drainage volume, were estimated and detailed below.

4.9.1 Foam Expansion (FE)

The foam expansion of the cold plasma-treated pineapple pulp foam was found to be increased with the SMP concentrations ($p<0.05$). The foaming concentrations and whipping time positively affected the expansion volume, as presented in Table 4.22. The FE of the pineapple pulp foam significantly varied from 143.66 to 189.67% with the SMP concentrations. The increased expansion volume with SMP (%) addition might be due to the milk protein, i.e., casein, in skimmed milk powder (SMP). The protein in SMP promotes air-liquid incorporation at the interface of the produced foam. Protein gets denatured at the air-liquid interface during whipping, which interacts with other foaming agents to form a stable foam. In all SMP concentrations, it was observed that the expansion volume of the foam increased up to 90 seconds of WT; thereafter, the foam expansion volume slightly decreased, which might be due to the higher whipping time breaking the bubble structure, and thus the expansion volume of the foam decreased. However, the maximum expansion value was 189.67 at SMP-6% and WT for 90 s. The decrease in expansion volume after 90 s of whipping time was observed for all the treatment conditions in the present investigation. Asokapandian et al. (2016) also investigate a similar interpretation of the effect of whipping time on foaming. Whipping foam for longer results in the foam's destruction, as observed in the study by Lau and Dickinson (2005). However, the egg albumin used as a foaming agent positively affects the expansion volume and foam density (Azizpour et al., 2014). The increased foaming agent increased the foam expansion and reduced the foam density. The increased foaming volume could be due to the incorporation of air during whipping, which is entrapped at the air-water interface. Protein in SMP denatures during whipping, interacts with the interface, and holds the bubbles to produce stable foam for the foaming process. Khodifad & Kumar (2020) also revealed that methyl cellulose significantly affected foam formation.

4.9.2 Foam density (FD)

Foam density is the measure of the developed foam whipping properties. The more air is incorporated into foam volume, the lower the density (Bag et al., 2011). The experimental studies suggested that as the SMP and whipping time increased, the foam density decreased from (798-505.31 $kg.m^{-3}$) as reported in Table 4.22. Similar findings were obtained for all the combinations of foam. Foam expansion and foam density were inversely related to each other. Lower foam density implied more air was incorporated during whipping, resulting in higher foam expansion. Higher expansion volume and lower density are desirable criteria

for the best foaming process. The desirable foam density was obtained at SMP-6% and 60 s of WT. The addition of SMP concentration significantly decreased the foam density ($p<0.05$). Foam with a higher expansion volume produced the lighter, denser foam. Raharitsifa et al. (2006) found that foam density was inversely linked with the whipping time until it reached a minimum, suggesting that overbeating or excessive whipping may result in foam collapse. Bag et al. (2011) also reported that after an optimum whipping time value, no significant density changes were observed in the foaming.

4.9.3 Foam stability and drainage volume

Cold plasma treatment enhanced the stability of the pineapple pulp foam. Drainage volume measures the foam's stability and capacity to retain its air-water interface. The foam's minimum drainage volume was 1 mL, while the maximum was 5 mL (Table 4.22). The stability of the foam was found to be 94.75-99.00%. No significant changes were observed with the increased concentration of SMP from 2-6% at 60 s of WT, although there is a slight change in the values. The minimum drainage volume and foam stability desirable for the foam mat drying were 1 mL and 99%, respectively, at 6% SMP and 90 s of WT. The enhanced foam stability might be due to the higher surface activity of the surfactant (protein) in SMP, which reduces the foam’s surface tension. The carboxymethyl cellulose (CMC) added as a foam stabilizer also helped to stabilize the foam for longer, which led to lower drainage volume and greater stability. Carboxymethyl cellulose, or anionic cellulose ethers, is a cellulose-like compound usually dissolved in water to form colloidal solutions. The presence of hydroxyl and hydrophobic groups, which exhibit a high thickening efficacy, may cause the creation of colloidal solutions. It can increase the foam's consistency, resist the bubbles' structure from rupture, and develop a viscoelastic layer in the foam interface. The incorporation of CMC during foaming interacts with the foaming agent (protein) and produces a viscoelastic interfacial film around the foam lamella bubbles, stabilizing the foam and lowering the drainage volume. SMP concentrations of 2-6% at 60 s of whipping time showed no significant changes in DV in the present investigations. Lower drainage volume indicates good foam stability in that the foam can hold the air-liquid interface and stabilize the foam for a longer time, resulting in faster product drying. The higher drainage volume measures the lower air-liquid holding capacity of foam. The lower drainage volume and higher air-liquid holding capacity reflect the better stability of the foam (Lau & Dickinson, 2005).

Table 4.22 Foaming properties of cold plasma-treated pineapple pulp

Foaming conditions	WT (min)	Foam Expansion (FE) (%)	Foam density (FD) (kg/m^3)	FS (%)	DV (mL)
CP_SMP_2%	60 s	143.66±1.41^a	798±1.41^c	94.75±0.354^a	5.25±0.353^a
CP_SMP_4%		163.54±0.30^b	691±2.12^b	95±1.414^a	5±1.414^a
CP_SMP_6%		182±1.88^c	572±4.24^a	98±0.707^a	2±0.710^a
CP_SMP_2%	90 s	149.00±0.47^a	763.30±7.07^c	95.50±0.710^{ab}	3.50±0.707^{ab}
CP_SMP_4%		172.67±1.88^b	630.30±21.21^b	95.50±0.710^a	4.5±0.710^b
CP_SMP_6%		189.67±1.41^c	505.31±9.89^a	99.00±0.707^b	1±0.707^a
CP_SMP_2%	120 s	146±0.94^a	775.3±4.24^c	94.25±1.06^a	5±0.00^a
CP_SMP_4%		168±0.94^b	677.10±2.12^b	95.5±0.707^a	4.5±0.707^a
CP_SMP_6%		187.65±0.45^c	540.20±12.02^a	97±0.710^a	3±0.710^a

Superscripts with different letters are significant at $p<0.05$ with varying SMP at constant WT.

4.10 Drying characteristics of the foam

The pineapple pulp foam has been dried using a tray dryer at 60 ^oC. The loss in weight has been recorded every 30 minutes. The drying process continues until the desired moisture content reaches 0.06 g of moisture/g of dry solid. The MR versus time plots were fitted with the various mathematical models, and their model coefficients were estimated and presented in Table 4.23. The model coefficient shown in the table indicates how their coefficients change with the foaming concentrations. Page's model coefficient (k- and n) value slightly changes with the SMP (%) and whipping time. Page's coefficient (k-value) slightly increased, while the opposite trend can be observed in the n values. Page's model fits well with ($0.984> \left| R^2 \right| <0.999$) and RMSE <0.048. At the same time, the Henderson, Wang, and Singh model fits the data with ($0.921> \left| R^2 \right| <0.999$) and ($0.793> \left| R^2 \right| <0.998$), respectively. All the models were well fitted with all the experimental combinations, with good determination (R^2) and the lowest error/RMSE. The highest R^2 with the lowest RMSE obtained for Page's model showed a good prediction for explaining the drying behavior of foam. The Page's model coefficient n>1 in all the cases showed super diffusion phenomena. The moisture movement from the pulp sample might be due to this phenomenon occurring during drying. The value of the model coefficient (k-) for Page's and Henderson and Pabis models slightly changes; however, it showed no significant effect on the foaming concentration and whipping. The larger surface area of the bubble helped reduce moisture content, so the drying rate increased. Djaeni et al. (2015) reported that adding a foaming

agent (egg albumin) enlarged the foam's pore size, thus allowing for quicker product drying. Drying of tomato juice also showed similar behavior (egg albumin 10%, WT 5 min) (Kadam & Balasubramanian, 2011). The SMP, carboxymethyl cellulose, and pulp starch helped stabilize the foam for a long time without collapsing. Azizpour et al. (2014) successfully dried the shrimp powder using this technology.

4.11 Powder characteristics of the pineapple powder sample

SMP concentrations had a positive impact on the powder properties. The higher bulk density at higher SMP might be due to SMP's higher molecular weight protein. All the powder properties were significantly increased with the increasing SMP concentrations from (2-6%) at 60 s, 90 s, and 120 s of WT. The Carr index and Hausner ratio values of less than 12% and 1.20 indicated their good flow ability and low powder cohesiveness. Bulk density is an important index affecting powdered food's reconstitution, packaging, transportation, and storage.

The quality of particulates can be better predicted by knowing the bulk and particle densities (Seerangurayar et al., 2017). SMP concentration positively influenced the bulk density of pineapple powder ($p \leq 0.05$) (Table 4.24). The bulk density of the powder was increased with the increased SMP concentrations compared to the whipping time. As seen from Table 4.24, increased bulk density might be due to SMP added to pineapple foam, producing thicker foam that may affect the porous structure and thus enhance the density. Higher molecular weight proteins in SMP and adding CMC and starch during whipping affected the bulk density. Shaari et al. (2017) also investigated similar behavior. The powder produced with SMP-6% had a significantly higher tapped density for all the whipping time combinations than SMP-2% and SMP-4% (Table 4.24). The increase in SMP concentrations produces more lumps; therefore, the particles stick together, limiting the powder flow during tapping. Tapped density for all the whipping time combinations of the powder was significantly ($p<0.05$) higher than the bulk density. Higher tapped density might be due to the tapping operation during the experiment, allowing the smaller particles to be tapped and achieving a dense packing state. A similar pattern of observation could also be seen in the studies performed by Mitra et al. (2017).

Table 4.23 Thin Layer Drying Models of Foam Mat Dried Pineapple Pulp

Model	SMP (%)	WT (s)	K	n	a	b(×10^{-5})	R^2	RMSE
Page	2	60	0.0002	1.679			0.994	0.028
	2	90	0.003	1.257			0.996	0.022
	2	120	0.006	1.170			0.989	0.034
	4	60	0.003	1.335			0.996	0.020
	4	90	0.008	1.167			0.986	0.039
	4	120	0.0001	1.891			0.984	0.048
	6	60	0.006	1.218			0.998	0.128
	6	90	0.002	1.486			0.997	0.017
	6	120	0.0208	1.004			0.999	0.016
Henderson and Pabis	2	60	0.008		1.105		0.951	0.083
	2	90	0.010		1.044		0.985	0.043
	2	120	0.013		1.016		0.985	0.041
	4	60	0.015		1.037		0.986	0.040
	4	90	0.017		1.017		0.983	0.043
	4	120	0.007		1.119		0.921	0.108
	6	60	0.016		1.027		0.993	0.025
	6	90	0.018		1.044		0.981	0.047
	6	120	0.021		1.002		0.999	0.011
Wang and Singh	2	60			-0.005	0.64	0.988	0.042
	2	90			-0.006	1.21	0.998	0.013
	2	120			-0.008	1.57	0.967	0.061
	4	60			-0.009	1.73	0.943	0.081
	4	90			-0.009	1.96	0.924	0.092
	4	120			-0.004	1.98	0.977	0.058
	6	60			-0.008	1.54	0.902	0.100
	6	90			-0.009	1.86	0.906	0.103
	6	120			-0.009	**1.92**	**0.793**	**0.140**

Particle density indicates the mass of solid particles per unit volume, excluding the void space between the powder particles (Seerangurayar et al., 2017). The foaming concentrations significantly influenced particle densities of the dried powder. The powder produced with 6% SMP showed significantly higher particle density for all the whipping times than samples made with 2 and 4% SMP; a similar trend was observed in the bulk density. Particle density was found to be increased with the carrier agents (Bhusari et al., 2014). Seerangurayar et al. (2017) also demonstrated that the date powder developed from maltodextrin showed a particle density of 1.45-1.70 g/cm^3, more than that of powder made

with gum Arabic. The porosity of the powder sample is the void space between the powder particles (Bhusari et al., 2014). Porosity quantifies the amount of the total volume occupied by air and is related to bulk density (Seerangurayar et al., 2017). It is possible to verify from Table 4.24 that the porosity of powders with the SMP concentrations varied from 46.27 to 57.04%. Increased SMP concentrations create more void space in the intermolecular space between the particles.

Table 4.24 Physical and rehydration properties of foam dried pineapple powder

Sample	Bulk density (kg/m^3)	Tapped density (kg/m^3)	Particle density (kg/m^3)	Porosity (%)	Carr index (%)	Hausner ratio (-)	RR (-)
2% SMP-60s	478.18±6.17^a	555.33±7.23^a	1033.74±13.88^a	46.27±0.01^a	13.89±0.01^a	1.16±0.00^a	2.17±0.03^a
4% SMP-60s	502.75±1.48^b	593.54±5.17^b	1220.56±2.78^b	51.55±0.35^b	15.29±0.52^b	1.18±0.01^b	2.34±0.02^b
6% SMP-60 s	569.33±0.84^c	699.67±1.03^c	1572.38±4.06^c	55.50±0.07^c	18.63±0.01^c	1.22±0.02^c	2.33±0.02^b
2% SMP-90s	493.02±1.05^a	553.53±1.22^a	1056.57±2.20^a	47.61±0.01^a	10.81±0.01^a	1.12±0.00^a	2.16±0.03^a
4% SMP-90s	515.59±1.52^b	587.68±5.12^b	1239.21±2.82^b	52.79±0.34^b	12.26±0.54^b	1.14±0.01^b	2.33±0.02^b
6% SMP-90 s	583.86±0.86^c	692.77±1.02^c	1596.41±4.12^c	56.60±0.07^c	15.72±0.01^c	1.18±0.01^c	2.32±0.01^b
2% SMP-120s	503.653±1.07^a	553.425±1.23^a	1067.137±2.23^a	48.139±0.01^a	8.993±0.01^a	1.099±0.0001^a	2.190±0.03^a
4% SMP-120s	526.008±1.55^b	587.564±5.12^b	1251.604±2.85^b	53.055±0.34^b	10.473±0.55^b	1.117±0.01^b	2.358±0.02^b
6% SMP-120s	595.664±0.88^c	692.633±1.02^c	1612.377±4.17^c	57.043±0.07^c	14.000±0.0000 1^c	1.163±0.0001^c	2.349±0.01^b

An increase in SMP increased foam expansion due to the creation of several bubbles, as observed in Table 4.24. The porosity of spray-dried tamarind pulp increased from 43.8% to 77.6% with carrier agents (Bhusari et al., 2014). The rehydration ratio was between 2.16 and 2.36, and the addition of SMP enhanced the rehydration quality of the powder (Table 4.24). A high rehydration ratio is desirable for dried powdery samples for convenient mixes, including fruit juice powder. The addition of SMP significantly increased the CI and HR values ($p<0.05$) (Table 4.24). The low CI value indicated good powder flowability; the lowest CI was associated with the lowest SMP level of 2%. The Hausner ratio (HR) was between 1.16 and 1.18, which means the powder has a low and intermediate extent of cohesiveness.

4.12 Interrelation between/among rheological, foam parameters, and powder attributes

PCA analysis in the present investigations was carried out to develop an interrelation between independent variables and dependent functions. The plot shown in Fig. 4.8 represents the principal component 1 and principal component 2, which account for 92.10% and 7.90%, respectively. Total variation (>95%) implied their good prediction of the PCA in the present context.

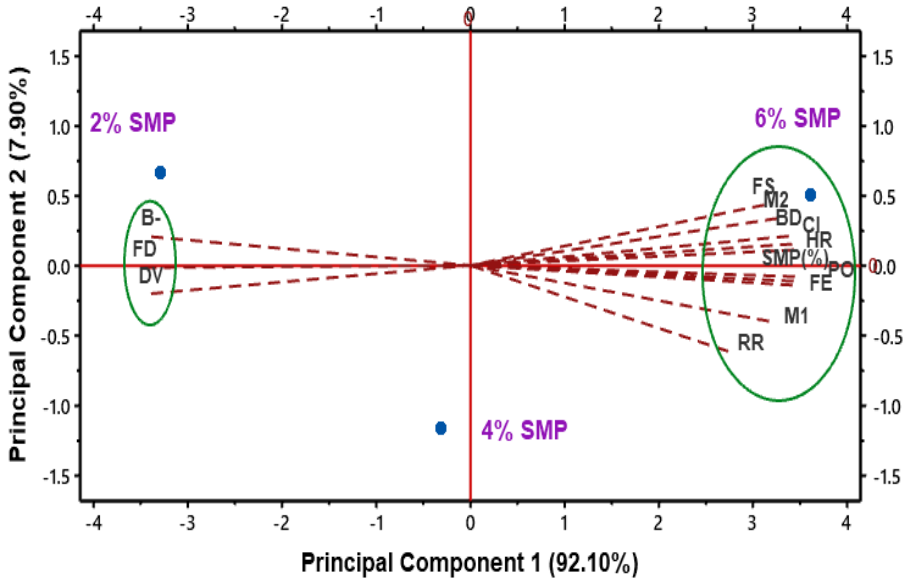

Figure 4.8 Principal component analysis (PCA) biplot among independent variable (SMP concentration) and dependent functions (foaming and powder properties)

The PCA biplot shown in Fig. 4.8 shows that the powder properties, such as HR, BD, PO, and RR, and foaming properties (FE and FS), form one group. The smallest angle between these parameters showed their strong correlation among themselves (Fig. 4.8). However, the parameters of the group mentioned above were negatively linked to DV and FD values due to their positions in different quadrants. The parameters B-, FD, and DV lie in the 2nd and 3rd quadrants and form one group. The experimental studies also obtained similar results, as shown in Table 4.22.

4.12.1 PCA interpretation

The coefficients of the correlation matrix showed the relationship between SMP and foaming properties (physical) and powder properties, as presented in Table 4.25. The correlation coefficients of foaming properties (FE and FS) with SMP were 0.287 and 0.261,

respectively, indicating that they were positively correlated ($p<0.01$) with SMP. However, the foaming properties of DV and B values negatively correlated with SMP. The addition of SMP increased the surrounding liquid's viscosity, preventing the developed foam's drainage-induced instability and structural breakdown. High SMP concentrations markedly increased the viscosity, significantly enhancing the physical properties of the foam. The DV value was inversely related to SMP while positively correlated with FS.

4.13 Chemical properties of powder

The powder had a pH of 3.57-5.29 and a moisture content of 6.25%. The pH of the powder was significantly increased with the increasing SMP concentrations ($p<0.05$) (Table 4.26). The low pH characteristics of the powder are responsible for product safety and shelf-life enhancement. SMP concentrations also showed a positive impact on the protein and ash content of the powder. Protein and ash content of the powder properties were obtained in the 0.436-1.432 mg/100g range and 10.212-13.513%, respectively. Adding skimmed milk powder to the sample during foaming significantly enhanced the protein content.

4.14 Standardization of the foaming process

The statistical parameters for the responses of foam expansion, foam density, foam stability, and drainage volume are shown in Table 4.27.

The model was significant for the foaming process with an F-value of 456.63 and $p<0.05$. SMP concentrations showed a significant effect on the foaming process. Whipping time (WT) also showed a similar impact on foaming. However, the p-value was lower at SMP than WT, which showed a more significant effect of SMP on foaming $p<0.05$. Foam expansion is one of the critical parameters for a successful foaming process. Higher expansion volume indicates more air in the pulp during whipping. Similar observations were also obtained in our investigations, as presented in Table 4.21 and explained in Section 4.11. Foam density model parameter F-198.19 and $p<0.05$ indicate the significance of the model. Foam density is the reverse of the foam expansion. Both the SMP concentrations and WT had a significant effect on foam density. Model parameter of foam stability and drainage volume also signifies their considerable impact on the foaming process. Higher stability and lower foam drainage volume are desirable for a good foaming process.

Table 4.25 Lower half correlation matrix among foaming and powder properties of foam

Variable	SMP	FE	FD	FS	DV	B-	M1	M2	BD	PO	CI	HR	RR
SMP	0.288												
FE	0.287	-0.111											
FD	-0.289	-0.016	-0.2										
FS	0.261	0.425	0.195	-0.087									
DV	-0.283	-0.198	-0.26	0.538	0.193								
B-	-0.283	0.201	0.016	-0.01	0.46	-0.316							
M1	0.265	-0.392	-0.26	-0.159	0.127	-0.213	-0.367						
M2	0.272	0.33	-0.16	-0.138	0.022	0.138	0.342	-0.28					
BD	0.283	0.205	-0.05	0.455	0.009	-0.569	-0.173	-0.078	0.255				
PO	0.286	-0.139	0.37	0.066	0.076	0.136	0.205	0.181	-0.168	0.38			
CI	0.286	0.15	-0.07	-0.174	-0.209	0.19	-0.172	0.029	-0.008	0.104	-0.789		
HR	0.287	0.109	-0.69	-0.121	0.017	0.106	-0.051	0.214	0.192	0.098	0.087	0.04	
RR	0.229	-0.603	0.027	-0.167	0.013	0	-0.127	0.477	0.409	-0.075	0.115	-0.104	-0.338

Table 4.26 Chemical properties of the pineapple pulp powder

Sample	pH	Protein (mg/100g)	Ash (%)	Moisture (db)
2% SMP	3.57±0.01[a]	0.436±0.031[a]	10.212±0.06[a]	6.25±0.05%
4% SMP	4.71±0.03[b]	0.812±0.013[b]	11.321±0.13[b]	
6% SMP	5.29±0.13[c]	1.432±0.016[c]	12.513±0.21[c]	

Table 4.27 Statistical analysis of the table for responses to foam expansion, foam density, foam stability, and drainage volume

Responses	Foam expansion		Foam density		Foam stability		Drainage volume	
Source	**F-value**	**p-value**	**F-value**	**p-value**	**F-value**	**p-value**	**F-value**	**p-value**
Model	456.63	<0.0001	198.19	<0.0001	27.00	0.0010	34.14	0.0005
A-SMP	883.43	<0.0001	376.88	<0.0001	27.00	0.0010	34.14	0.0005
B-WT	29.82	0.0039	19.50	0.0087				
R^2	0.9978		0.9950		0.9000		0.9192	
Adjusted R^2	0.9956		0.9900		0.8667		0.8923	

The addition of SMP concentration significantly enhanced the stability and reduced the drainage volume, as shown in Table 4.21. The criteria selected for standardizing the drying process are presented in Table 4.28. The foaming process was standardized by choosing the foam density, stability, and drainage volume as minimum, maximum, and minimum, respectively, giving the importance of 3. Based on the selection criteria, SMP-6% and WT-120s were found to be optimum for the foaming process, fulfilling all the desirable criteria as shown in Table 4.29. The validation of the standardized condition was carried out by conducting the experiments under optimum conditions. The closeness of the values can be interpreted for validation of the process, as shown in Table 4.30. From Table 4.27, we can see that SMP affected the foaming process more than WT. Hence, the foaming was prepared by varying the SMP concentrations from 2-6% at WT-120 s to carry out the studies of objective 3.

Table 4.28 Criteria for standardization of the foaming process

Name	Goal	Limit		Weightage		Importance
		Lower	Upper	Lower	Upper	
A: SMP	is in range	2	6	1	1	3
B: WT	is in range	60	120	1	1	3
Foam expansion	is in range	143.66	189.67	1	1	3
Foam density	minimize	505	798	1	1	3
Foam stability	maximize	95	99	1	1	3
Drainage volume	minimize	1	5	1	1	3

Table 4.29 Solutions of foaming standardization

Number	SMP	WT	Foam expansion	Foam density	Foam stability	Drainage volume	Desirability	
1	**6**	**120**	**186.747**	**541.778**	**98.000**	**1.333**	**0.844**	**Selected**

Table 4.30 Validation of the standardized combination

Parameters	Unit	Actual	Predicted	% deviation
SMP	%	6	6	
WT	min	2	2	
Foam expansion	%	**186.747**	190	1.74
Foam density	$Kg\text{-}m^{-3}$	541.778	560	3.36
Foam stability	%	98	99	1.02
Drainage volume	mL	1.333	1.300	2.31

4.15 Rheological characterization of foam

Rheological study of emulsion-based food products is important in the food industry, as it helps characterize and control the texture, mouthfeel, and stability of products such as ice cream, salad dressings, and beverages.

In this context, understanding the time-dependent, steady-state, and dynamic rheological properties of pineapple pulp foam directly impacts industrial food processing. Enhanced foam stability and viscoelasticity at higher SMP levels can improve texture and shelf stability in aerated products such as foamed beverages, desserts, and foam mat dried

powders. The rheological models applied here can be used to predict processing behavior during pumping, mixing, or drying operations, aiding in equipment design and process optimization. Moreover, the thixotropic behavior suggests that shear conditions during processing must be carefully controlled to prevent premature foam collapse, ensuring consistent product quality in large-scale manufacturing.

4.15.1 Time-dependent flow characteristics of foam

Non-Newtonian fluid foods are time-dependent and usually show a time-dependent shear-thinning property. The shear stress required for these fluids to flow depends on the shear rate and shearing time (Bhattacharya et al., 1992). The Weltman model parameters (A_W and B_W) of the pineapple pulp foam increased with an increase in shear-rate (1-50 s^{-1}) (Table 4.31). The initial stress (A_w), an indication of the force required to initiate flow, increased with increasing shear rate and SMP concentration, which is due to the stability of the foam. The proteins in SMP (such as casein and whey) acted as the surface-active agents. Due to high surface activity resulting in stable foam, they tended to get adsorbed rapidly at the air-water interface. The B_W values indicated the changes in the extent of time-dependent shear-thinning behavior. The change in B_W from 3.65-12.58 $Pa \cdot s^{-1}$ and 1.130-7.422 for untreated and cold plasma-treated samples with shear-rate (1-50 s^{-1}) might be attributed to the time-dependent shear-thinning behavior of foam. The proteins in SMP are amphiphilic, meaning they are adsorbed to hydrophobic surfaces. Thus, they reduced the interfacial stress in aqueous foam by developing viscoelastic interfacial film bubbles, which could stabilize the foam. However, thinning the film between adjacent bubbles resulted in the foam's collapse as the shear rate increased. The overall result was the coalescence of bubbles that could ultimately exhibit the foam's structural breakdown. Pineapple jam also showed a similar pattern of time-dependent behavior, as reported by Basu et al. (2007). Hahn model parameter A_H showed more changes with shear rate than B_H values for both the treated and untreated samples, while the equilibrium stress (σ_e) was also increased for both samples with shear rates. The Weltman model parameters (A_W and B_W) and Hahn model parameters (A_H and B_H) are expected to behave similarly. However, in the results, it was not observed (Table 4.31); this might be due to an additional parameter, i.e., the Hahn model's equilibrium stress (σ_e). Bhattacharya (1999) also obtained a similar behavior for mango pulp. The present study's equilibrium stress (σ_e) varied from 1.01 to 4.13 Pa and 10.986 to 59.687 Pa for untreated and treated samples, respectively. The Figoni and Shoemaker model showed insignificant effects on the A_{FS} values (Table 4.31). The shear

stress and time of shearing of foamed pineapple pulp could fit well with Weltman as $|R^2|$= 0.796-0.995, and RMSE (0.448-3.681). The Hahn ($|R^2|$= 0.938-0.997 and RMSE=0.470-2.872) and Figoni and Shoemaker ($|R^2|$= 0.939-0.998 with RMSE of (0.221-2.871) models were also suitable. Similar patterns can also be seen for the CP-treated samples. However, among all the models, the Hahn, Figoni and Shoemaker model was the best fit to explain the time-dependent behavior of pineapple pulp foam, as the R^2-values were marginally better with the lowest RMSE. The best-fit model in the present study was thus based not only on the coefficient of determination (R^2) but also on the experimental error, like RMSE.

The sample plot (Figs 4.9 and 4.10) showed the decreasing shear stress with increased shearing time, indicating the time-dependent thixotropic characteristics of pineapple foam. Time-dependent characteristics or thinning with time reflected how the structure continuously broke down or rearranged as sheared; the phenomenon was prominent in the initial shearing phase. The experimental points were close to model-predicted lines to indicate the suitability of these three models to characterize the thixotropic flow behavior in the present context.

4.15.2 Steady rheology of foam

A steady rheology test of the pineapple pulp was conducted and presented in Fig. 4.11. Viscosity versus shear rate plots shown in Fig. 4.11 indicate the samples' flow behavior. Steady rheology of the samples with the increased SMP from 2-6% showed more viscosity than those with lower SMP. Viscosity for both samples was higher at higher SMP concentrations than at lower SMP concentrations. All the foaming samples showed similar behavior. The foam with the highest concentration produced a more concentrated foam, requiring higher stress (yield) to initiate its flow.

The experimental stress versus shear rate data obtained from the steady rheological experiments were fitted with various rheological models, viz., Power, Bingham plastic, and Casson models (Table 4.32). The Power model coefficient (k-) value increased with the increased SMP concentrations for both samples. At the same time, slight changes were observed in the n-value. Power model coefficients were well explained with the correlation coefficient R^2<0.992 and RMSE <1.486. Bingham plastic model coefficient ($\boldsymbol{\sigma_{B)}}$ increased with the increased SMP (%), which indicates that the added SMP produced thicker foam, and hence, it initially requires more stress to initiate its flow. Similar behavior can be seen

for all the experimental combinations. Casson model yield stress (σ_C) and Herschel Bulkley yield stress (σ_{HB}) also showed the inclined pattern with the SMP. The Casson model coefficient and the Bingham plastic coefficient implied a similar interpretation. The values for both the model coefficients were expected to be the same, but in prediction, it was not found; that might be due to the slight modification in the Casson model equation.

The correlation coefficient of R^2<0.857 and R^2<0.930 for the Bingham plastic and Casson models, respectively. Both models were well fitted with the experimental shear stress versus shear rate data, with a good coefficient of determination (R^2) and the lowest error/RMSE. However, based on the statistical parameter, the Power model was better fitted for the model prediction than the Casson and Bingham Plastic models.

4.15.3 Dynamic rheology of pineapple pulp foam

The dynamic rheological parameter (G', G") of the pineapple pulp foam is shown in Table 4.33. All the parameters at a 1 Hz frequency have been considered for better comparisons. Storage modulus values were significantly increased with the increasing SMP concentrations, while the opposite trend was observed for the loss modulus. Storage modulus exceeds the loss modulus, showing the viscoelastic behavior of the foam. In all foaming processes, the storage modulus values exceeded the loss modulus, indicating the foam's viscoelastic behavior. With increasing SMP (%), the viscoelastic behavior of the foam increased, which resulted in (G'>G"). A Similar investigation of the dynamic rheology was also obtained by Pereira et al. (2008). The protein in SMP is denatured and unfolds, which causes aggregation through hydrophobic interaction. This results in the formation of the gel-like network within the continuous phase of the foam system, consequently enhancing the solid elastic properties of the foam (G' over G"). The addition of SMP had a significant effect on the foaming process. Higher loss modules signify the fluid-like viscous behavior of the foam. The loss modulus of foam at a frequency of 1 Hz varied from 45.825-141.040 Pa (Table 4.33). The loss modulus of the pulped foam was decreased with the incorporation of SMP. Lower (G″) values observed in the samples with the increased SMP showed a more solid-like behavior than viscous behavior. The loss modules of the pineapple pulp foam may be interlinked with the drainage volume of the foam. Foam at lower SMP concentration had a higher loss modulus and a higher drainage volume. This problem might be due to the poor viscoelastic interfacial strength of the air-liquid interface, which could collapse the bubbles and increase the drainage volume.

Table 4.31 Suitability of different rheological models for pineapple pulp foam obtained with varying levels of skimmed milk powder (SMP) at different shear rates

SMP (%)	Shear- rate (s^{-1})	Experimental value		Weltman model			RMSE	Hahn model			RMSE	Figoni and Shoemaker model		RMSE
		σ_{max}(Pa)	σ_e (Pa)	A_w (Pa)	B_w(Pa.s^{-1})	R^2		A_H (Pa)	B_H (×10^{-3} Pa.s^{-1})	R^2		A_{FS} (s^{-1})	R^2	
Untreated pineapple pulp foam														
2	1	11.80±0.48	1.01±0.26	28.64±1.56	3.65±0.41	0.888	1.18	2.55±0.09	2±0.05	0.962	0.686	0.0017±0.0005	0.965	0.676
	10	18.10±0.13	1.525±0.79	35.45±1.19	4.16±0.13	0.952	0.846	2.75±0.02	2±0.07	0.985	0.470	0.0016±0.0007	0.987	0.459
	50	27.57±0.79	2.23±0.71	66.08±2.09	8.01±0.99	0.796	3.681	3.44±0.04	2±0.02	0.919	2.323	0.0010±0.0002	0.917	2.321
4	1	19.02±1.60	1.16±0.09	36.59±2.45	4.79±0.24	0.980	0.611	2.91±0.04	3±0.10	0.997	0.220	0.0019±0.003	0.998	0.221
	10	27.16±2.12	1.79±0.06	51.64±3.10	6.78±0.87	0.995	0.448	3.19±0.12	2±0.01	0.986	0.665	0.0021±0.0001	0.987	0.663
	50	41.29±2.05	3.85±1.62	78.86±2.27	10.31±0.03	0.993	0.577	3.68±0.003	3±0.01	0.991	0.656	0.0028±0.0001	0.993	0.652
6	1	22.86±1.66	2.18±0.13	41.42±2.38	4.92±0.07	0.977	0.683	2.96±0.12	2±0.08	0.977	0.676	0.0014±0.0008	0.979	0.674
	10	52.45±2.76	3.01±0.35	86.05±2.11	11.34±1.64	0.978	1.546	3.82±0.12	3±0.03	0.971	1.747	0.0035±0.0003	0.975	1.743
	50	59.22±1.59	4.13±0.33	96.75±0.57	12.58±0.16	0.986	1.230	3.84±0.07	3±0.07	0.938	2.872	0.0026±0.00008	0.939	2.871
Cold plasma-treated pineapple pulp foam														
2	1	4.440±2.13	10.986±1.53	15.965±7.814	1.130±0.471	0.771	0.875	2.073±0.270	3.3±0.01	0.858	0.297	3.3±0.01	0.857	0.291
	10	10.615±0.75	17.906±1.25	26.055±6.456	1.977±0.726	0.940	0.372	2.227±0.052	1.0±0.09	0.993	0.156	1.0±0.09	0.995	0.154
	50	17.713±1.05	24.560±1.23	37.200±1.018	3.730±1.657	0.961	0.615	2.642±0.365	4.0±0.3	0.974	0.561	4.0±0.3	0.975	0.559
4	1	6.932±1.23	9.708±0.23	15.475±0.389	1.449±0.024	0.981	0.185	1.652±0.010	2.0±0.01	0.988	0.145	2.0±0.01	0.991	0.141
	10	9.880±1.13	18.831±0.45	28.585±0.841	2.395±0.085	0.952	0.481	2.282±0.095	9.0±0.04	0.990	0.224	1.0±0.04	0.997	0.222
	50	21.364±1.43	37.400±1.05	51.610±0.707	3.977±0.180	0.995	0.256	2.644±0.048	1.7±0.001	0.979	0.528	1.7±0.001	0.986	0.580
6	1	7.123±1.25	19.885±1.02	32.565±0.389	3.377±0.130	0.992	0.270	2.488±0.040	1.7±0.01	0.990	0.313	1.7±0.01	0.993	0.311
	10	16.708±2.21	36.752±1.31	54.160±0.877	5.003±0.194	0.999	0.146	2.898±0.035	2.3±0.01	0.984	0.579	2.3±0.01	0.987	0.573
	50	28.835±2.05	59.687±2.51	84.270±7.538	7.422±0.725	0.995	0.451	3.312±0.082	2.6±0.2	0.975	1.054	2.6±0.2	0.976	1.051

Values are reported as mean ± standard deviation.

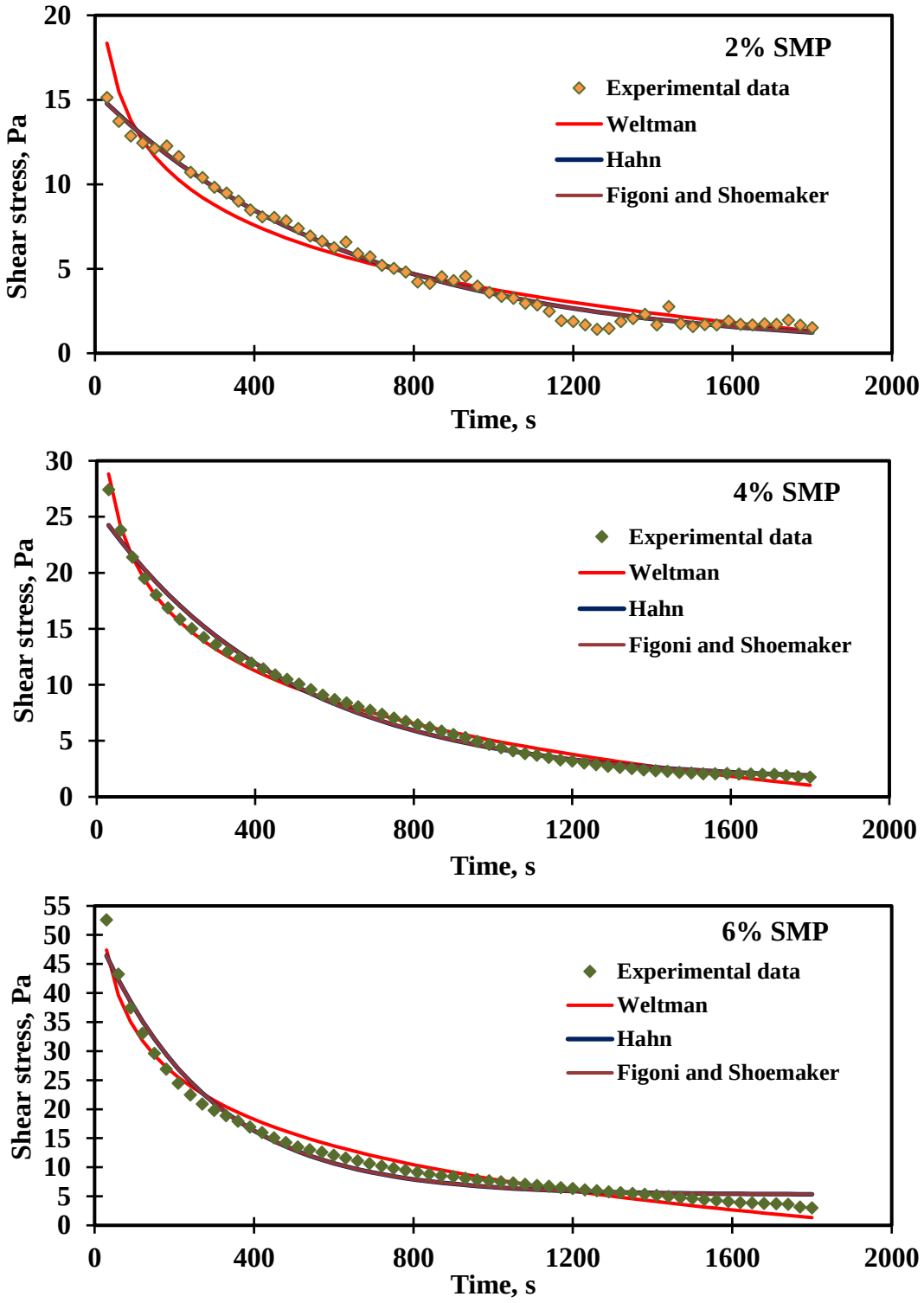

Figure 4.9 Sample shear stress versus time plot of experimental data and model fitting for pineapple pulp at a shear rate of 10 s^{-1} with 2%, 4%, and 6% skimmed milk powder (SMP) that were whipped for 2 min

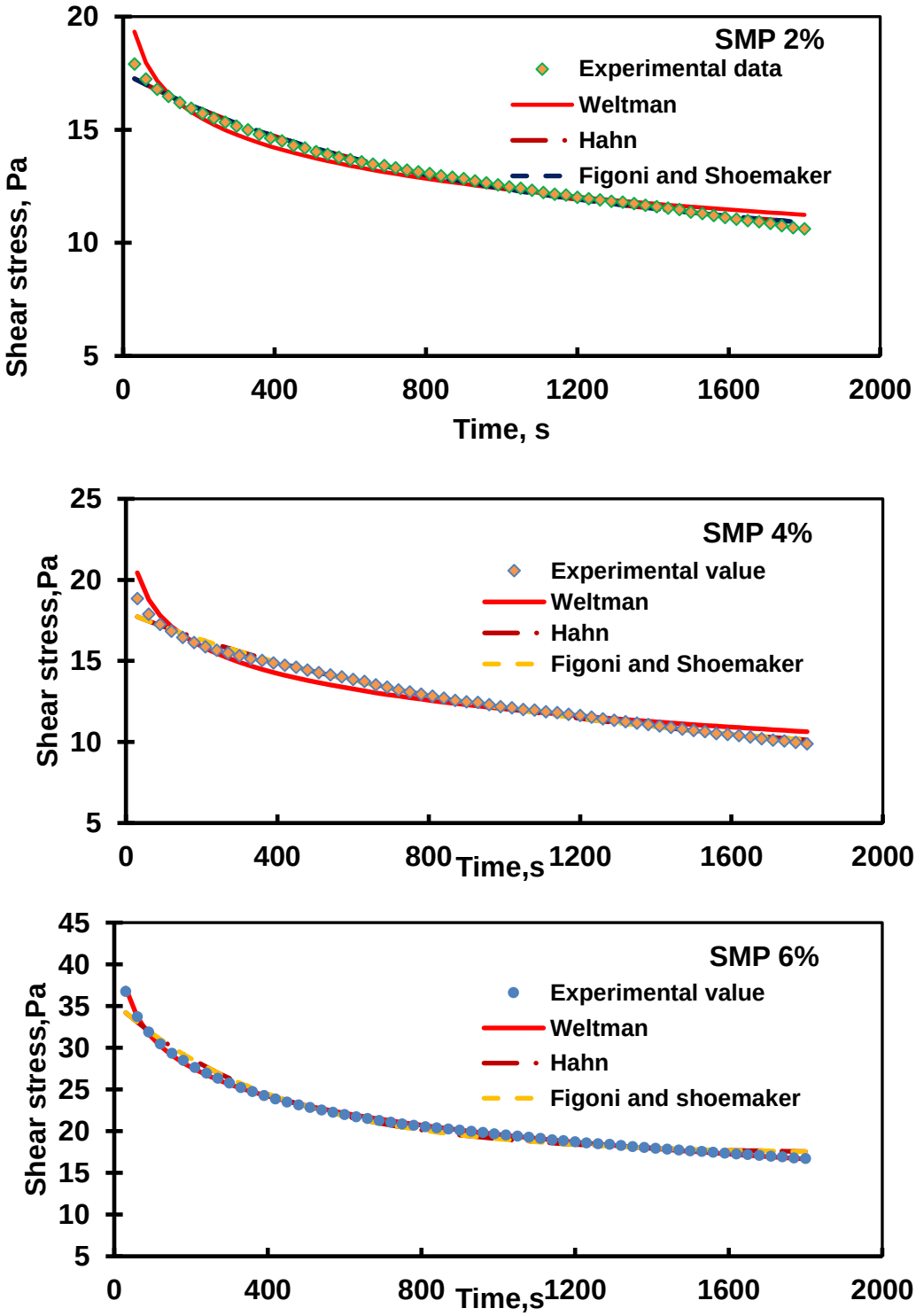

Figure 4.10 Sample shear stresses versus time plot of experimental data and model fitting for cold plasma-treated pineapple pulp at a shear rate of 10 s^{-1} with 2%, 4%, and 6% skimmed milk powder (SMP) that were whipped for 2 min

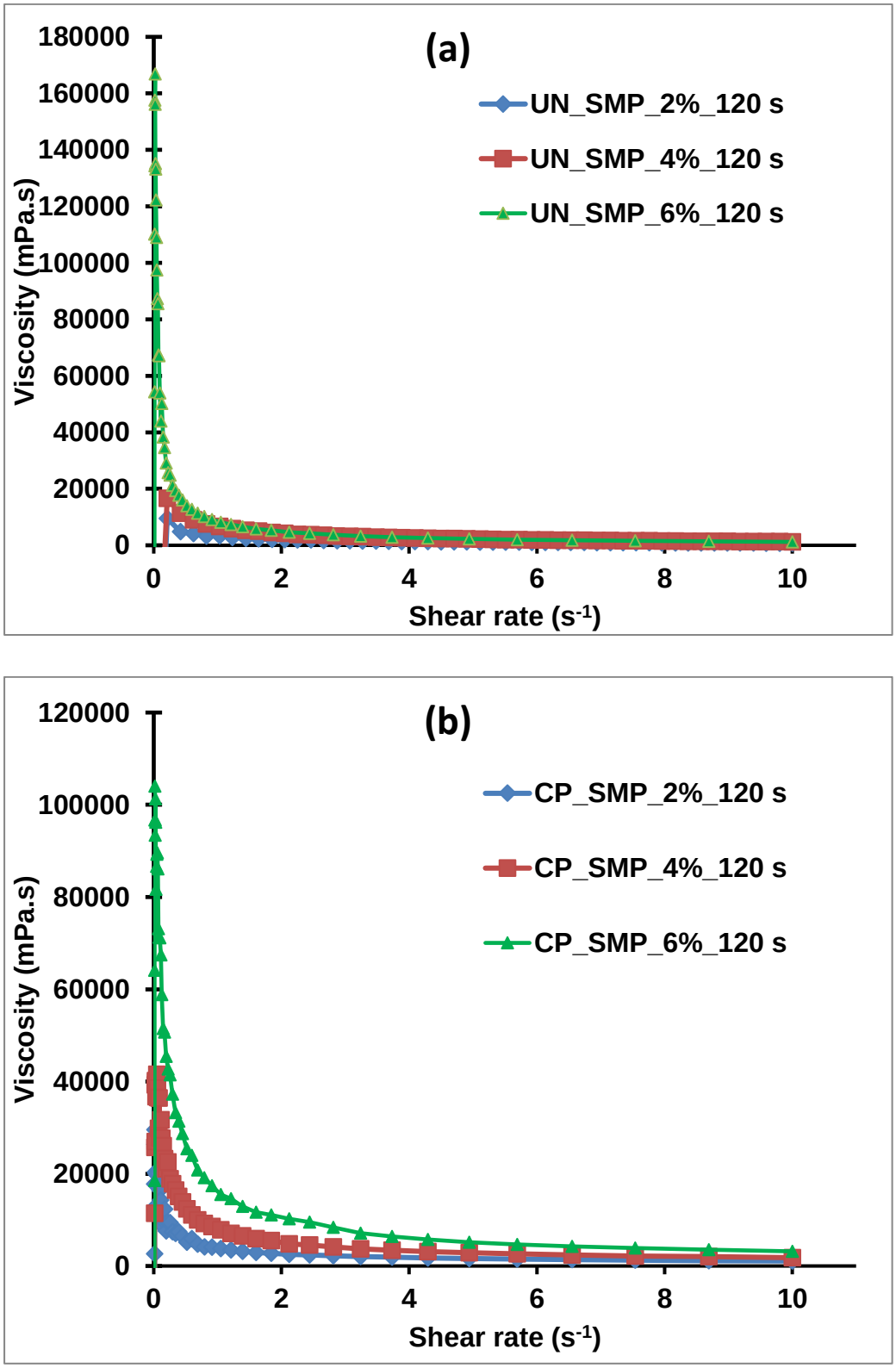

Figure 4.11 Steady rheology of cold plasma-treated pineapple pulp foam with (a) 2% SMP, (b) 4% SMP, and (c) 6% SMP whipped for 120 s

Table 4.32 Various drying models fitted with pineapple pulp foam prepared with different levels of skimmed milk powder (SMP)

Combinations	Power law model				Bingham plastic model				Casson model				Herschel-Bulkley model				
	k	n	R^2	RMSE	σ_B	k_B	R^2	RMSE	σ_c	k_c	R^2	RMSE	σ_{HB}	k_{HB}	n	R^2	RMSE
UN-SMP-2%	3.107	0.384	0.983	0.232	2.674	0.542	0.857	0.664	1.662	0.479	0.930	0.466	0.00000	15.220	0.343	0.975	1.486
UN-SMP-4%	6.813	0.282	0.963	0.517	6.251	0.765	0.728	1.406	4.418	0.501	0.847	1.055	$1.40x10^{-10}$	6.813	0.2818	0.9632	0.5166
UN-SMP-6%	6.693	0.214	0.935	0.688	4.419	0.842	0.595	1.713	3.595	0.509	0.760	1.318	$8.49x10^{-9}$	6.693	0.2136	0.9347	0.6877
CP-SMP-2%	3.829	0.453	0.992	0.265	1.593	1.140	0.874	1.068	1.031	0.782	0.945	0.703	0.00000	3.829	0.453	0.992	0.265
CP-SMP-4%	7.610	0.393	0.985	0.650	3.495	1.916	0.808	2.300	2.402	0.968	0.906	1.613	0.00000	7.610	0.393	0.985	0.650
CP-SMP-6%	15.220	0.343	0.975	1.486	7.740	3.251	0.740	4.755	5.584	1.200	0.863	3.450	0.00000	15.220	0.343	0.975	1.486

* σ_B and σ_c are the Bingham and Casson yield plastic, respectively

However, its values decreased with the increased SMP. The loss modulus of date syrup was obtained with more G″ over G′, implying the date syrup foam's viscous fluid behavior (Mohamed & Hassan, 2016).

The phase angle determines energy loss for stored energy during phase deformation. The phase angle 0° implied the foam's solid-like (elastic) behavior. At the same time, 90^{o} indicates the liquid-like (viscous) behavior, and in between their range indicates the viscoelastic behavior of the sample. The investigation from the study showed that the phase angle (δ) of pineapple foam was in the range of 23.670- 43.435^{o} at 25 ^{o}C, which confirmed the solid-like (viscoelastic) behavior of the pineapple pulp foam for all the SMP (%). The elastic behavior of the foam might be due to the addition of SMP, starch, and CMC during whipping. The lower phase angle (viscoelastic) of foam can reduce its drainage volume and enhance its stability.

Complex viscosity measures the total resistance to the flow of material. The complex viscosity of pulp foam with SMP varied from 10.636 to 42.147 Pa-s (Table 4.33). It is reported that the sample's viscosity may reduce the foam's drainage volume. The viscosity of pulp foam was higher at higher SMP concentrations, which might be due to the incorporation of more SMP-produced thick foam. The viscoelastic nature of the foam can be easily poured on a Petri plate, retaining its structure (stability) during drying.

Table 4.33 Dynamic rheological parameters of cold plasma-treated pineapple pulp (1 Hz)

Combinations	Storage Modulus (Pa)	Loss Modulus (Pa)	Phase Shift Angle (o)	Complex Viscosity (Pa-s)
UN-SMP-2%	97.136±3.223^{a}	66.010±1.332^{b}	34.205±0.346^{c}	18.758±0.839^{a}
UN-SMP-4%	120.610±1.697^{b}	61.440±0.634^{a}	26.995±0.091^{b}	21.633±1.308^{a}
UN-SMP-6%	172.695±1.096^{c}	75.703±0.527^{c}	23.670±0.014^{a}	30.142±2.028^{b}
CP-SMP-2%	48.419±3.108^{a}	45.825±2.473^{a}	43.435±0.289b	10.636±0.153^{a}
CP-SMP-4%	68.730±3.231^{b}	63.347±2.458^{b}	42.675±0.233b	14.921±0.456^{a}
CP-SMP-6%	200.350±3.705^{c}	141.040±3.309^{c}	35.145±0.134^{a}	42.147±2.141^{b}

The increased viscosity of incorporating SMP reduced the drainage volume and foam stability. It was observed from the experimental studies that the drainage volume of the foam decreased with increased SMP. The higher viscosity of the foam with the SMP can

prevent liquid flow from the air-liquid interface due to gravity/capillary action. The complex viscosity signifies the shear-thinning behavior of the foam with a frequency sweep from 1 to 10 Hz. The shear thinning of the foam was due to the rapid increase of shear, which may damage the structure of the air-liquid dispersed foam (Karaman et al., 2011). The complex viscosity increased with increasing SMP and WT. All the foaming combinations in the present investigations showed the shear-thinning flow behavior of the pulped foam.

4.16 **Physical characteristics of foam**

4.16.1 Foam properties (foam expansion, stability, and drainage volume)

The foam expansion (FS) and foam stability (FS) of pineapple pulp foam significantly increased, while drainage volume decreased with an increase in SMP concentration (Table 4.34 and Table 4.35). Higher FS had lowered the DV of foam with time. The addition of SMP could increase the stability of pineapple pulp. Foam expansion is commonly used to determine the whipping process. An increase in FS with SMP concentration indicated the higher incorporation of air in the pineapple pulp during whipping. SMP is a foaming agent that reduces interfacial tension around the foam bubbles. Khamjae and Rojanakorn (2018) also reported similar findings for foam mat-dried passion fruit aril. They reported that the methylcellulose used as a foaming agent increased the FS from 0.75 to 2.25%, significantly increasing it from 109% to 187%.

Foam stability can be defined as the foam's half-life or the time needed to shrink to half its original volume (Huppertz, 2010). In the present study, the foam stability increased with SMP concentration; the highest FS was obtained with 6% SMP. This phenomenon of increased FS could be attributed to the milk composition, which consists mainly of protein and polar lipids, monoglycerides, diglycerides, free fatty acids, and phospholipids. Both surfactants have important roles in the stabilization of foam. With the Gibbs–Marangoni mechanism, polar lipids aid in foam stabilization by facilitating the quick adsorption of surfactants from the bulk phase to the region of lower concentration in the adsorbed film (Gibbs effect). During interface deformation, equilibration of the concentration gradient may occur due to diffusion of molecules in the surface layer (Maragoni effect) (van Kempen et al., 2014). Thus, SMP consisting of both surfactants could lower the surface tension and provide a high molecular interface, acting as an excellent foam stabilizer. The stability of *totapuri* mango pulp foam has been reported to increase with added egg albumen

(Dehghannya et al., 2018; Rajkumar et al., 2006). More stable foam could hold the air-liquid interface and efficiently remove water from the foamed pulp (Azizpour et al., 2014).

The drainage volume (DV) of the pineapple foam inversely decreased with SMP concentration, which could be correlated with the foam's stability (Tables 4.34 and 4.35). The foam drainage phenomenon can be seen due to the capillary action and gravity. The gravitational force caused an upward movement or creaming of air bubbles due to the density differences between the air bubbles. The continuous phase (Huppertz, 2010) resulted in the drainage and deformation of foam bubbles. It is also possible that the viscosity of the surrounding liquid prevented drainage-induced instability. Similarly, adding protein (WPC) decreased drainage, resulting in improved foam stability (Martinez-Padilla et al., 2014).

Table 4.34 Thixotropic model coefficients and physical properties of untreated pineapple foam with varying SMP and shear rates

Skimmed milk powder (SMP) (%)	Shear-rate (s^{-1})	B-value (Pa.s)	M-value (Pa.s) at		Relaxation time, λ (s)	FE (%)	FS (%)	DV (mL)
			1-10 (s^{-1})	10-50 (s^{-1})				
2	1	2.64±0.05	4.34±0.20	0.77±0.01	434.8	62.9±0.8[a]	65±0[a]	35±0[c]
	10	0.36±0.04			416.7			
	50	0.12 ±0.01			333.3			
4	1	4.48±0.72	6.15±0.33	0.88±0.03	476.2	71.1±1.4[b]	87±1[b]	13±1[b]
	10	0.63±0.05			434.8			
	50	0.48±0.01			384.6			
6	1	4.92±0.11	7.87±0.65	2.16±0.10	526.3	88.7±1.3[c]	96±1[c]	4±1[a]
	10	1.23±0.18			500.0			
	50	0.88±0.01			476.2			

Alphabets with different superscripts in the same column are significantly different at $p<0.05$

* FE: Foam expansion, FS: Foam stability, and DV: Drainage volume

4.16.2 Rheological properties (B and M values and relaxation time (λ))

The model coefficients (B, M, and λ) were determined from Eqs. (3.31), (3.32), and (3.33), and are shown in Table 4.34 and Table 4.35. The time coefficient (B) decreased markedly with increased shear rates but increased with SMP concentrations. The increase in B-values with SMP was attributed to the high stability of the pineapple foam due to the presence of surfactants in SMP that helped to reduce surface tension in the foam. Similarly, M values decreased with increased shear rate, but increased with SMP concentrations.

The relaxation time (λ) of pineapple foam decreased with increased shear rate but increased with SMP concentration. The collapse of bubbles in the foam might have occurred at a higher rate when the shear rate was higher. Further, a low relaxation time indicated a liquid-like material (Jimenez-Junca et al., 2011) that occurred when the SMP concentration was lowest. In that situation, less relaxation time was due to low viscosity, which showed more liquid-like behavior due to faster drainage. The thickness of the foam possibly increased with SMP, and hence, the sample required more time to relax. Higher SMP concentration was also associated with increased viscosity of the surrounding liquid, significantly lowering the drainage volume but retaining the foam stability, as observed in the present study.

4.17 Quality attributes of powder

SMP concentrations positively impacted the Bulk density of the powder sample. Similar effects of SMP can be observed for the tapped and particle densities of the control and treated samples. The powder produced with SMP-6% showed maximum density for the control and treated samples (Table 4.36). The porosity of powders was varied from (48.14-57.04%) with the increased SMP.

Table 4.35 Thixotropic model coefficients and physical properties of cold plasma-treated pineapple foam with varying SMP and shear rates

Skimmed milk powder (SMP) (%)	Shear-rate (s^{-1})	B-value (Pa.s)	M-value (Pa.s) at 1-10 (s^{-1})	M-value (Pa.s) at 10-50 (s^{-1})	Relaxation time, λ (s)	FE (%)	FS (%)	FD (kg/m^3)	DV (mL)
CP-SMP_2%	1	2.64±0.05	**3.29±0.15**	**0.66±0.08**	557.21	146±0.94	95±0.50	775±0.03	5±0.50
	10	2.51±0.04			514.21				
	50	0.43 ±0.01			498.75				
CP-SMP_4%	1	4.48±0.72	**6.27±0.04**	**0.76±0.02**	598.07	168±0.94	95±0.99	677±0.04	4±0.50
	10	1.28±0.06			567.27				
	50	0.70±0.001			531.71				
CP-SMP_6%	1	3.12±0.06	**7.04±0.09**	**1.54±0.04**	602.17	187.65±0.45	97±1.23	540±0.03	1±0.00
	10	0.49±0.02			587.23				
	50	0.15±0.007			557.19				

Cold plasma treatment showed a similar impact on the pineapple powder's porosity, as seen in Table 4.36. CI and HR values for both samples were changed significantly with SMP ($p<0.05$) (Table 4.36). The low CI value obtained at SMP-2% for both the controlled and treated samples implied the good flowability of the powder. Similarly, Hausner ratio (HR) of the powder was found to be in the range of (1.10-1.163), showing the powder's low and intermediate extent of cohesiveness. Insignificant changes were observed in the control and

treated samples ($p>0.05$). The use of SMP significantly enhanced the WAI and WSI values of the control and cold plasma-treated pineapple powder ($p<0.05$) (Table 4.36). An increase in values, observed in the treated samples, might be due to the solubilization of the food constituents upon exposure to cold plasma. SMP concentrations had an insignificant effect on the dispersibility of the powder for both samples, as explained in detail ($p>0.05$). The increase of all these powder properties with the increased SMP concentration is explained in section 4.11 of objective 2.

4.18 Pearson correlation

The coefficients of the correlation matrix showed the relationship between SMP and foaming properties (physical and rheological) and powder properties, as presented in Table 4.37 and Table 4.38. The correlation coefficients of foaming properties (FE and FS) with SMP were 0.966 and 0.968, respectively, indicating that they were strongly correlated ($p<0.01$) with SMP (Table 4.37). However, the foaming properties of DV and B values negatively correlated with SMP. The SMP in pulp produces a viscoelastic interfacial film around the air-liquid interface, which can prevent drainage-induced instability and structural breakdown of the developed foam. SMP showed strong correlations with RT, M1, and M2 ($r=0.870$, 0.976, and 0.891, respectively) at $p<0.01$. High SMP concentrations markedly increased the viscosity, which significantly enhanced the rheological properties of the foam. The B value was inversely related to SMP while positively correlated with DV. The strong relationship between DV and B value ($r=0.978$, $p<0.01$), FS and M1 ($r=0.976$, $p<0.01$) implied the good stability of the foam. Powder properties (PO, CI, HR, RR, WAI, and WSI) were significantly ($p<0.01$) correlated with BD. A similar interpretation for treated samples is shown in Table 4.38. However, the coefficient shown in the table implied a stronger relationship among the treated samples. SMP showed positive interrelation with the foaming properties (FE and FS), rheological (RT, M1, and M2), and powder properties (BD, PO, CI, HR, RR, WAI, and WSI).

The solubility of the powder of both the untreated and treated samples was good due to the addition of SMP, since it produced smaller bubbles with a larger surface area of the foam, leading to enhanced penetrability and solubility. Poor powder dispersibility (DI) correlation was observed in the powders with SMP concentration, foaming properties, rheological properties, and other powder properties.

4.19 Interrelation between/among rheological, foam parameters, and powder attributes

The multivariate analysis was conducted to develop the inter-relationship among the independent variables (SMP concentration) and dependent functions (time-dependent rheological parameters, foaming, and powder properties). The principal component analysis (PCA) biplot (Fig. 4.12 and Fig. 4.13) showed that PC1 and PC2 accounted for 82.5% and 14.8%, and 85.90% and 14.10% for untreated and treated samples, respectively, meaning a much higher loading on the principal component axis 1. A total variation of more than 97% by PC1 and PC2 of both the untreated and treated samples indicated the suitability of the PCA method in the present context.

In the PCA biplot, the powder dispersibility (DI) was an outlier, meaning that the dispersibility of pineapple powder had little interrelationship with the foaming and rheological properties for both the treated and control samples, as shown in Fig. 4.12 and Fig. 4.13. The powder properties like HR, BD, CI, WAI, WSI, PO, RR, foam expansion, and rheological properties (RT and M2) formed one group. Their smallest angle showed a positive interrelationship among themselves (Figs. 4.12 and 4.13). However, the parameters of the above-mentioned group were negatively linked to DV and B values due to their positions in different quadrants. However, the DV and B values formed a small cluster. The physical properties of the foam and a high concentration of SMP potentially reduced the DV and B values by lowering the viscoelastic interfacial tension of the bubbles. The FS and M1 were also positively correlated with the foam properties. It indicated that the higher FS and M1 values resulted in higher RT values to reduce the structural damage during foam formation. The trend was also noticed in the physical and rheological studies of pineapple pulp foam. Similar findings were observed as FS varied with the SMP concentration (Tables 4.37 and 4.38).

Table 4.36 Physical and rehydration properties of foam-dried pineapple powder

Skimmed milk powder (SMP) (%)	Density(kgm^{-3})			Porosity (%)	Carr index (CI) (%)	Hausner ratio (-)	Properties of powder		
	Bulk	Tapped	Particle				WAI(g/g)	WSI (%)	Dispersibility (%)
SMP-2%	498.67±1.07^{a}	547.95±1.21^{a}	1056.57±2.21^{a}	48.14±0.01^{a}	8.99±0.01^{a}	1.100±0.00^{a}	5.24±0.05^{a}	43.09±1.26^{a}	87.25±1.61^{a}
SMP-4%	520.80±1.54^{b}	581.74±5.07^{b}	1239.21±2.83^{b}	53.06±0.34^{b}	10.47±0.55^{b}	1.120±0.01^{b}	5.37±0.21^{a}	56.41±0.23^{b}	85.45±5.60^{a}
SMP-6%	589.76±0.87^{c}	685.80±1.02^{c}	1736.99±5.13^{c}	57.04±0.07^{c}	14.00±0.00^{c}	1.160±0.00^{c}	6.31±0.40^{b}	59.72±0.75^{c}	86.24±1.09^{a}
CP-2% SMP	503.653±1.07^{a}	553.425±1.23^{a}	1067.137±2.23^{a}	48.139±0.01^{a}	8.993±0.01^{a}	1.099±0.0001^{a}	5.34±0.07^{a}	43.39±0.76^{a}	87.57±0.14^{b}
CP-4% SMP	526.008±1.55^{b}	587.564±5.12^{b}	1251.604±2.85^{b}	53.055±0.34^{b}	10.473±0.55^{b}	1.117±0.01^{b}	5.68±0.16^{a}	56.68±0.38^{b}	86.045±0.09^{a}
CP-6% SMP	595.664±0.88^{c}	692.633±1.02^{c}	1612.377±4.17^{c}	57.043±0.07^{c}	14.000±0.00001^{c}	1.163±0.0001^{c}	6.88±0.13^{b}	59.25±0.93^{b}	87.07±0.19^{b}

Alphabets with different superscripts in the same column are significantly different at $p<0.05$

Table 4.37 Lower half correlation matrix of untreated pineapple pulp among foaming, rheological, and powder properties of foam

	SMP	FE	FS	DV	RT	B-value	M1	M2	BD	PO	CI	HR	RR	WAI	WSI
FE	0.966**														
FS	0.968**	0.873**													
DV	-0.968**	-0.873**	-1.000**												
RT	0.870**	0.968**	0.724**	-0.724**											
B-value	-0.897**	-0.753**	-0.978**	0.978**	-0.564*										
M1	0.976**	0.903**	0.976**	-0.976**	0.776**	-0.937**									
M2	0.891**	0.973**	0.750**	-0.750**	0.989**	-0.603**	0.819**								
BD	0.961**	10.000**	0.863**	-0.863**	0.972**	-0.741**	0.900**	0.979**							
PO	0.997**	0.944**	0.984**	-0.984**	0.832**	-0.927**	0.985**	0.855**	0.938**						
CI	0.963**	0.997**	0.869**	-0.869**	0.961**	-0.751**	0.899**	0.973**	0.996**	0.939**					
HR	0.961**	0.997**	0.864**	-0.864**	0.964**	-0.745**	0.895**	0.975**	0.997**	0.936**	1.000**				
RR	0.833**	0.664**	0.944**	-0.944**	0.457	-0.991**	0.884**	0.495*	0.650**	0.871**	0.663**	0.656**			
WAI	0.880**	0.864**	0.818**	-0.818**	0.799**	-0.749**	0.916**	0.860**	0.872**	0.877**	0.852**	0.853**	0.667**		
WSI	0.940**	0.823**	0.994**	-0.994**	0.655**	-0.992**	0.960**	0.689**	0.812**	0.962**	0.822**	0.816**	0.970**	0.791**	
DI	0.032	0.259	-0.194	0.194	0.447	0.361	-0.116	0.430	0.272	-0.047	0.295	0.302	-0.455	0.026	-0.257

*Significant at ($p<0.05$) level of significance **Significant at ($p<0.01$) level of significance

Table 4.38 Lower half correlation matrix of treated samples among foaming, rheological, and powder properties of foam

	SMP (%)	FE	FS	DV	RT	B-value	M1	M2	BD	PO	CI	HR	RR	WAI	WSI
FE	.999*														
FS	.866	.849													
DV	-.961	-.951	-.971												
RT	.968	.976	.713	-.861											
B-value	-.992	-.996	-.797	.919	-.992										
M1	.947	.957	.659	-.820	.997*	-.979									
M2	.913	.899	.995	-.990	.782	-.855	.733								
BD	.959	.949	.972	-1.000**	.857	-.916	.816	.991							
PO	.998*	1.000*	.834	-.942	.981	-.998*	.964	.887	.940						
CI	.973	.965	.958	-.999*	.885	-.937	.847	.982	.998*	.958					
HR	.970	.961	.962	-.999*	.877	-.931	.839	.985	.999*	.953	1.000**				
RR	.841	.858	.458	-.658	.950	-.902	.971	.548	.653	.872	.695	.683			
WAI	.931	.918	.989	-.996	.809	-.878	.763	.999*	.996	.907	.990	.992	.585		
WSI	.943	.953	.650	-.814	.996	-.977	1.000**	.726	.809	.961	.841	.833	.973	.756	
DI	-.393	-.423	.119	.123	-.611	.505	-.669	.015	-.116	-.448	-.172	-.156	-.828	-.029	-.677

*Significant at ($p<0.05$) level of significance **Significant at ($p<0.01$) level of significance

High FS, in combination with a high concentration of SMP, resulted in less structural breakdown and low DV, which finally offered the good drying characteristic of the product at a low temperature, as observed for the drying behavior of foam. The highest distance of SMP-6%, located in the first quadrant, showed a more substantial effect on parameters of foaming, rheological, and powder properties (BD, HR, CI, WAI, PO, WSI, and RR) than other SMP concentrations. A similar interpretation can be seen in Fig. 4.13. The higher stability produced at 6 % SMP for 2 min was considered the best combination for the powder produced with good attributes.

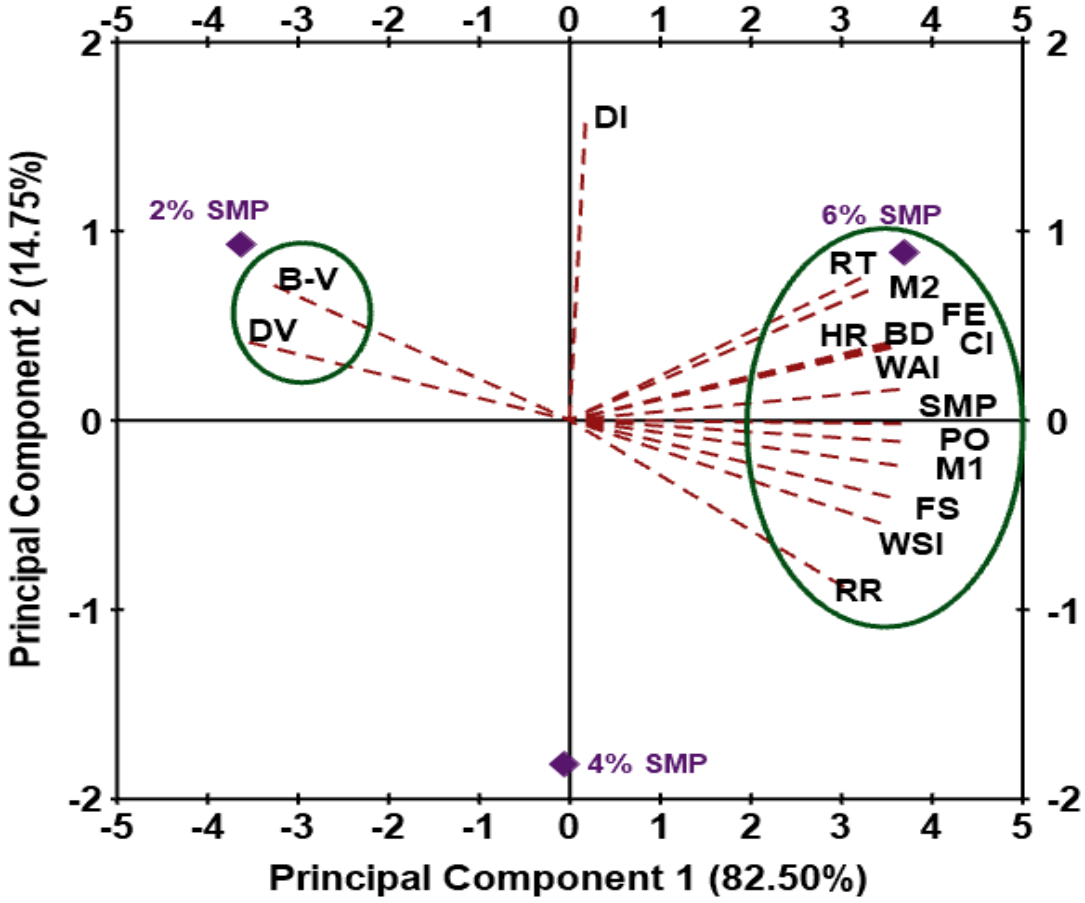

Figure 4.12 Principal component analysis (PCA) biplot of untreated pineapple pulp among independent variables (SMP concentration) and dependent functions (time-dependent rheological parameters, foaming, and powder properties)

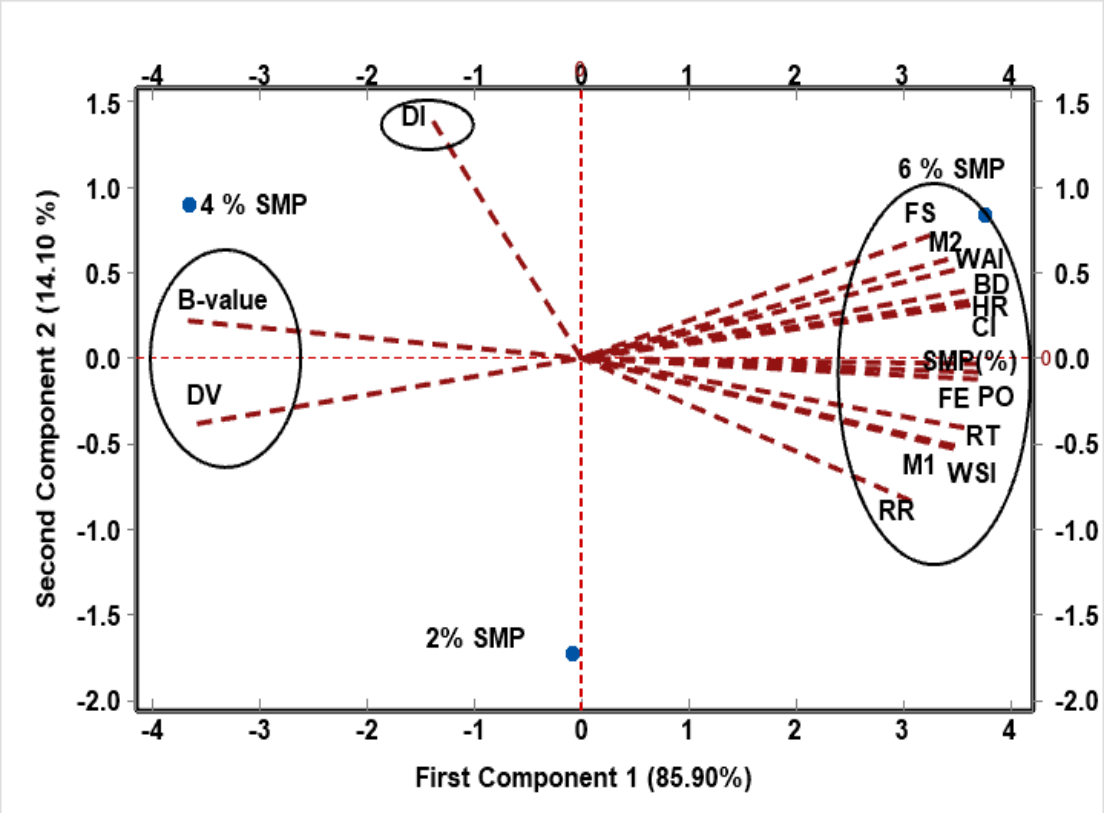

Figure 4.13 Principal component analysis (PCA) biplot of cold plasma-treated pulp among independent variables (SMP concentration) and dependent functions (time-dependent rheological parameters, foaming, and powder properties).

4.20 Storage study of powder

4.20.1 Moisture sorption isotherm of pineapple powder

Pineapple powder produced with **SMP-6% and WT-120 s** was stored at different temperatures (30, 40, and 50 °C) to investigate the adsorption isotherm. The change in adsorption isotherms of the powder with temperature is presented in Table 4.39. Equilibrium moisture content versus water activity is shown in plot 4.14, which illustrates that the increase in water activity increases the EMC of the powder. The hydrophilic nature of the carbohydrate (sugar) and protein in the pineapple powder may increase EMC. The EMC increases linearly with water activity, and a drastic increase in the EMC was observed at higher water activity in the condensation region (Muzaffar et al., 2016). A similar behavior can also be seen in many sugar-rich and acid-rich fruits (Muzaffar et al., 2016; Goula et al., 2008; Kaymak-Ertekin et al., 2004; Sormoli et al., 2015). The patterns of isotherms obtained in this study showed Type-II isotherms for all the temperature combinations. This downward concavity (Type-II isotherm) of the curve is most commonly

found in sugar-rich foods. A high-sugar food powder absorbs moisture quickly in a higher relative humidity environment. The composition and constituents of the food products can also affect the moisture sorption capacity, as reported by Labuza & Altunakar (2008). Sorption isotherms of many food products were studied by several researchers and fitted with various mathematical models to predict their isotherm behavior (Quirijns et al., 2005).

Experimental isotherm data were fitted with the different mathematical models, as shown in Table 4.39. The coefficient predicted from the mathematical model equations gives an idea for selecting the equilibrium moisture content of the foam-dried powder. All five fitted models were well fitted to the experimental observations of the powder with R^2>0.851 and RMSE<0.012. However, the GAB model fits best in the present investigations with the highest (R^2≤0.996) and lowest RMSE<0.003. This model was also best fitted for describing the isothermal studies of tamarind, orange juice, and tomato pulp powder (Muzaffar et al., 2016; Goula et al., 2008; Kaymak-Ertekin et al., 2004; Sormoli et al., 2015). GAB model parameter (M_G) indicates the monolayer moisture content associated with the deteriorative reaction in the food products. M_G is the critical moisture value in food products for food stability. The moisture value below this critical value represents the rate of deteriorative reactions at a negligible rate due to the strong binding of water to the surface (Abdullah et al., 2020). The M_G of the powder in this investigation inversely decreased with temperature. This might be due to the weakening of the hydrogen bonds of the water molecules as the temperature increases. The value obtained for the powder was found to be in the range for agro-based foods. Labuza and Altunakar (2008) reported that the optimum monolayer moisture of dehydrated products was found to be in the range of 0.2 to 0.3, which shows the products' stability and maximum shelf life. Above this moisture content value, lipid oxidation occurs. The caking and stickiness of the powder were found to be 0.35 to 0.50, and the optimum water activity for microbial spoilage was mentioned to be 0.6. Monolayer moisture content for the present investigation was found to be below 0.12, which indicated its maximum shelf-life stability. The same trend has also been observed for drying orange juice powder over the temperature range of 20-50 °C (Sormoli & Langrish, 2015).

Table 4.39: Isotherm model parameters with their statistical performance parameters of pineapple powder packed in PP and AL pouches.

Model (s)	Temp.	Model Parameters			R^2	RMSE	Model Parameters			R^2	RMSE
		PP pouches					AL pouches				
GAB	30	M_G=0.137	C_G=27.110	K_G=0.588	0.996	0.003	M_G=0.112	C_G=26.71	K_G=0.6555	0.9901	0.0040
	40	M_G=0.123	C_G=63.730	K_G=0.581	0.996	0.002	M_G=0.109	C_G=64.50	K_G=0.6343	0.9912	0.0034
	50	M_G=0.109	C_G=75.360	K_G=0.543	0.986	0.003	M_G=0.089	C_G=408.80	K_G=0.6014	0.9449	0.0068
Smith	30	A=0.053	B=-0.029		0.969	0.005	A_S=0.0537	B_S=-0.0266		0.9547	0.0060
	40	A_S=0.053	B_S=-0.025		0.974	0.004	A_S=0.0520	B_S=-0.0244		0.9883	0.0028
	50	A_S=0.054	B_S=-0.019		0.995	0.001	A_S=0.0510	B_S=-0.0195		0.9867	0.0024
Henderson	30	A_H=716	B_H=2.686		0.993	0.003	A_H=1215	B_H=2.8720		0.9867	0.0033
	40	A_H=1511	B_H=2.929		0.991	0.002	A_H=1954	B_H=3.0040		0.9824	0.0034
	50	A_H=9905	B_H=3.583		0.974	0.003	A_H=9531	B_H=3.5160		0.9245	0.0056
Oswin	30	A_{Os}=0.074	B_{Os}=0.215		0.980	0.004	A_{Os}=0.073	B_{Os}=0.2016		0.9692	0.0050
	40	A_{Os}=0.072	B_{Os}=0.194		0.985	0.003	A_{Os}=0.069	B_{Os}=0.1955		0.9913	0.0024
	50	A_{Os}=0.069	B_{Os}=0.161		0.997	0.001	A_{Os}=0.065	B_{Os}=0.1709		0.9690	0.0036
Iglesias and Chirife	30	A_{IC}=0.067	B_{IC}=0.006		0.851	0.012	A_{IC}=0.0670	B_{IC}=0.0053		0.8259	0.0118
	40	A_{IC}=0.066	B_{IC}=0.005		0.863	0.010	A_{IC}=0.0638	B_{IC}=0.0050		0.9031	0.0080
	50	A_{IC}=0.063	B_{IC}=0.004		0.936	0.005	A_{IC}=0.0600	B_{IC}=0.0041		0.9596	0.0041

The moisture absorbed in the powder packaged in PP material was slightly higher than in ALP materials. The M_G value obtained from the GAB model also identifies a similar interpretation. Sormoli & Langrish (2015) investigated the isothermal study of orange juice powder, for which the GAB model provided a better explanation.

The sample plot in Fig. 4.14 represents the EMC of the samples under different temperature conditions. Experimental data for each equilibrium moisture content at fixed temperature were fitted with various mathematical models, viz., Henderson, Smith, and Oswin models, to identify the behavior of their predicted models with the experimental values. The plots show that all the models were close to the experimental values and showed good fitness of the selected fitted models in the present investigations. Fig. 4.14 was for the Moisture sorption isotherms of pineapple powder packed in PP, while Fig. 4.15 was for the sorption isotherms of pineapple powder packed in AL pouch at 30, 40, and 50 °C. All these models fit well with the experimental values of the powder stored under both packing conditions. However, it was observed that the models were closer to the actual data of samples stored under AL packing conditions than the powder packed in the PP pouch. A similar pattern was also obtained from the predicted model parameters, as presented in Tables 4.39 and explained in section 4.20.1.

4.20.2 A_f and B_f value for the model validation

The accuracy of the fitness was analyzed by determining the accuracy (A_f) and bias (B_f) factors and comparing their values to identify the accurate model. These models' values were close to 1 (Table 4.40). However, the A_f values were found to be slightly higher in the case of the GAB model, Henderson model, and Oswin model, followed by the Smith, Iglesias, and Chirife models. A higher A_f value in the observations indicates that the predicted values deviate from the actual observations. The models with higher A_f values showed unsatisfactory results in explaining the sorption isotherm. While the A_f value obtained in the Smith model was well explained, the prediction of moisture sorption isotherms was achieved with the highest accuracy among them.

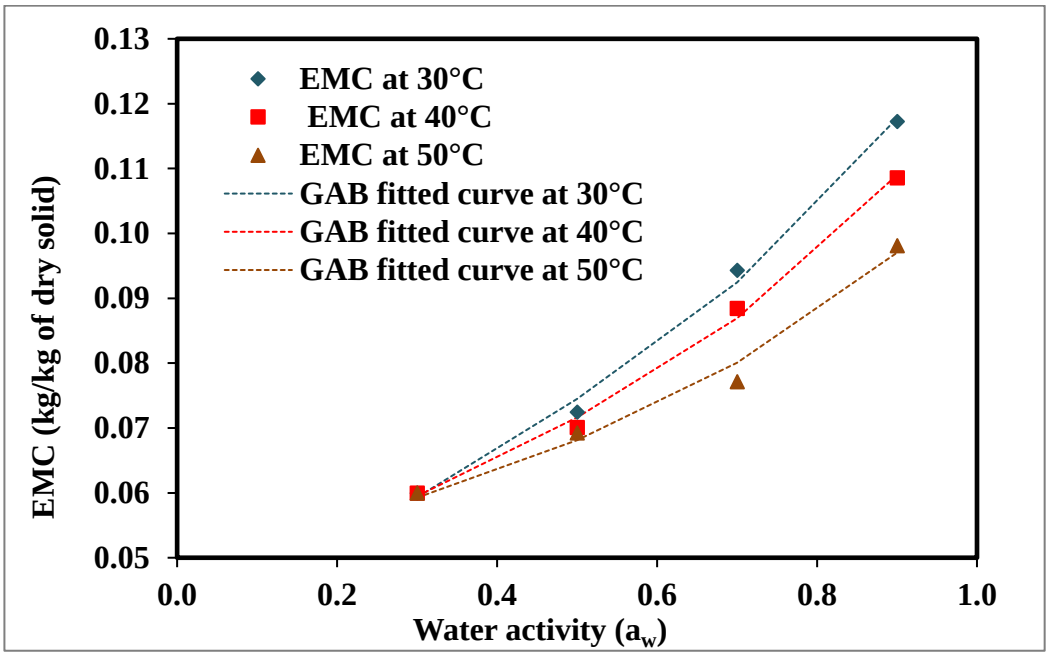

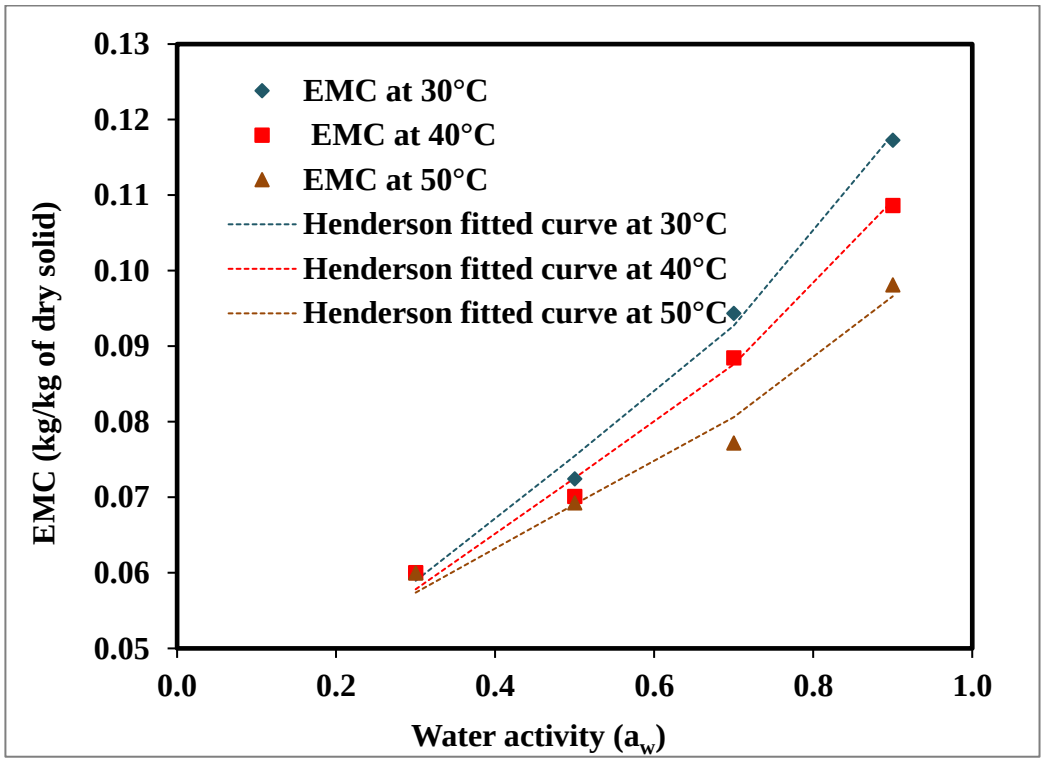

Figure 4.14 Moisture sorption isotherms of pineapple powder packed in PP pouch at 30, 40, and 50 ºC showing the fitted curves of the GAB and Henderson models

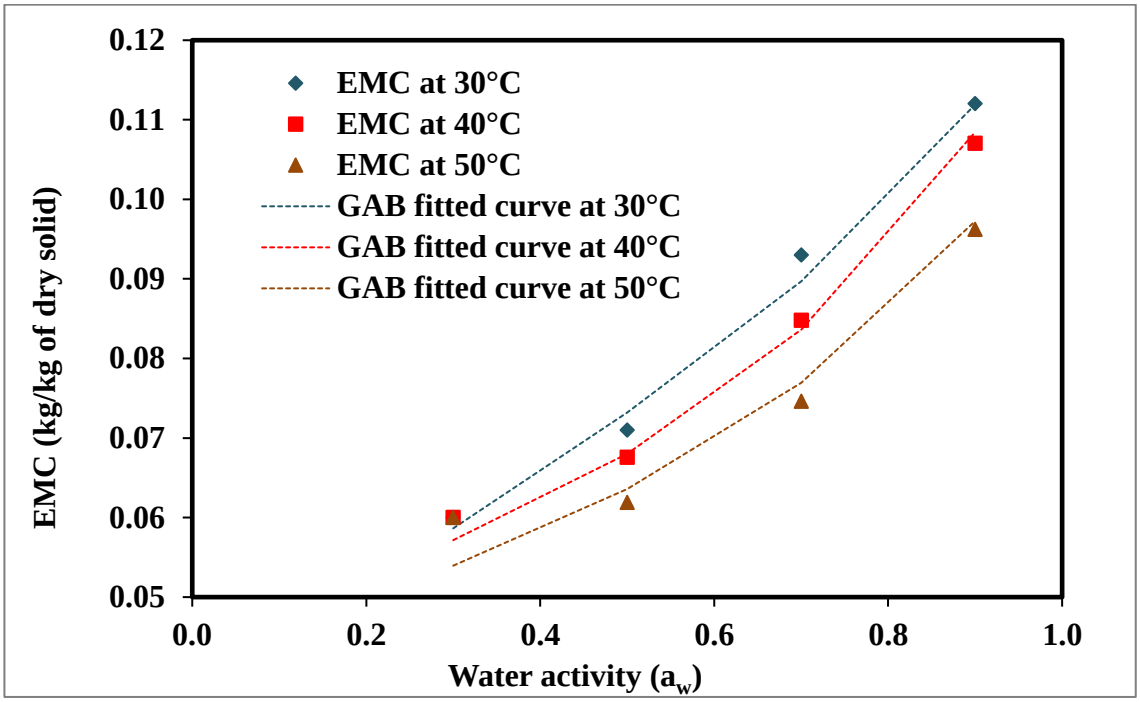

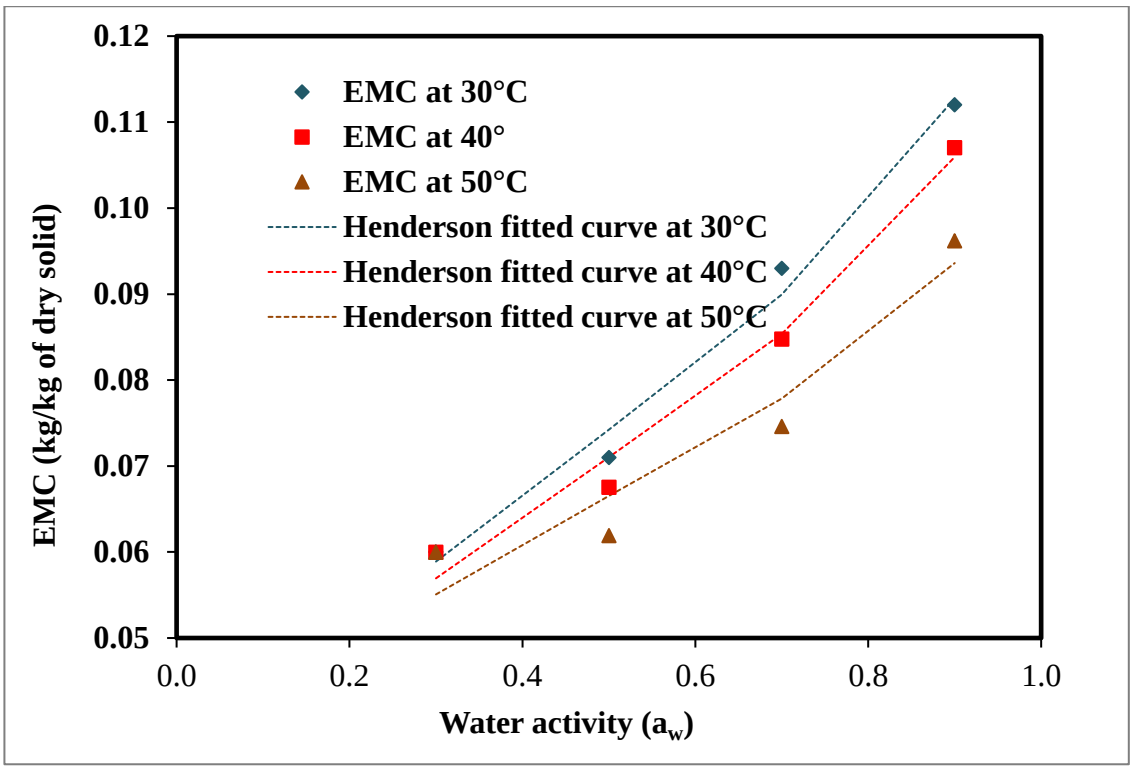

Figure 4.15: Moisture sorption isotherms of pineapple powder packed in an AL pouch at 30, 40, and 50 °C showing the fitted curves of the GAB and Henderson models

The B_f value for all the models was found to be the same ($B_f \approx 1$), which signifies the excellent prediction of the models. Although the values were slightly different, they had no significant differences. Muzaffar & Kumar. (2016) also revealed that the Smith model better described the moisture sorption isotherm of tamarind pulp. Esua et al. (2022) also used the accuracy and bias factors to validate their fitted models. They reported that the best fitness was obtained in the model where the A_f and B_f were found to be in the range of (0.970–1.006) and (0.995–1.031), respectively.

4.20.3 AIC and BIC values for the model validation

Various mathematical models had been fitted with the moisture sorption isotherms data to investigate their behavior. The present investigations determined AIC and BIC values to identify the best models among the fitted models. The best-selected models were identified based on their estimations, as shown in Table 4.40. Lower AIC values were observed in the Smith, Iglesias, and Chirife models, followed by the Oswin and Henderson models. A low AIC value implied a better prediction of the models than the observed one. The Smith model presented in Table 4.40 showed the smallest AIC value for all the isotherm conditions, signifying their substantial support for validating the models for the isotherm study. Similar patterns had also been observed for the AL-30, AL-40, and AL-50, respectively. BIC values for all the models were the same for all the models. However, the Smith model had the lowest value compared to other fitted models. With respect to AIC, the models were ranked in the following order: Smith>Iglesias and Chirife>GAB> Oswin and Henderson model. The observation shows that the Smith models were best as predicted from the accuracy factor (A_f and B_f) and the model validation parameters AIC and BIC. A similar trend was also obtained for the inactivation kinetic study by Esua et al. (2022). The model with the lowest AIC value is considered the best (Panigrahi et al., 2021; Petrossian et al., 2018).

4.21 Thermodynamic properties

4.21.1 Net Isosteric heat (Q_{st}) of sorption and sorption entropy

The study and investigation of the net isosteric heat were significant for optimizing the drying processes. The energy required to remove moisture can help design more efficient drying techniques (King, 1968).

Table 4.40: Model validation parameters (A_f and B_f) and selection parameters (AIC and BIC) of the moisture sorption isotherms of pineapple powder packed in PP and AL pouches at 30, 40, and 50 ºC

Conditions	GAB		Smith		Henderson		Oswin		Iglesias and Chirife	
	A_f	B_f	A_f	B_f	A_f	B_f	A_f	B_f	A_f	B_f
PP-30	1.000008	0.9999	1.0000	0.9999	1.0008	0.9991	1.000141	0.999859	1.000011	0.999989
PP-40	1.000077	0.999923	1.000002	0.999998	1.000078	0.999922	1.000075	0.999925	1.000013	0.999987
PP-50	1.000085	0.999915	1.000005	0.999993	1.000692	0.999308	1.010133	0.989969	1.000016	0.999984
AL-30	1.001893	0.998111	1.000015	1.000015	1.000116	0.999884	1.005926	0.994109	1.000008	1.000008
AL-40	1.001662	0.998341	1.000001	0.999998	1.000041	0.999959	1.000000	1.000000	1.000013	0.999987
AL-50	1.000837	0.999164	1.000020	0.999970	1.000275	0.999725	1.000106	0.999894	1.000014	0.999986
	AIC	**BIC**	**AIC**	**BIC**	**AIC**	**BIC**	**AIC**	**BIC**	**AIC**	**BIC**
PP-30	-95.134	-7.645	-109.679	-7.964	-67.420	-6.961	-81.949	-7.365	-102.046	-7.816
PP-40	-91.197	-7.557	-114.619	-8.054	-87.091	-7.490	-87.339	-7.496	-101.463	-7.804
PP-50	-90.993	-7.553	-106.436	-7.902	-70.184	-7.045	-48.904	-6.290	-100.196	-7.778
AL-30	-65.376	-6.858	-96.949	-7.711	-83.653	-7.407	-52.132	-6.425	-105.327	-7.881
AL-40	-66.820	-6.904	-118.303	-8.118	-92.436	-7.613	-135.050	-8.388	-101.472	-7.804
AL-50	-72.986	-7.091	-95.596	-7.682	-77.858	-7.259	-85.510	-7.453	-101.650	-7.808

Controlling moisture content is crucial for stability and self-life in the food industry, where powders are often produced. However, investigating the net isosteric heat can facilitate the formulation and maintain the appropriate moisture levels. It also helps in assessing the hygroscopic nature of the powder. High isosteric heat signifies the higher hygroscopicity of the powder, which can readily absorb moisture from the air. Q_{st} is the additional heat above the latent heat of pure water vaporization. Q_{st} indicates how strongly water vapor molecules adhere to solids by evaluating the excess heat required compared to the energy needed to vaporize pure water. This parameter helps in understanding the interaction forces between the vapor and solid phases, providing insight into how water vapor molecules are bound to or interact with various solid materials (Al-Muhtaseb et al., 2002; Wang & Brennan, 1991). The isosteric heat absorption model predicted by the GAB and Smith model is shown in Fig. 4.16. From the result, it can be seen that the Q_{st} value significantly decreased at a broader moisture value. The work carried out by Al-Muhtaseb et al., 2004 also obtained similar findings. This might be due to the strong interaction between the water molecules, sugar, and protein molecules present in the food matrix (Rizvi, 1995; Wang & Brennan, 1991). There is a strong repulsive interaction between the water molecules at high moisture content, as the absorbed water molecules are free and closer to each other. The repulsive interactions between the molecules reduced the net isosteric heat during further adsorption (Al-Muhtaseb et al., 2004). The net isosteric heat and Sorption entropy values were higher in the GAB prediction (ΔSG, Q_{st} G) than in the Smith prediction (ΔSSmi, Q_{st}Smi). The accuracy of the GAB prediction, as explained in section 4.20. Model validation parameters AIC, BIC, and accuracy factors A_f and B_f also suggest how well the GAB was fitted with the experimental observation to predict better the isotherm studies of the pineapple powder in the present context.

4.21.2 Enthalpy-Entropy Compensation Parameters

Sorption entropy and isosteric heat under different moisture contents were determined from Eq. 3.39 and plotted as isosteric heat versus sorption entropy, as shown in Fig. 4.17. The plot showed strong dependencies of entropy with an exponential trend followed by differential enthalpy. Similar results were also reported for the sorption isotherm studies of starch powder (Al-Muhtaseb et al., 2002). The plot obtained between the thermodynamic properties showed a linear relationship between entropy and enthalpy.

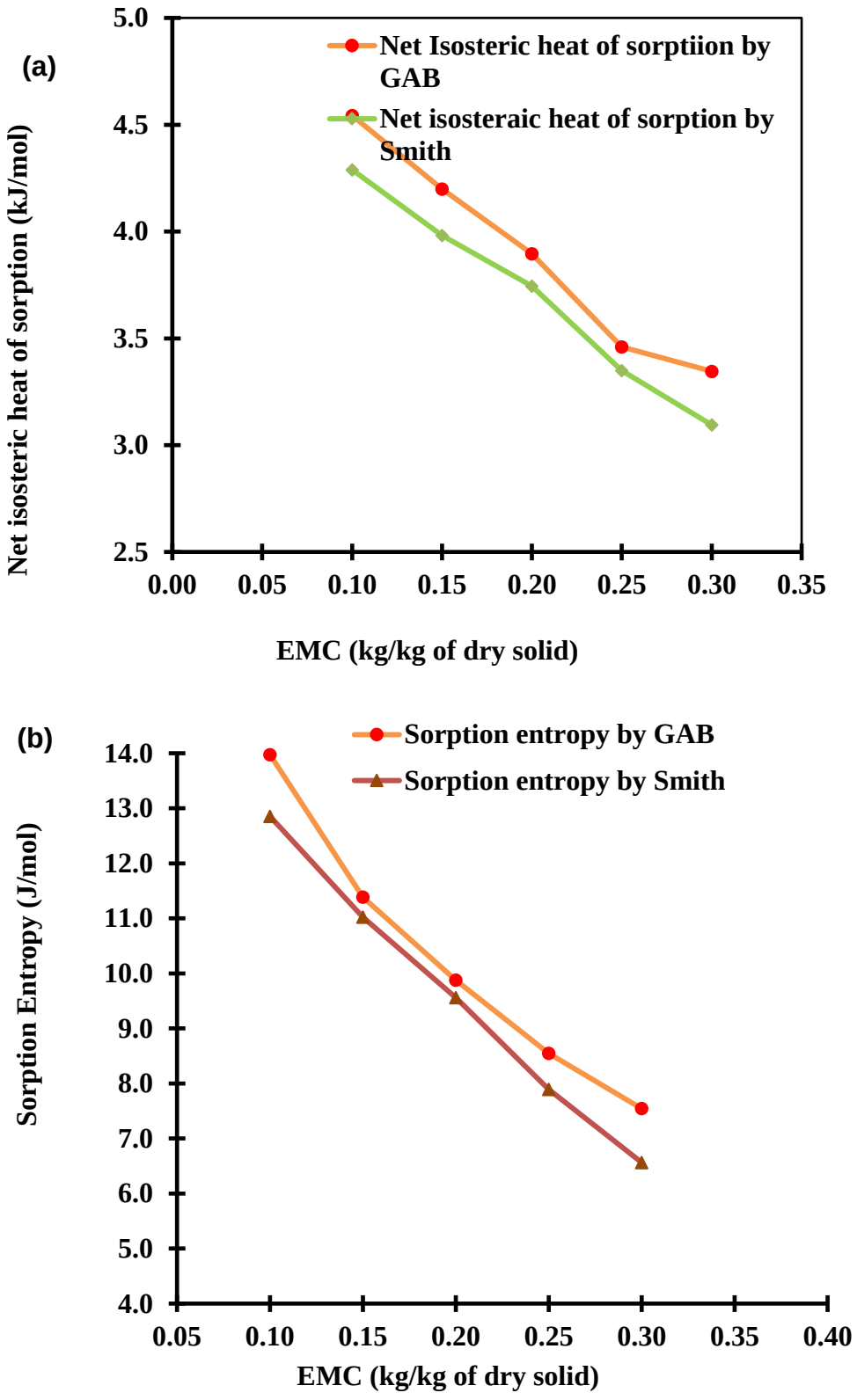

Figure 4.16 Effect of EMC on the (a) net isosteric heat of sorption and (b) sorption entropy of pineapple pulp powder using GAB and Smith models output.

For the GAB model, $\Delta Q\_st = 345.13\Delta S + 1883$ Eq.4.1

For the Smith model, $\Delta Q\_st = 339.53\Delta S + 1853$ Eq.4.2

The isokinetic temperature of the sorption obtained from the linear equations for the GAB and Smith model was T_B= 345.23 K and 333.53 K, respectively. The mean temperature of T_{hm} was calculated as T_{hm}=303 K. Hence, the T_B value for both models can be taken as 58-65 °C, which is significantly varied from the T_{hm} and represents the isokinetic theory's applicability to the pineapple powder water sorption isotherm. The entire process can be characterized as enthalpy-driven, as (T_B>T_{hm}).

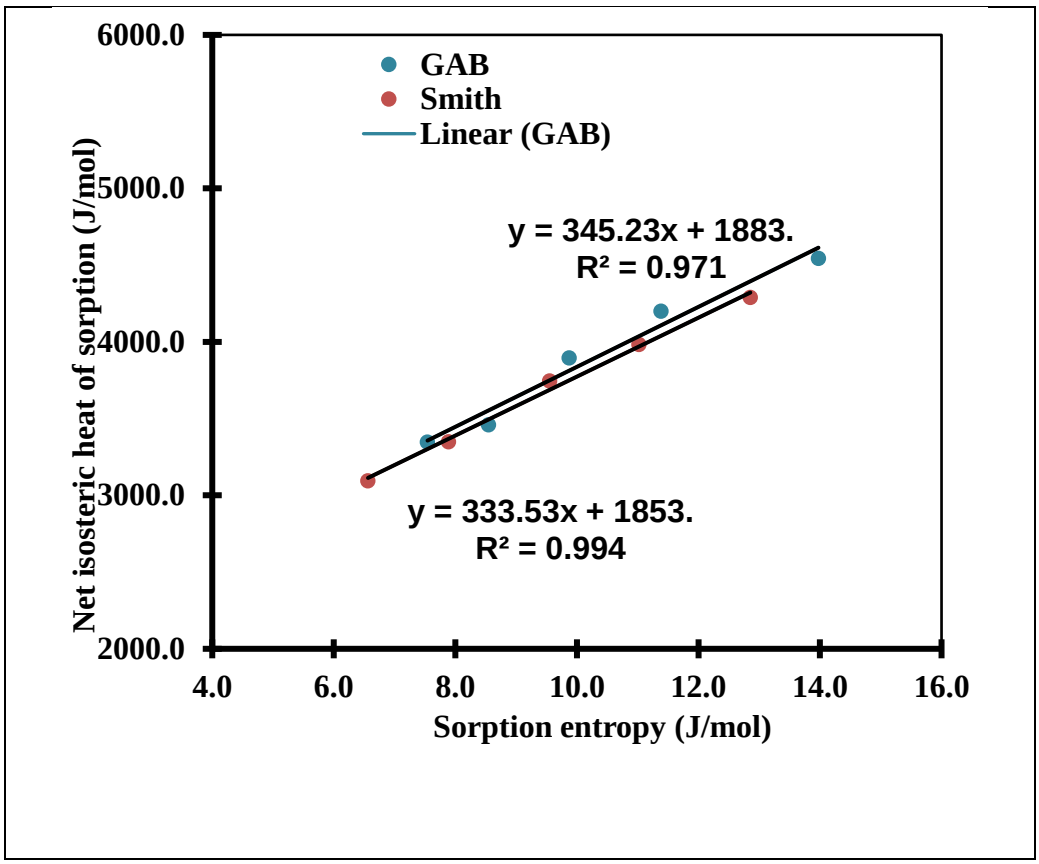

Figure 4.17 Sample plot of net isosteric heat of sorption versus sorption entropy

4.21.3 Interrelation between Sorption entropy and isosteric heat of foam-dried powder

The PCA biplot in Figure 4.18 represents the interrelation between the Sorption entropy and the isosteric heat predicted from the GAB and Smith model parameters. The first component 1 of the PCA biplot is shown on the x-axis, while the second component 2 is shown on the y-axis. The total variation of component 1 and component 2, more than 99%, indicates the suitability of the PCA method for correlating their interrelation.

The plot shown in the figure represents that the isosteric heat predicted by the GAB and Smith model and sorption entropy by the Smith model lied in the 4th quadrant and form a single loop, representing their strong correlation. However, entropy (***Δ***SG) predicted by GAB and water activity (a_w) lies in a separate quadrant. Entropy (***Δ***SG) lies in a separate quadrant. Entropy (***Δ***SG) lies in the 1st quadrant, while the water activity (a_w) lies in the 2nd quadrant. They are positioned opposite a quadrant, implying their inverse relationship with each other. At lower water activity, the sorption entropy was higher. However, its value decreased in the wider water activity range. This might be due to the strong interaction between the water molecules, sugar, and protein molecules present in the food matrix (Rizvi, 1995; Wang & Brennan, 1991). The same trend can also be seen in Fig. 4.16. A Small deviation between the entropy predicted by the Smith model (***Δ***SSmi) and the isosteric heat predicted by the same Smith model (QstSmi) implied a strong relation between them. The detailed science behind their interaction is described in section 4.20.

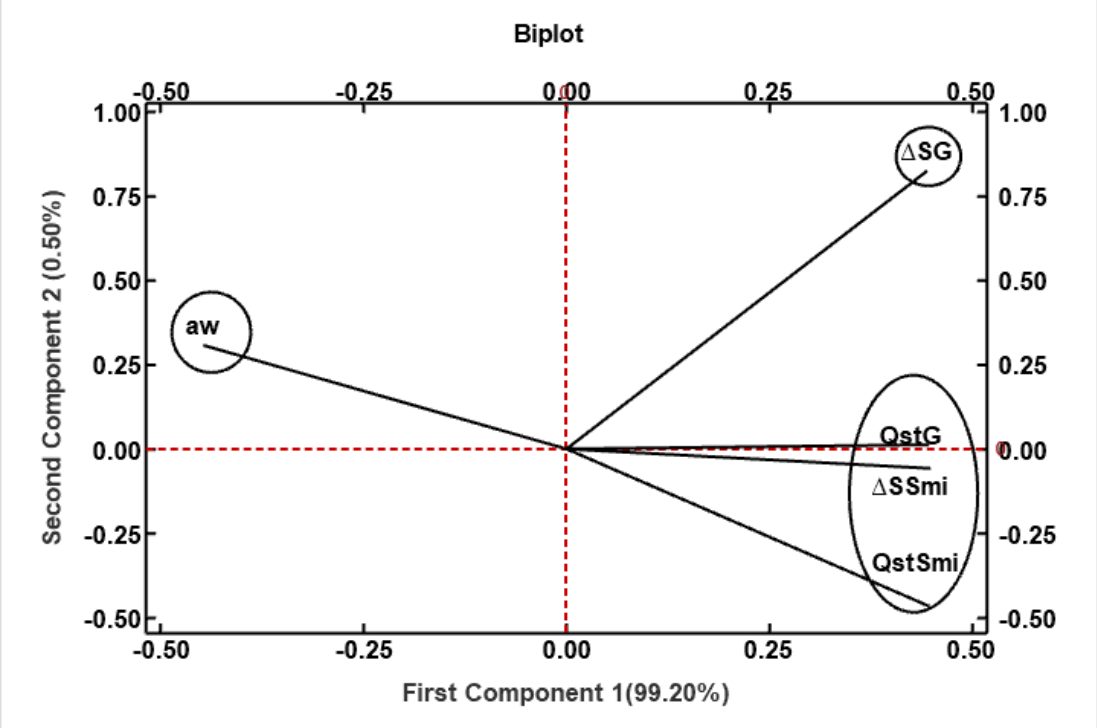

Figure 4.18 PCA Biplot of Sorption entropy and isosteric heat of foam dried pineapple pulp powder

Symbols: a_w: water activity, ***Δ***SG: entropy predicted by the GAB model, ***Δ***SSmi: entropy predicted by the Smith model, QstG and QstSmi : isosteric heat predicted by the GAB and Smith models, respectively

4.22 Physicochemical properties of powder during storage

The total phenolic content of the pineapple pulp powder stored in PP and ALP pouches under different storage conditions is presented in Table 4.41. TPC of pineapple pulp powder was slightly decreased with the storage days and temperature. It was observed that the storage temperature had more of an effect on TPC than storage days. However, no significant changes in TPC value were observed. Powder packed in ALP pouches showed less destruction of TPC during storage. Antioxidant activity of the pineapple pulp showed that the powder stored under the ALP package showed no significant changes during storage. In contrast, some changes were observed in the powder packed in the PP package. Though the values were slightly changed with the temperature, no significant changes were observed with the days of storage. With the increasing storage temperature, the TPC value was found to decrease at higher temperatures ($p<0.05$). Powder exposed to high temperatures might destroy the TPC value. Similar patterns were observed for the powder packed in ALP pouches.

In contrast, aluminum-laminated (ALP) pouches showed better retention than PP. The pH value of the powder during storage was analyzed for both packaging conditions after every 3-day interval. The values presented in Table 4.41 showed that the values were slightly changed with time. However, insignificant changes were observed during the storage period. The titrable acidity of the powder stored in PP and ALP pouches showed changes in the values during the studies. The TA value changed more in the powder packed in PP pouches than in ALP. However, the values were slightly changed with the storage conditions. The changes in the chemical values during storage studies might be due to the interaction of the various constituents in the pineapple powder. As Muzaffar & Kumar (2016) described, similar results have also been obtained. Packaging material slightly impacted the TA value (Table 4.41), possibly due to the reaction between the amine group of protein and the sugar in the pineapple powder, which caused the Millard reaction. Similar observations were obtained during the storage studies of tomato pulp powder and mango milk powder (Liu et al., 2010; Chauhan et al., 2013). However, insignificant changes can be seen for the conditions packed in PP and ALP pouches, respectively. Overall, the results indicate that AL pouches were more effective in preserving phenolics, antioxidant activity, and acidity balance of the juice, particularly under elevated storage temperatures, whereas PP pouches exhibited slight quality degradation.

Table 4.41: Physicochemical properties of foam mat dried powder stored in PP and AL pouches under accelerated storage conditions

	PP pouches											
	TPC (g GAE/ L juice)			**% Antioxidant Capacity**			**pH**			**Titrable acidity (TA) (%)**		
Storage (Temp_days)	**30ºC**	**40 ºC**	50 **ºC**	**30 ºC**	**40 ºC**	50 **ºC**	**30 ºC**	**40 ºC**	50 **ºC**	**30 ºC**	**40 ºC**	50 **ºC**
Control	**6.580±0.100^{cA}**	**6.580±0.100^{cA}**	**6.580±0.100^{cA}**	**63.751±0.683** ^{aA}	**63.751±0.683** ^{aA}	**63.751±0.683** ^{dA}	3.30±0.001 ^{aA}	3.30±0.001 ^{aA}	3.30±0.001 ^{aA}	0.843±0.02 ^{aA}	0.843±0.02 ^{aA}	0.843±0.02 ^{aA}
3	5.588±0.277^{bA}	5.326±0.059^{bA}	5.209±0.012^{aA}	62.553±0.755 ^{aA}	62.448±0.755 ^{aA}	60.936 ±1.153^{cdA}	3.33±0.001 ^{aA}	3.33±0.000 ^{aA}	3.33±0.001 ^{aA}	0.845±0.03 ^{aA}	0.932±0.05 ^{aA}	0.989±0.04 ^{aA}
6	5.255±0.006^{bA}	5.201±0.024^{bB}	5.151±0.012^{abAB}	62.448±0.712 ^{aA}	62.292 ±0.681 ^{aA}	59.947±1.017^{bcA}	3.35±0.002 ^{aA}	3.35±0.001 ^{aA}	3.35±0.004 ^{aA}	0.849±0.01 ^{aA}	0.936±0.09 ^{aA}	0.991±0.03 ^{aA}
9	4.972±0.029 ^{aA}	4.722±0.088^{aA}	4.934±0.212^{abA}	62.312±0.869 ^{aA}	62.149±1.100 ^{aA}	58.973±0.302^{bcA}	3.36±0.001 ^{aA}	3.36±0.003 ^{aA}	3.36±0.003 ^{aA}	0.901±0.04 ^{aA}	0.943±0.07 ^{aA}	0.993±0.01 ^{aA}
12	4.984±0.012 ^{aAB}	4.693±0.165^{aA}	5.030±0.018^{abB}	62.259±1.255 ^{aA}	62.095±1.331 ^{aA}	56.834±0.875^{abA}	3.35±0.001 ^{aA}	3.35±0.005 ^{aA}	3.35±0.001 ^{aA}	0.913±0.03 ^{aA}	0.965±0.01 ^{aA}	0.994±0.05 ^{aA}
15	4.951±0.012 ^{aA}	4.588±0.265 ^{aA}	4.801±0.236^{aA}	62.149±1.253 ^{aB}	61.985±1.176 ^{aB}	54.757±0.582^{aA}	3.35±0.003 ^{aA}	3.35±0.001 ^{aA}	3.35±0.005 ^{aA}	0.915±0.02 ^{aA}	0.986±0.01 ^{aA}	0.995±0.03 ^{aA}
	AL pouches											
Control	**6.580±0.100^{aA}**	**6.580±0.100^{aA}**	**6.580±0.100^{cA}**	**63.751±0.683^{aA}**	**63.751±0.683^{aA}**	**63.751±0.683^{cA}**	3.30±0.001^{aA}	3.30±0.001^{aA}	3.30±0.001^{aA}	0.843±0.03 ^{aA}	0.843±0.03 ^{aA}	0.843±0.03 ^{aA}
3	6.518±0.012^{aC}	6.493±0.001^{aB}	6.342±0.059^{bcA}	63.697±0.864^{aA}	63.228±1.822^{aA}	62.239±1.013^{bcA}	3.31±0.001^{aA}	3.35±0.000^{aA}	3.39±0.001^{aA}	0.843±0.01 ^{aA}	0.854±0.01 ^{aA}	0.873±0.01 ^{aA}
6	6.472±0.018^{aA}	6.409±0.071^{aA}	6.217±0.118^{abA}	63.698±0.422^{aA}	63.176±1.306^{aA}	61.927±0.018^{bcA}	3.34±0.002^{aA}	3.36±0.001^{aA}	3.40±0.004^{aA}	0.843±0.02 ^{aA}	0.861±0.03 ^{aA}	0.891±0.02 ^{aA}
9	6.468±0.035^{aB}	6.368±0.106^{aB}	6.122±0.018^{abA}	63.519±1.807^{aA}	63.123±1.523^{aA}	60.229±0.230^{abA}	3.36±0.001^{aA}	3.37±0.003^{aA}	3.41±0.003^{aA}	0.844±0.05 ^{aA}	0.863±0.04 ^{aA}	0.893±0.04 ^{aA}
12	6.447±0.006^{aB}	6.334±0.153^{aB}	6.038±0.018^{aA}	63.512±0.050^{aB}	63.017±0.750^{aB}	60.010±0.232^{abA}	3.33±0.001^{aA}	3.38±0.005^{aA}	3.37±0.001^{aA}	0.846±0.05 ^{aA}	0.864±0.02 ^{aA}	0.897±0.01 ^{aA}
15	6.509±0.177^{aB}	6.272±0.065^{aB}	5.951±0.024 ^{aA}	63.460±0.800^{a}	62.803±0.486^{aB}	58.914±0.859 ^{aB}	3.31±0.003^{aA}	3.38±0.001^{aA}	3.39±0.005^{aA}	0.846±0.03 ^{aA}	0.869±0.03 ^{aA}	0.899±0.03 ^{aA}

**mean± SD that do not share small letters are significantly different with the storage days

Table 4.42: Thermodynamic properties of foam mat dried powder stored in PP and ALP

	TPC				**% Antioxidant Capacity**			
Sample (s)	**k**	**T (K)**	**Ea(kJ/mol)**	**Q_{10}**	**k**	**T (K)**	**Ea(kJ/mol)**	**Q_{10}**
PP	0.0251	30	9.34	1.125	0.0021	30	14.601	1.203
	0.0305	40			0.0024	40		
	0.0269	50			0.0098	50		
ALP	0.0014	30	14.908	1.208	0.0003	30	17.509	1.248
	0.0034	40			0.0011	40		
	0.0074	50			0.0054	50		

The thermodynamic properties of foam-mat dried pineapple powder packed in PP and ALP materials are presented in Table 4.42. The reaction rate constant (k) obtained from the first-order model equation showed slight changes with temperature, indicating its effect on the degradation of quality parameters in both packaging materials. Although the "k" values varied with temperature, the activation energy values indicated negligible changes in these parameters during storage. The low Q_{10} values obtained for both cases suggest low temperature sensitivity of total phenolic content (TPC) and antioxidant capacity degradation in pineapple pulp powder. Q_{10} value of 1.208 indicates that storage temperature only slightly influences the degradation of total phenolic content (TPC) and antioxidant capacity in foam-mat dried pineapple powder. In other words, when the storage temperature increases by 10 °C, the rate of degradation increases by only about 20.8%**,** which reflects high stability and low temperature sensitivity of these bioactive compounds in the powder.

Bibliography

Abdullah, S., Keoh, S. C., Johar, H. M., Razak, N. A., Shaari, A. R., & Rukunudin, I. H. (2020, September). Mathematical modelling of moisture sorption isotherms by using the BET and GAB models. In *IOP Conference Series: Materials Science and Engineering* (Vol. 932, No. 1, p. 012037). IOP Publishing.

Almeida, F. D. L., Cavalcante, R. S., Cullen, P. J., Frias, J. M., Bourke, P., Fernandes, F. A., & Rodrigues, S. (2015). Effects of atmospheric cold plasma and ozone on prebiotic orange juice. *Innovative Food Science & Emerging Technologies*, *32*, 127–135.

Al-Muhtaseb, A. H., McMinn, W. A. M., & Magee, T. R. A. (2002). Moisture sorption isotherm characteristics of food products: a review. *Food and Bioproducts Processing*, *80*(2), 118–128.

Al-Muhtaseb, A. H., McMinn, W. A. M., & Magee, T. R. A. (2004). Water sorption isotherms of starch powders. Part 2: Thermodynamic characteristics. *Journal of Food Engineering*, *62*(2), 135–142.

Asokapandian, S., Venkatachalam, S., Swamy, G. J., & Kuppusamy, K. (2016). Optimization of foaming properties and foam mat drying of muskmelon using soy protein. *Journal of Food Process Engineering*, *39*(6), 692–701.

Azizpour, M., Mohebbi, M., Hossein Haddad Khodaparast, M., & Varidi, M. (2014). Optimization of foaming parameters and investigating drying temperature's effects on shrimp's foam-mat drying *(Penaeus indicus*). *Drying Technology*, *32*(4), 374–384.

Bag, S. K., Srivastav, P. P., & Mishra, H. N. (2011). Optimization of process parameters for foaming of bael (*Aegle marmelos L.*) fruit pulp. *Food and Bioprocess Technology*, *4*, 1450–1458.

Basu, S., Shivhare, U. S., & Raghavan, G. S. V. (2007). Time dependent rheological characteristics of pineapple jam. *International Journal of Food Engineering*, *3*(3).

Bhattacharya, S. (1999). Yield stress and time-dependent rheological properties of mango pulp. *Journal of Food Science*, *64*(6), 1029–1033.

Bhattacharya, S., Bhat, K. K., & Raghuveer, K. G. (1992). Rheology of Bengal gram (*Cicer arietinum*) flour suspensions. *Journal of Food Engineering*, *17*(2), 83–96.

Bhusari, S. N., Muzaffar, K., & Kumar, P. (2014). Effect of carrier agents on physical and microstructural properties of spray dried tamarind pulp powder. *Powder Technology*, *266*, 354–364.

Bußler, S., Ehlbeck, J., & Schlüter, O. K. (2017). Pre-drying treatment of plant related tissues using plasma processed air: Impact on enzyme activity and quality attributes of cut apple and potato. *Innovative Food Science & Emerging Technologies*, *40*, 78–86.

Chauhan, A. K., & Patil, V. (2013). Effect of packaging material on storage ability of mango milk powder and the quality of reconstituted mango milk drink. *Powder Technology*, *239*, 86–93.

Dasan, B. G., & Boyaci, I. H. (2018). Effect of cold atmospheric plasma on inactivation of Escherichia coli and physicochemical properties of apple, orange, tomato juices, and sour cherry nectar. *Food and Bioprocess Technology*, *11(2)*, 334-343.

Davies, K. J., & Delsignore, M. E. (1987). Protein damage and degradation by oxygen radicals. III. Modification of secondary and tertiary structure. *Journal of Biological Chemistry*, *262*(20), 9908–9913.

Dehghannya, J., Pourahmad, M., Ghanbarzadeh, B., & Ghaffari, H. (2018). Heat and mass transfer modeling during foam-mat drying of lime juice as affected by different ovalbumin concentrations. *Journal of Food Engineering*, *238*, 164-177.

Djaeni, M., Prasetyaningrum, A., Sasongko, S. B., Widayat, W., &Hii, C. L. (2015). Application of foam-mat drying with egg white for carrageenan: drying rate and product quality aspects. *Journal of Food Science and Technology*, *52*(2), 1170-1175.

Esua, O. J., Sun, D. W., Ajani, C. K., Cheng, J. H., & Keener, K. M. (2022). Modelling of inactivation kinetics of Escherichia coli and Listeria monocytogenes on grass carp treated by combining ultrasound with plasma functionalized buffer. *Ultrasonics Sonochemistry*, *88*, 106086.

Fernandes, F. A., & Rodrigues, S. (2021).Cold Plasma Processing on Fruits and Fruit Juices: A Review on the Effects of Plasma on Nutritional Quality. *Processes*, *9*(12), 2098.

Goula, A. M., Karapantsios, T. D., Achilias, D. S., & Adamopoulos, K. G. (2008). Water sorption isotherms and glass transition temperature of spray dried tomato pulp. *Journal of Food Engineering*, *85*(1), 73–83.

Grzegorzewski, F., Ehlbeck, J., Schlüter, O., Kroh, L. W., & Rohn, S. (2011). Treating lamb's lettuce with a cold plasma–Influence of atmospheric pressure Ar plasma immanent species on the phenolic profile of Valerianella locusta. *LWT-Food Science and Technology*, *44*(10), 2285–2289.

Hayashi, N., Kawaguchi, R., & Liu, H. (2009). Treatment of Protein Using Oxygen Plasma Produced by RF Discharge. *Journal of Plasma and Fusion Research Series*, 8, 552–555.

Huppertz, T. (2010). Foaming properties of milk: A review of the influence of composition and processing. *International Journal of Dairy Technology*, *63*(4), 477-488.

Illera, A. E., Chaple, S., Sanz, M. T., Ng, S., Lu, P., Jones, J., & Bourke, P. (2019). Effect of cold plasma on polyphenol oxidase inactivation in cloudy apple juice and on the quality parameters of the juice during storage. *Food chemistry: X*, *3*, 100049.

Jimenez-Junca, C. A., Gumy, J. C., Sher, A., & Niranjan, K. (2011). Rheology of milk foams produced by steam injection. *Journal of Food Science*, *76*(9), E569-E575.

Kadam, D. M., & Balasubramanian, S. (2011). Foam mat drying of tomato juice. *Journal of Food Processing and Preservation*, *35*(4), 488–495.

Karaman, S., Yilmaz, M. T., Dogan, M., Yetim, H., & Kayacier, A. (2011). Dynamic oscillatory shear properties of O/W model system meat emulsions: linear viscoelastic analysis for effect of temperature and oil concentration on protein network formation. *Journal of Food Engineering*, *107*(2), 241-252.

Kaymak-Ertekin, F., & Gedik, A. (2004). Sorption isotherms and isosteric heat of sorption for grapes, apricots, apples and potatoes. *LWT-Food Science and Technology*, *37*(4), 429-438.

Khamjae, T., & Rojanakorn, T. (2018). Foam-mat drying of passion fruit aril. *International Food Research Journal*, *25*(1), 204–212.

Khodifad, B. C., & Kumar, N. (2020). Foaming properties of custard apple pulp and mathematical modelling of foam mat drying. *Journal of Food Science and Technology*, *57(2)*, 526–536.

King, C. J. (1968). Rates of moisture sorption and desorption in porous dried foodstuffs. *Food Technology*, *22*(4), 509.

Labuza, T. P., & Altunakar, B. (2020). Water activity prediction and moisture sorption isotherms. *Water activity in foods: Fundamentals and Applications*, 161-205.

Lau, C. K., & Dickinson, E. (2005). Instability and structural change in an aerated system containing egg albumen and inverted sugar. *Food Hydrocolloids*, *19*(1), 111–121.

Liu, F., Cao, X., Wang, H., & Liao, X. (2010). Changes of tomato powder qualities during storage. *Powder Technology*, *204*(1), 159–166.

Martínez-Padilla, L. P., García-Mena, V., Casas-Alencáster, N. B., & Sosa-Herrera, M. G. (2014). Foaming properties of skim milk powder fortified with milk proteins. *International Dairy Journal*, *36*(1), 21–28.

Misra, N. N., Keener, K. M., Bourke, P., Mosnier, J., & Cullen, P. J. (2014). In-package atmospheric pressure cold plasma treatment of cherry tomatoes. *Journal of Bioscience and Bioengineering*, 118(2), 177–182. https://doi.org/10.1016/j.jbiosc.2014.02.005

Misra, N. N., Patil, S., Moiseev, T., Bourke, P., Mosnier, J. P., Keener, K. M., & Cullen, P. J. (2014). In-package atmospheric pressure cold plasma treatment of strawberries. *Journal of Food Engineering*, *125*, 131–138.

Mitra, H., Pushpadass, H. A., Franklin, M. E. E., Ambrose, R. K., Ghoroi, C., & Battula, S. N. (2017). Influence of moisture content on the flow properties of basundi mix. *Powder Technology*, *312*, 133–143.

Mohamed, I. O., & Hassan, E. (2016). Time-dependent and time-independent rheological characterization of date syrup. *Journal of Food Research*, *5*(2), 13–22.

Muzaffar, K., & Kumar, P. (2016). Moisture sorption isotherms and storage study of spray dried tamarind pulp powder. *Powder Technology*, *291*, 322-327.

Ozen, E., & Singh, R. K. (2020). Atmospheric cold plasma treatment of fruit juices: A review. *Trends in Food Science & Technology*, *103*, 144–151.

Panigrahi, C., Mishra, H. N., & De, S. (2021). Modelling the inactivation kinetics of Leuconostoc mesenteroides, Saccharomyces cerevisiae and total coliforms during ozone treatment of sugarcane juice. *LWT-Food Science and Technology*, *144*, 111218.

Panigrahi, C., Vishwakarma, S., Mishra, H. N., & De, S. (2021). Kinetic modeling for inactivation of polyphenoloxidase and peroxidase enzymes during ozonation of sugarcane juice. *Journal of Food Processing and Preservation*, *45*(1), e15094.

Pankaj, S. K., Misra, N. N., & Cullen, P. J. (2013). Kinetics of tomato peroxidase inactivation by atmospheric pressure cold plasma based on dielectric barrier discharge. *Innovative Food Science & Emerging Technologies*, *19*, 153-157.

Pankaj, S.K., Wan, Z., Colonna, W., & Keener, K. M. (2017). Effect of high-voltage atmospheric cold plasma on white grape juice quality. *Journal of the Science of Food and Agriculture*, *97*(12), 4016-4021.

Pereira, E. A., Brandão, E. M., Borges, S. V., & Maia, M. C. (2008). Influence of concentration on the steady and oscillatory shear behavior of umbu pulp. *Revista Brasileira de Engenharia Agrícola e Ambiental*, *12*, 87–90.

Petrossian, G. A., & Maxfield, M. (2018). An information theory approach to hypothesis testing in criminological research. *Crime Science*, *7(1)*, 1–14.

Planinić, M., Velić, D., Tomas, S., Bilić, M., Bucić, A. (2005).Modeling of drying and rehydration of carrots using Peleg's model. *European Food Research and Technology*, *221(3)*, 446-451.

Quintão-Teixeira, L. J., Soliva-Fortuny, R., Mota Ramos, A., & Martín-Belloso, O. (2013). Kinetics of peroxidase inactivation in carrot juice treated with pulsed electric fields. *Journal of Food Science*, *78*(2), E222-E228.

Quirijns, E. J., Van Boxtel, A. J., Van Loon, W. K., & Van Straten, G. (2005). Sorption isotherms, GAB parameters and isosteric heat of sorption. *Journal of the Science of Food and Agriculture*, *85*(11), 1805-1814.

Raharitsifa, N., Genovese, D. B., & Ratti, C. (2006). Characterization of apple juice foams for foam-mat drying prepared with egg white protein and methylcellulose. *Journal of Food Science*, *71*(3), E142-E151.

Rajkumar, P., & Kailappan, R. (2006). Optimizing the process parameters for foam mat drying of totapuri mango pulp. *Madras Agricultural Journal*, *93*(Jan-Jun), 1.

Ramazzina, I., Berardinelli, A., Rizzi, F., Tappi, S., Ragni, L., Sacchetti, G., & Rocculi, P. (2015). Effect of cold plasma treatment on physico-chemical parameters and antioxidant activity of minimally processed kiwifruit. *Postharvest Biology and Technology*, 107, 55–65. https://doi.org/10.1016/j. postharvbio.2015.04.008.

Rizvi, S. S. H. (1995). Thermodynamic properties of food in dehydration. In M. A. Rao, & S. S. H. Rizvi (Eds.), *Engineering Properties of Foods* (pp. 223–309). New York: Marcel Dekker Inc.

Rodríguez, Ó., Gomes, W. F., Rodrigues, S., & Fernandes, F. A. (2017). Effect of indirect cold plasma treatment on cashew apple juice (*Anacardium occidentale L.). LWT-Food Science and Technology*, *84*, 457–463.

Seerangurayar, T., Manickavasagan, A., Al-Ismaili, A. M., & Al-Mulla, Y. A. (2017). Effect of carrier agents on flowability and microstructural properties of foam-mat freeze dried date powder. *Journal of Food Engineering*, *215*, 33–43.

Shaari, N. A., Sulaiman, R., Rahman, R. A., & Bakar, J. (2018). Production of pineapple fruit (*Ananas comosus*) powder using foam mat drying: Effect of whipping time and egg albumen concentration. *Journal of Food Processing and Preservation*, *42*(2), e13467.

Sormoli, M. E., & Langrish, T. A. (2015). Moisture sorption isotherms and net isosteric heat of sorption for spray-dried pure orange juice powder. *LWT-Food Science and Technology*, *62*(1), 875–882.

Sreedevi, P., Jayachandran, L. E., & Rao, P. S. (2019). Kinetic modeling of high-pressure induced inactivation of polyphenol oxidase in sugarcane juice (*Saccharum officinarum*). *Journal of the Science of Food and Agriculture*, *99*(5), 2365–2374.

Surowsky, B., Fischer, A., Schlueter, O., Knorr, D. (2013). Cold plasma effects on enzyme activity in a model food system. *Innovative Food Science & Emerging Technologies*, 19, 146–152.

Takai, E., Kitano, K., Kuwabara, J., & Shiraki, K. (2012). Protein Inactivation by Low-temperature Atmospheric Pressure Plasma in Aqueous Solution. *Plasma Processes and Polymers*, 9(1), 77-82.

Tappi, S., Berardinelli, A., Ragni, L., Dalla Rosa, M., Guarnieri, A., & Rocculi, P. (2014). Atmospheric gas plasma treatment of fresh-cut apples. *Innovative Food Science & Emerging Technologies*, 21, 114–122.

van Kempen, S. E., Schols, H. A., van der Linden, E., & Sagis, L. M. (2014). Molecular assembly, interfacial rheology and foaming properties of oligofructose fatty acid esters. *Food & Function*, *5*(1), 111-122.

Wang, N., & Brennan, J. G. (1991). Moisture sorption isotherm characteristics of potatoes at four temperatures. *Journal of Food Engineering*, *14*(4), 269–287.

Zhong, K., Wu, J., Wang, Z., Chen, F., Liao, X., Hu, X., & Zhang, Z. (2007). Inactivation kinetics and secondary structural change of PEF-treated POD and PPO. *Food Chemistry*, *100*(1), 115–123.